Dissertation

submitted to
the Combined Faculties for the Natural Sciences and for Mathematics
of the
Ruperto-Carola University of Heidelberg, Germany

for the degree of
Doctor of Natural Sciences

put forward by

Dipl.-Phys. Lisa Marie Haas

born in Nürtingen, Germany

Oral examination: 19th of October 2012

On the phase diagram of QCD

Referees:

Prof. Dr. Jan M. Pawlowski
Prof. Dr. Michael G. Schmidt

On the phase diagram of QCD

Abstract

In this thesis we study two flavour Quantum Chromodynamics (QCD) with the Functional Renormalisation Group (FRG). We compute the QCD phase diagram at imaginary and real chemical potential in the chiral limit. We introduce dual order parameters which originate in the matter sector but are sensitive to center symmetry breaking. For real and imaginary chemical potential we find that the chiral and the confinement–deconfinement transitions agree. At vanishing chemical potential we obtain for the chiral transition $T_c = 181$ MeV and for the confinement–deconfinement crossover $T_c \approx 178$ MeV. The dual density and the Polyakov loop agree within the percent level. At imaginary chemical potential the phase diagram shows the expected Roberge–Weiss periodicity. This constitutes the first calculation of the QCD phase diagram at imaginary chemical potential in the chiral limit. At real chemical potential our results agree with lattice, DSE and FRG model studies. Then we compare the Yang–Mills (YM) and the glue Polyakov loop potential and match the temperature scales as the matter contributions to the gauge dynamics do not alter the form of the potential but the temperature scale. We use the translation of the two temperature scales in a Polyakov Quark Meson model, where we study the order parameters and the thermodynamic observables. The Polyakov loop potential thus approximates the glue dynamics instead of the YM dynamics. We find very good agreement for the thermodynamic observables with lattice results.

Zum Phasendiagramm der QCD

Kurzfassung

In dieser Arbeit untersuchen wir Quantenchromodynamik (QCD) mit der Funktionalen Renormierungsgruppe (FRG). Dazu berechnen wir das Phasendiagramm der QCD mit imaginärem und reellem chemischem Potenzial mit zwei masselosen Quark flavour. Wir führen duale Ordnungsparameter ein, die aus dem Materiesektor der QCD stammen, aber sensitiv auf die Brechung von Zentrumssymmetrie sind. Unsere Resultate zeigen, dass sowohl für imaginäres als auch reelles chemisches Potenzial der chirale und der confinement–deconfinement Phasenübergang übereinstimmen. Bei verschwindendem chemischem Potenzial finden wir für den chiralen Phasenübergang eine kritische Temperatur von $T_c = 181$ MeV und für den confinement–deconfinement crossover eine Übergangstemperatur von $T_c \approx 178$ MeV. Der Polyakov loop und die duale Dichte stimmen sehr gut überein. Das Phasendiagramm mit imaginärem chemischem Potenzial zeigt die erwartete Roberge–Weiss Periodizität und ist die erste Rechung mit verschwindenden Quarkmassen. Unsere Ergebnisse für das Phasendiagramm mit rellem chemischem Potenzial stimmen mit DSE und FRG Modellrechnungen überein. Zum Schluss vergleichen wir das Polyakov loop Potenzial von Yang–Mills (YM) und glue Rechnungen. Die Form des Potenzials ändert sich kaum, dafür allerdings die Temperaturskala. Wir verwenden die Temperaturskalenanpassung in einem Polyakov Quark Meson Modell, in dem wir die Ordnungsparameter und die thermodynamischen Größen berechnen. Die Ergebnisse stimmen sehr gut mit Gitter Resultaten überein.

Contents

Chapter 1

Introduction

Quantum Chromodynamics (QCD) is the quantum field theory of the strong interaction of the standard model describing the microscopic correlations in nuclear and elementary particle physics. Its intrinsic properties are currently explored at colliders like the LHC at CERN, RHIC at Brookhaven and are planned at FAIR at Darmstadt and NICA at Dubna.

At microscopic scales, that is at very high energies, the degrees of freedom of QCD are quarks and gluons. Additionally to Quantum Electrodynamics (QED) the fermions (quarks) and the gauge fields (gluons) carry colour charge. These supplementary degrees of freedom eventually give rise to the self-interactions of the gluons and the formation of bound states consisting of three identical fermions that are only distinguished by their colour charge. In the ultraviolet regime (UV), i.e. at high energies, the coupling strength of the interactions between the quarks and the gluons is very small and it increases towards lower energies, i.e. in the infrared (IR). This behaviour is called asymptotic freedom [1, 2] as the interaction strength between the quarks and gluons becomes arbitrarily small for high energies. In the IR regime they are bound in macroscopic states and it is not possible to observe a single quark or gluon. In fact these macroscopic confined objects are colour charge neutral bound states called hadrons.

Through the Higgs mechanism all fundamental and massive particles of the standard model acquire their mass. However the two lightest quarks, the u and the d, which also constitute protons and neutrons, obtain only very small masses of about $3 - 5$ MeV. Therefore the Higgs mechanism does not account for the large neutron and proton masses of about 1 GeV. Consequently another mechanism is responsible for the masses of the hadrons. In the UV, quarks exhibit chiral symmetry which is dynamically broken for increasing coupling strength due to the formation of bound states. This spontaneous breaking of chiral symmetry is the mechanism that gives rise to the hadron masses. It is an example why understanding the phase transitions of QCD is crucial for our comprehension of elementary particle physics.

In collider experiments the fundamental processes of QCD are studied. They aim at the transition between the deconfined high temperature plasma phase, the Quark Gluon Plasma (QGP), see e.g. [3–6], and the hadronic phase at low temperatures. First hints from RHIC

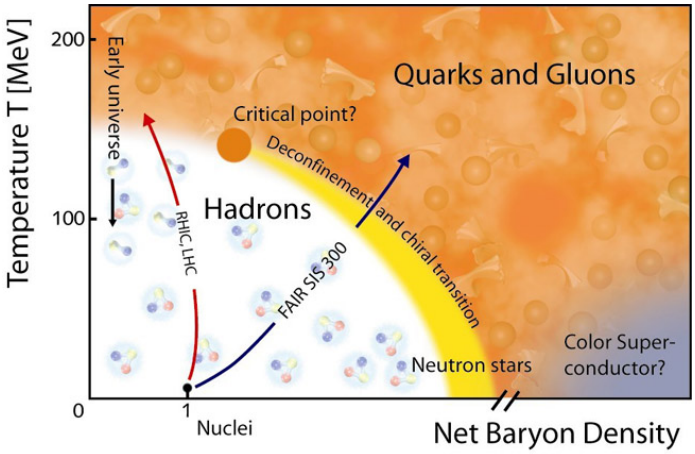

Figure 1.1: A sketch of the QCD phase diagram [9]. At high temperatures and chemical potentials quarks and gluons are deconfined whereas at low temperatures and densities they are bound in hadrons.

opened the discussion to whether the QGP is strongly coupled [7]. Up to then it was expected to be weakly coupled with basically freely moving quarks and gluons similar to the photons and electrons in the QED plasma. So far, this issue has not been resolved but is under investigation at the LHC. Most importantly the properties of the phases and the critical temperature of the transition are studied.

The transition between the deconfined QGP and the confined hadronic phase does not only occur at vanishing density but persists also for larger densities. One can plot the phase boundary as a function of temperature and chemical potential, resulting in the QCD phase diagram. This can be probed by collider experiments. The LHC and RHIC study small chemical potential, see Fig. 1.1, and NICA and FAIR investigate the structures of the phase diagram at large chemical potential. It is believed that the trajectory of the early universe cooling down stayed close to the temperature axis, so at very small chemical potential, undergoing the QCD transition at about $T_c \approx 180$ MeV and ending in the hadronic (nuclear) phase at low temperatures and small densities. Compact objects such as neutron stars are very dense but cold objects. Thus they are located close to the chemical potential axis at small temperatures and high chemical potential. The strong interactions are thought to play a crucial role in their composition and life-cycle, see e.g. [8] and references therein. Therefore an understanding of the QCD phase diagram and its properties is crucial to understanding the processes in elementary particle physics.

The large coupling strength in the IR is also the reason for the break down of perturbation theory, which expands in powers of the coupling α_s. At about $\Lambda_{\mathrm{QCD}} \approx 200$ MeV the perturbative ansatz for the strong coupling runs into a Landau pole, predicting its own failure. Consequently non-perturbative methods have to be used to study QCD. This is also part of the reason why QCD has not been solved.

A non-perturbative ansatz is to calculate QCD on a lattice. There one has to introduce a finite lattice spacing and a finite space-time extension as the calculations are done numerically on each lattice point using Monte–Carlo sampling techniques. Lattice QCD has proven to be very successful, e.g. in determining the hadron particle spectrum [10]. Unfortunately it is still not fully understood how to extrapolate to the continuum and finite-size effects as well as large quark masses, which have to be introduced due to the problems of implementing chiral symmetry on a discrete lattice, still play a major role, see e.g. [11–17]. Another obstacle is non-zero chemical potential, where due to the complex fermionic determinant, no interpretation of the weight of the generating functional in terms of a probability is applicable and hence Monte–Carlo methods cannot be utilised. This is called the sign-problem of lattice QCD [18, 19] and probably the second reason why QCD has not yet been fully understood.

Low temperature effective models, like the Quark–Meson (QM) model and the Nambu-Jona–Lasinio (NJL) model [20, 21] capture the characteristics of the matter sector of QCD well – like chiral symmetry breaking, but fail to describe confinement which is triggered by the glue dynamics. This has the consequence that their range of validity concentrates on low temperatures and larger chemical potentials where the dominant characteristics stem from the matter sector of QCD. A way to incorporate confinement is to additionally include an ansatz for the effective potential of the order parameter of the gauge sector of QCD, the Polyakov loop. The models are therefore called the Polyakov–Quark-Meson (PQM) and Polyakov–Nambu-Jona–Lasinio (PNJL) models [22–26]. However in QCD both, the gauge and the matter sector, couple to each other. This has the consequence that characteristics like the critical temperature of the QCD phase boundary is shifted which is unfortunately hard to include in model studies. Additionally they suffer from parameter dependence and use a fit to the thermodynamics of lattice QCD with infinitely heavy quarks which does not represent the correct thermodynamics with dynamical quarks.

Non-perturbative approaches that do not suffer from the sign problem and do not necessarily exhibit the parameter dependence are Renormalisation Group (RG) studies. They can incorporate bound state formation naturally through the rebosonisation technique [27–33]. The aim is to deduce the behaviour of the hadrons, i.e. the macroscopic degrees of freedom from the interactions of the quarks and gluons, i.e. the microscopic degrees of freedom. Unlike in perturbation theory, where one integrates out all momentum modes in the same step, this is done gradually. Here the idea is very similar to Kadanoff's block spin transformation [34], where one averages over a block of spins, keeping the effective information in a resulting effective spin. This is then done again with the resulting effective spins of several blocks repeatedly until the desired macroscopic scale is reached. This way, the relevant information is transported to the next scale until one arrives in the IR. This idea was extended to the continuum by Wegner [35] and Wilson [36, 37], integrating out fluctuations in small momentum shells yielding a flow equation for the theory. The formulation in terms of the effective average action is given by the Wetterich equation [38] and this particular formulation in terms of functionals is therefore called the Functional Renormalisation Group (FRG). It can be applied to a broad variety of theories and does not rely on weak coupling strengths.

For reviews and its applications in QCD and effective models, non-equilibrium gauge theories, ultra cold atoms, atomic and nuclear physics and quantum gravity, see e.g. [31, 39–67]. In this thesis we make use of the FRG to gain insight into the phase diagram of QCD.

The Wetterich equation is an exact equation and it allows to incorporate chemical potential in QCD studies. It also includes the full back-coupling and the dynamics of the two sectors of QCD, namely the gauge and the matter sector. Due to its formulation all quantum fluctuations are included step-wise and it also incorporates all non-perturbative effects. However this comes at the price of choosing a suitable truncation, see Subsec. 3.2.1, where it must be chosen such that all relevant physical information is self-consistently contained.

This thesis is organised as follows. Chapter 2 gives a short introduction to QCD and the QCD phase diagram. We discuss the order parameters of the chiral and the confinement–deconfinement phase transition and their effective potentials. In Chapter 3 we derive the flow equation of the FRG from the generating functional of QCD and explain its properties. Then we introduce rebosonisation, which dynamically enables bound state formation during the flow from the bare action in the UV to the full quantum effective action in the IR. Chapter 4 is a technical chapter where we explain our truncation and give the propagators and vertices we use in our computations. Then we derive the rebosonised flow equations for the couplings and anomalous dimensions, at vanishing and non-zero chemical potential and temperature. In Chapter 5 we introduce imaginary chemical potential and discuss the resulting properties of the extended QCD phase diagram. We introduce new order parameters for the confinement–deconfinement phase transition, the dual order parameters, and show our findings for the pressure difference, the dual quark mass and the pion decay constant. Subsequently we discuss the properties of the effective potential of the gauge sector, the Polyakov loop potential, at imaginary chemical potential. We show the order parameters, the chiral condensate, the dual density and the Polyakov loop at vanishing chemical potential in the chiral limit for two flavours. Our results show that the transitions agree within the width of the crossover and we find a chiral critical temperature of $T_c \approx 178$ MeV and a crossover temperature of $T_c = 181$ MeV. We plot the phase diagram at imaginary chemical potential, showing the phase boundary for the chiral and the confinement–deconfinement phase transition. This is the first calculation of the QCD phase diagram at imaginary chemical potential in the chiral limit from first principles. In Chapter 6 we discuss results at vanishing temperature and chemical potential for the masses of the matter sector and compute the QCD phase diagram for real chemical potential. Our results show that both the chiral and the confinement–deconfinement transition agree. The results also compare very well to DSE and FRG PQM model studies. Then we compare the YM and the glue Polyakov loop potential and match the temperature scales. This is applied in a PQM model with an logarithmic ansatz for the effective potential. We present the order parameters and the thermodynamic observables of the system and find that they agree very well with lattice results. Thus the translation of the two temperature scales can aid model studies to incorporate glue dynamics. The last chapter concludes this thesis with a short summary.

This thesis was solely written by the author, however the results presented here are based on work in collaboration with Jens Braun, Leonard Fister, Florian Marhauser, Jan M. Pawlowski, Jürgen Schaffner–Bielich and Rainer Stiele. Chapter 5 is based on Refs. [68, 69] and Chapter 6 includes Refs. [70–73], which are to be published.

Chapter 2

Quantum Chromodynamics

Quantum Chromodynamics (QCD) is the quantum field theory of the strong interaction. At high energy scales QCD exhibits asymptotic freedom [1, 2] as the coupling strength becomes arbitrarily small, see Fig. 2.1. Its intrinsic scale is $\Lambda_{\mathrm{QCD}} \approx 200$ MeV, where perturbation theory, the expansion in powers of the coupling α_s, predicts a divergent coupling strength, it runs into a Landau pole.

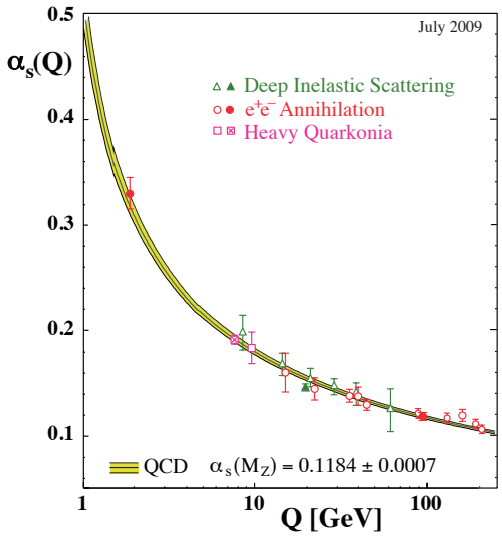

Figure 2.1: Summary of experimental data of α_s as a function of energy scale Q fitted with 4−loop predictions of perturbation theory [74].

In QCD as opposed to QED, the fermions, quarks, as well as the gauge fields, gluons, carry colour charge and due to the self-interactions of the gluons the strong force is of short range. The degrees of freedom at high energies are massive quarks and massless gluons whereas at low energies they are confined in colourless composite massive bound states, hadrons. The relatively small quark masses of the u and d quark of about $3 - 5$ MeV from the Higgs mechanism do not account for the comparatively large meson masses like the pions, which are composed of the u and d quark and have masses of about 140 MeV, and the even much

bigger masses for the other mesons and baryons. The generation of these hadron masses cannot be explained by the Higgs mechanism, but by the dynamical (spontaneous) breaking of chiral symmetry which is an intrinsic property of the quark fields at high energies.

At low energies there are no free quarks and gluons, i.e. coloured objects but only confined colour charges in colour-neutral objects as the energy needed to separate two quarks rises proportional to their distance. Consequently one can also picture a phase at very high energies and densities where quarks and gluons are deconfined. This is called the Quark Gluon Plasma (QGP).

2.1 The QCD action

QCD is the non-Abelian Quantum Field Theory of the strong interaction. Its microscopic degrees of freedom are the quarks (fermions) and the gluons (gauge fields). The microscopic action in $d = 4$ Euclidean momentum space is given by

$$S = \int \frac{d^4p}{(2\pi)^4} \left\{ \frac{1}{4} F^a_{\mu\nu} F^a_{\mu\nu} + \bar{\psi}^f_i \left(i \not{D}_{ij} + i m_\psi \, \delta_{ij} \right) \psi^f_j \right\}, \tag{2.1}$$

where the gauge fields are given in the adjoint representation of the $SU(N_c = 3)$ gauge group and the quarks are composed of two Weyl spinors in the fundamental representation. The field strength tensor and the Dirac operator in momentum space are given by

$$F^a_{\mu\nu} = \frac{i}{g}[D_\mu, D_\nu] = \partial_\mu A^a_\nu - \partial_\nu A^a_\mu + g f^{abc} A^b_\mu A^c_\nu \tag{2.2}$$

$$i \not{D}_{ij} = i \gamma_\mu (D_\mu)_{ij} = \gamma_\mu (p_\mu \, \delta_{ij} + g A^a_\mu t^a_{ij}), \tag{2.3}$$

where in the adjoint representation the colour (gauge group) degrees of freedom range from $a = 1, \ldots, N_c^2 - 1$, so in total there are 8 colour degrees of freedom, as there are eight generators which are given by

$$(t^a)_{ij} = \frac{(\lambda^a)_{ij}}{2}. \tag{2.4}$$

The λ^a are the Gell–Mann matrices, see App. A.3. They are 3×3 unitary traceless Hermitian matrices. The indices i, j refer to the fundamental representation of $SU(3)$ and range therefore from $1, \ldots, 3$. The quark fields are Dirac spinors which are composed of two Weyl spinors and can thus be written in terms of an independent left and right handed part

$$\psi = \begin{pmatrix} \psi_L \\ \psi_R \end{pmatrix}, \qquad \bar{\psi} = \left(\bar{\psi}_R, \bar{\psi}_L \right). \tag{2.5}$$

Additionally, the quarks carry also flavour degrees of freedom, ranging $f = 1, \ldots, N_f$, where QCD has six flavours $N_f = 6$. The Greek indices above stand for the Lorentz degrees of freedom and range in Euclidean space from $\mu = 0, \ldots, 3$. We use Hermitian Dirac γ-matrices which obey the anti-commutation relation

$$\{\gamma_\mu, \gamma_\nu\} = 2\delta_{\mu\nu} \mathbb{1}_4. \tag{2.6}$$

The generators defined in Eqn. 2.4 determine the structure constants appearing in the field strength tensor via the commutation relation and the trace in group space

$$[t^a, t^b] = i f^{abc} t^c \tag{2.7}$$

$$\mathrm{Tr}\, t^a t^b = \frac{1}{2}\delta^{ab}. \tag{2.8}$$

Note that in full QCD all fields, masses, couplings and wave function renormalisations of Eqn. (4.1) are scale dependent, for a better readability we dropped the subscript k.

2.2 The phase diagram of QCD

Similar to the phase diagram of water, one can draw a phase diagram of quarks and gluons where the phase boundary as a function of temperature and density or chemical potential is shown, see Fig. 1.1. The temperatures and densities of QCD cover a wide range, from the matter surrounding us to the early and hot state of the universe or the dense states of neutron stars. The phase diagram of full QCD has so far not been calculated which is due to the coupling strength of α_s and the intrinsic properties of the quarks. For reviews on the QCD phase diagram see e.g. [75–80].

At high temperatures and densities the degrees of freedom of QCD are quarks and gluons which are deconfined in the Quark Gluon Plasma and the matter sector of QCD exhibits chiral symmetry. At low temperatures and densities the quarks and gluons are confined in hadronic bound states and chiral symmetry is broken. Naturally one would expect these phase transitions for vanishing chemical potential to occur around the intrinsic scale of QCD, $\Lambda_{QCD} \approx 200$ MeV.

For infinitely heavy quarks QCD reduces to a $SU(3)$ Yang–Mills theory and exhibits center symmetry at low temperatures which is broken at high temperatures. Lattice QCD studies find a first order transition at about $T_c \simeq 270$ MeV [81]. Including physical quark masses, the symmetry only holds approximately and so the transition is weakened to a crossover, see e.g. lattice and DSE calculations of the phase transitions at vanishing temperature and chemical potential with non-vanishing quark masses [82–86]. For $2+1$ quark flavours with physical masses, the transition temperature is about $T_c \approx 150 - 200$ MeV [87, 88]. This picture is also found by Renormalisation Group studies, see e.g. for $2+1$ flavours with physical quark masses [86]. For one and two flavours in the chiral limit, chiral symmetry is not explicitly broken and hence one expects a second order chiral transition and a crossover for the confinement-deconfinement transition, see [68, 84, 85, 89].

For non-vanishing chemical potential it is suggested by Renormalisation Group and model studies [24, 84–86, 90–96] that the crossover ends at a second order critical point and continues in a first order line towards smaller temperatures to the chemical potential axis. However the exact picture after the critical endpoint is under strong debate as large N_c calculations expect

a triple point instead of the second order endpoint and that the chiral and the deconfinement transition separate and another phase, the so-called quarkyonic phase appears [97]. Also the location of the conjectured endpoint is not clear, as it strongly depends on all parameters of the model and very strongly on the back-coupling of the gauge sector to the matter sector and the masses of the mesonic degrees of freedom [90, 91, 98–100].

In Ref. [101] it is argued from experimental data that at vanishing chemical potential the chemical freeze-out temperature is close to or serves as an upper bound on the critical temperature of the chiral and confinement–deconfinement transition temperature. Whether or not their arguments hold is not yet clear, as they find a first order transition and no crossover which is not confirmed by lattice [102], FRG [68] and DSE [84–86] studies. However they find a critical temperature of $T_{\text{chem}} = 176$ MeV which agrees with lattice and RG findings within the estimated errors of the theoretical and experimental studies. Up to now it is not fully clear how to compare the very different definitions of the transitions, as even the definitions within the RG and within the lattice communities differ.

At low temperatures and non-vanishing chemical potential, hadrons begin to form and for large chemical potential dominate the mesonic degrees of freedom as the energetic costs of producing a baryon decrease with increasing chemical potential. For densities smaller than normal nuclear matter density small droplets appear and for increasing density undergo a first order transition to the liquid matter phase just when the density equals the normal nuclear matter density. The transition is weakened for increasing temperature so that the first order line ends approximately at $10 - 20$ MeV in a second order point and then turns into a crossover at higher temperatures.

For lower temperatures and larger chemical potentials, the location of the phase boundaries is not so clear. Baryonic degrees of freedom definitely play a dominant role [80, 103] and as of now they haven't been included in $N_c = 3$ RG studies. However there are results for $N_c = 2$ RG [103, 104], model [105, 106] and lattice studies [107–109], where the relativistic crossover from a Bose–Einstein condensate (BEC) to a Bardeen–Cooper–Schriefer (BCS) phase have been investigated. The baryons in $N_c = 2$ are then simply given by the condensate of two quarks and are therefore bosons. They find that there is no critical endpoint [103]. From there baryons in $N_c = 3$ QCD then are the next step.

For very large chemical potentials and close to zero temperature weak coupling methods are applicable for the ground state of QCD, and in analogy to electrons in metal in QED, quarks in very dense matter exhibit colour superconductivity [8, 77, 110–114]. These phases might appear in extremely dense objects such as neutron stars or possibly quark stars, however this is at the moment under investigation.

The coupling strength and the importance of the long range interactions make the QCD

phase diagram hard to access. Perturbative methods lose their predictability already at high temperatures as non-trivial thermal fluctuations come into play.

At vanishing and imaginary chemical potential, lattice QCD is applicable, for a review see e.g. [115]. There one discretises QCD on a lattice with spacing a and volume V and use Monte Carlo importance sampling techniques to obtain quantities like the critical temperature T_c of the phase transition or the thermodynamic quantities. This method captures well the microscopic dynamics of QCD, however one has to perform two extrapolations, one is the continuum limit $a \to \infty$ and the other is the thermodynamic limit $V \to \infty$. This renders the results with statistical errors stemming from the importance sampling and systematical errors from the extrapolations. Unfortunately at non-zero chemical potential one faces the so-called sign problem, as the fermionic determinant at finite real chemical potential is complex so that no interpretation in the sense of probabilities is possible [18, 19]. This can only be circumvented by a purely imaginary chemical potential which renders the fermionic determinant real.

In general, quarks are hard to include in lattice calculations due to the controversy of implementing chiral symmetry on a discrete lattice. Nowadays, there are calculations with very light quarks, however they are very costly in terms of computing power and time, see e.g. [116, 117]. At vanishing chemical potential lattice studies show that the phase transition is a crossover and, depending on different definitions of such a crossover temperature, different implementations of the quarks and different lattice spacings and volumes, they find a critical temperature of about $T_c \approx 150 - 200$ MeV [82, 87, 118–120].

A way to circumvent the sign problem is to study models which capture the matter sector well and self-consistently but then have more difficulties to incorporate confinement. The big advantage is that a non-vanishing chemical potential is easily included and poses no problems in the calculations. For high chemical potential and low temperatures the matter sector of QCD plays the dominant role over the gauge sector. Here models are a very effective tool to capture QCD like behaviour, see e.g. for (P)QM/(P)NJL [20–26, 79, 80, 90–92, 121–127] studies. However for smaller chemical potential and higher temperatures the gauge sector plays a very dominant role which is not captured by the models.

Complementary to lattice one can approach QCD with the RG. This has the advantage that one does not have to discretise the theory and then later take the infinite volume and thermodynamic limit and chiral fermions are easy to implement. One can also include a chemical potential without having to deal with the sign-problem as RG studies usually do not utilise Monte-Carlo methods. The RG provides methods to approach the QCD phase diagram from an analytical side, valid for all temperatures and chemical potentials. The question arising[1] is where to truncate the infinitely many coupled differential equations, see Sec. 3.2.1. This has to be chosen carefully and in such a manner that the subset of equations

[1] There is no such thing as a free lunch.

is self-consistant and incorporates all relevant physical aspects. So the RG is applicable for all temperatures and chemical potentials being able to incorporate the dynamics of the glue and the matter sector of QCD in a fully coupled manner for all coupling strengths. For a study of the QCD phase boundary of one flavour in the chiral limit see [89], for two flavours see [68, 85] and for $N_f = 2 + 1$ with physical quark masses see [86].

2.3 The chiral phase transition

For massless quarks, the matter sector of QCD exhibits an exact global $U(N_f)_L \times U(N_f)_R$ flavour symmetry. This symmetry is broken explicitly by non-vanishing quark masses as such mass terms mix left and right handed quarks. The two lightest quarks, the u and the d quark, are almost massless compared to all other quarks, so that the chiral limit with $N_f = 2$ seems a reasonable approximation. The chiral limit guarantees that the left and the right handed parts of the quark fields can be treated independently and QCD is invariant under an exchange of the left and right handed fields. We can decompose this flavour symmetry into its components

$$SU(2)_L \times SU(2)_R \times U(1)_L \times U(1)_R. \tag{2.9}$$

One can now associate conserved currents with these symmetries, where the sum of the left and right handed currents results in the vector currents and the difference gives the axial currents. Therefore we can rewrite Eqn. (2.9) in terms of the vector and axial symmetries

$$SU(2)_V \times SU(2)_A \times U(1)_V \times U(1)_A. \tag{2.10}$$

The $U(1)_V$ vector symmetry corresponds to baryon number conservation, whereas the $U(1)_A$ subgroup corresponds to the chiral anomaly. The $SU(2)_V$ symmetry corresponds to isospin symmetry and is only broken by non-vanishing quark masses. In the following we see that the spontaneous breaking of the $SU(2)_A$ symmetry gives rise to pseudoscalar Goldstone bosons, which are the pions.

The $SU(2)_L \times SU(2)_R$ symmetry is spontaneously broken down to $SU(2)_V$ by a non-zero value of the chiral condensate: In the vacuum, the energy cost of creating an extra quark–anti-quark pair for massless quarks is small, so that the vacuum can also be thought of as a condensate of quark–anti-quark pairs. Of course they must have zero total and angular momentum, so that the condensate can only contain combinations of the form left handed quark and right handed anti-quark or vice versa. The condensate then is

$$\langle \bar{\psi}\psi \rangle = \langle \bar{\psi}_L \psi_R + \bar{\psi}_R \psi_L \rangle. \tag{2.11}$$

From this we see immediately that the vacuum mixes the two quark helicities which allows the u and d quarks to obtain effective masses as they pass through the vacuum although they themselves are massless. These effective masses break the $SU(2)_L \times SU(2)_R$ symmetry to $SU(2)_V$. This means that whenever $\langle \bar{\psi}\psi \rangle \neq 0$, chiral symmetry is spontaneously broken. Hence the chiral condensate serves as an order parameter for the chiral phase transition.

Through the Hubbard Stratonovich transformation [128, 129] one can relate it to the sigma-meson

$$\langle\sigma\rangle = -\frac{ih}{m_\sigma^2}\langle\bar{\psi}\psi\rangle. \tag{2.12}$$

In the UV, i.e. at high temperatures and chemical potentials, chiral symmetry holds and it is broken spontaneously (or dynamically) at low temperatures and chemical potentials. The $N_f^2 - 1$ massless Goldstone bosons associated with the spontaneous symmetry breaking are for $N_f = 2$ the pions. In the case of non-zero quark masses, the symmetry is not exact and hence the Goldstone bosons have also non-vanishing masses. Due to the breaking of $SU(N_f)_A$ symmetry, the pions are pseudoscalars.

2.4 The effective potential

In the case of two massless quark flavours, QCD falls into the $O(4)$ universality class [130, 131]. Through the spontaneous breaking of the global $SU(N_f)_A$ symmetry, the Goldstone bosons appear. These are associated with oscillations in the tangential direction of the effective potential in the ground state whereas the radial direction gives rise to a massive bound state, the sigma-meson. In this case, for two quark flavours, the effective potential is given by a Mexican hat type potential. If the minimum of the potential ϕ_0 acquires a non-vanishing expectation value, the $O(4)$ symmetry is broken and we are left with the $O(3)$ symmetry reflected by the trough of the potential where the pions live. One can picture a second order phase transition as a continuous deformation of a potential that looks like an x^2-potential into a Mexican hat potential, where the minima continuously move away from zero. So the minimum ϕ_0 is the order parameter, as it vanishes in the symmetric phase and has a non-zero value in the broken phase. From the arguments above it is precisely given by the oscillations in the radial direction and hence by the mass of the sigma-meson. The potential is in our

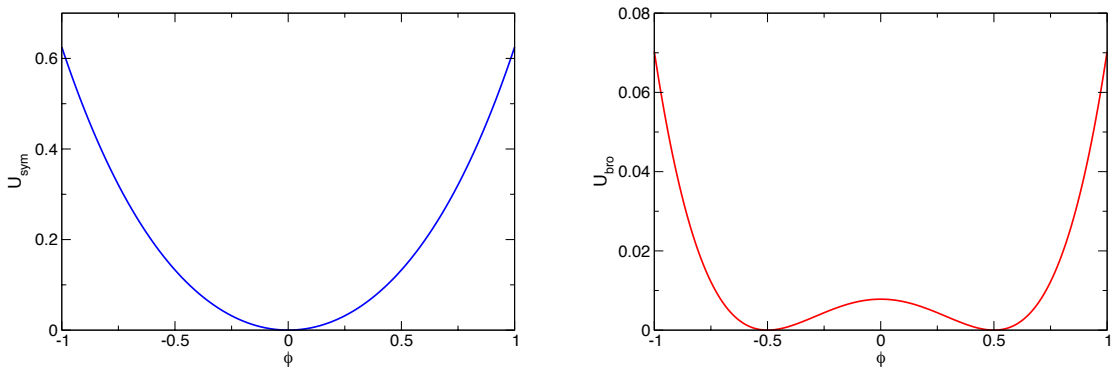

Figure 2.2: The effective potential of the matter sector for the symmetric (left panel) and the broken phase (right panel). To showcase we set $\phi_0 = 0.5$. A second order transition corresponds to a continuous deformation from the symmetric to the symmetry broken potential.

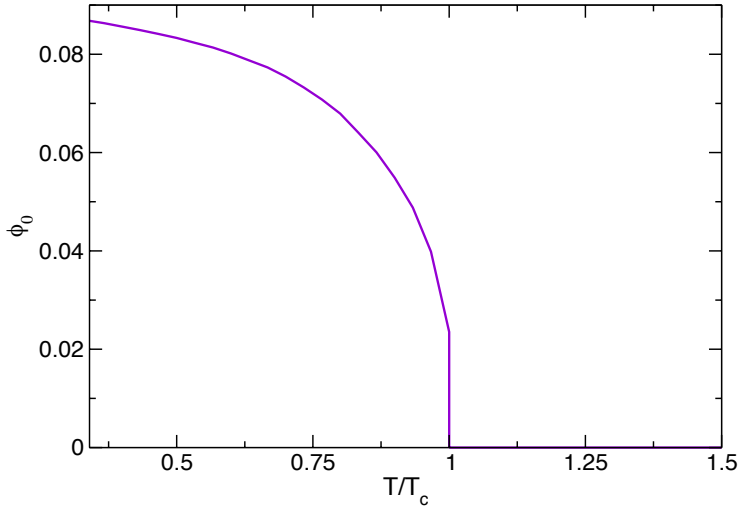

Figure 2.3: The minimum of the effective potential as a function of temperature. At temperatures above the phase transition in the symmetric phase the order parameter vanishes, below in the symmetry broken phase it has a non-zero value.

truncation, see Sec. 4.1, given by

$$\begin{aligned} U_{\text{sym}}(\phi^2) &= \frac{m_\sigma^2}{2}\phi^2 + \frac{\lambda_\sigma}{8}\phi^4 \\ U_{\text{bro}}(\phi^2) &= \frac{\lambda_\sigma}{8}(\phi^2 - \phi_0^2)^2 \end{aligned} \tag{2.13}$$

where the scalar field is composed of the pions and the sigma-meson $\phi = (\sigma, \vec{\pi})^T$. Eqn. (2.13) corresponds to the two potentials given in Fig. 2.2 in 2 dimensions, think of cutting through the higher dimensional potentials in the radial direction.

2.5 The confinement–deconfinement phase transition

For infinitely heavy quark masses, the gauge sector of QCD shows a different symmetry, a global center symmetry, as QCD reduces in this case to a pure $SU(N_c)$ gauge theory. The symmetry is broken in the presence of dynamical quarks. A center transformation is given by

$$U_z^{-1}(0, \vec{x}) U_z(\beta, \vec{x}) = z, \tag{2.14}$$

where $U_z(t, \vec{x})$ is a gauge transformation, $\beta = 1/T$ and z is an element of the center $Z(SU(N_c)) \equiv Z_{N_c}$ of the gauge group. The elements z are given by $z = \mathbb{1}\, e^{2\pi i \theta_z}$ from the condition $\det(z) = 1$ which means that the sum with respect to the angle θ_z vanishes $\sum_{\theta_z} e^{2\pi i \theta_z} = 0$, note that $\theta_z = k/N_c$ where k takes integer values $0, \ldots, N_c - 1$, as there are N_c elements that belong to the set of center elements. For $SU(3)$ the angle θ_z takes the values $\theta_z = 0,\ 1/3,\ 2/3$. It follows immediately that any observable that transforms non-trivially

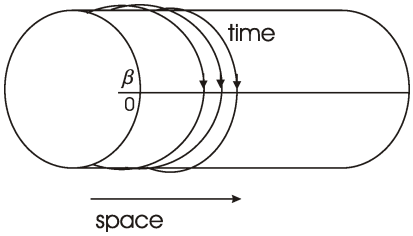

Figure 2.4: Sketch of the Polyakov loop. The time direction is curled up and has length $\beta = 1/T$.

under center transformations, i.e. that is sensitive to center transformations, can serve as an order parameter for center symmetry as it vanishes in the symmetric phase and it does not vanish in the broken phase. One example is the Polyakov loop $\langle L \rangle$ where the Polyakov loop variable $L(\vec{x})$ is given by

$$L(\vec{x}) = \frac{1}{N_c} \mathrm{Tr}\, \mathcal{P}\, e^{ig \int_0^\beta dt\, A_0(t,\vec{x})}, \tag{2.15}$$

where $\mathcal{P}$ stands for path ordering, the trace is evaluated in the fundamental representation and A_0 is the zero component of the gauge field. One can picture the Polyakov loop as an infinitely heavy quark moving only in the time direction, which is periodic in Euclidean time with length β, see Fig. 2.4, as $L(\vec{x})$ is related to the operator that generates a static quark [132]. The Polyakov loop variable L is not invariant under center transformations,

$$L \to zL, \tag{2.16}$$

which has the consequence that the vev of L, the Polyakov loop $\langle L \rangle$, vanishes in the symmetric phase and is non-zero in the broken phase, see e.g. [133]. Moreover, the Polyakov loop is proportional to the free energy of a quark F_q [2]

$$\langle L \rangle \sim e^{-\beta F_q} \tag{2.17}$$

so if the energy one needs to insert a quark into the theory is infinite, the Polyakov loop vanishes which means that the theory is confining. If the free energy is finite, the Polyakov loop does not vanish and we are in the deconfined phase. So we can link center symmetry and confinement.

In contradistinction to lattice QCD we compute $L[\langle A_0 \rangle]$. The expectation value of the Polyakov loop used in lattice calculations $\langle L \rangle_{\mathrm{ren}}$ involves a non-trivial renormalisation factor which amounts to $\langle L \rangle_{\mathrm{ren}}$ being larger than 1 for some temperature range. In Ref. [134–136], they showed that in Polyakov gauge $\langle A_0 \rangle$ is sensitive to topological defects which are related to confinement. Using the Jensen inequality, $L[\langle A_0 \rangle] \geq \langle L[A_0] \rangle$, $L[\langle A_0 \rangle]$ is an upper bound on $\langle L[A_0] \rangle$ and we have $L[\langle A_0 \rangle] \leq 1$ in the broken phase. In the symmetric phase $L[\langle A_0 \rangle]$ vanishes strictly [137].

[2] Actually it is related to half of the free energy of a quark-antiquark pair $F_{q\bar{q}}$ which is separated by an infinite distance.

2.6 Non-zero temperature

At non-zero temperature, the (imaginary) time axis is compactified on a torus with circumference $\beta = 1/T$, breaking the $O(4)$ symmetry to $O(3)$. This means that the zero components of the momenta are periodic and singled-out by the heat bath. This has two immediate consequences: the propagator of the gauge fields have now one component proportional and one perpendicular to the heat bath and the formalism for the zero-component of the momenta, which are now periodic, changes. One uses therefore the Matsubara formalism, where the integral over the zero-component of the momentum, which is now periodic with period $[0, \beta]$, is replaced by the sum over all Matsubara frequencies.

Due to their intrinsic characteristics, the fermions have anti-periodic boundary conditions and therefore have odd Matsubara frequencies, the bosons have periodic boundary conditions and hence even Matsubara frequencies

$$p_0 \to \nu_n = \begin{cases} 2n\,\pi T & \text{bosons} \\ (2n+1)\,\pi T & \text{fermions} \end{cases}, \quad n \in \mathbb{Z}.$$

So then we replace the integral at vanishing temperature over 4d momentum space with a sum over the zero-direction and a 3d integration

$$\int \frac{d^4p}{(2\pi)^4} \to T \sum_{n=-\infty}^{\infty} \int \frac{d^3p}{(2\pi)^3}. \tag{2.18}$$

At infinite temperature, i.e. $T \to \infty$, QCD reduces to a purely spatial theory as the circumference of the torus reduces to $\beta = 0$, the symmetry is given by $\mathbb{R}_3$. This can easily be seen by considering the propagators. E.g. the $4d$ quark and gluon propagators, which we derive in detail in the following chapter, are proportional to

$$G^{4d}_{\bar{\psi}\psi} \sim \frac{1}{T^2 + \vec{p}^2 + m^2_\psi} \quad \text{or} \quad G^{4d}_{AA} \sim \frac{1}{T^2 + \vec{p}^2} \tag{2.19}$$

so for $T \to \infty$ they vanish due to their proportionality to the inverse temperature. We can also relate the $3d$ propagators to the $4d$, as the temporal integration gives a contribution proportional to $\beta = 1/T$, we find $G^{3d} \sim T\, G^{4d}$, and hence as $G^{4d} \sim 1/T$ the $3d$ propagators obtain some non-vanishing value for $T \to \infty$. This also means that at infinitely high temperatures we enter the perturbative regime but with a $3d$ version of QCD[3].

So for large temperatures we expect to be able to use perturbative methods to describe QCD. This can be done e.g. by using a weak coupling expansion in powers of g, where the zeroth order gives a free gas of quarks and gluons, this is called the ideal QGP. The next orders, up to g^5 have been calculated so far [138, 139], but only converge poorly due to thermal fluctuations which strongly depend on the momentum scale considered. Even though the weak coupling expansion seems justified at such temperatures, the thermal fluctuations

[3]Perturbation theory of $4d$ QCD is found for infinite energy $E \to \infty$.

and the $3d$ theory complicate the picture, see e.g. [140–142]. At temperatures close to the phase transition, about $(1-2)\,T_c$, the predictive power using the weak coupling expansion is lost. Here, the system enters the strongly coupled regime.

2.7 The Polyakov loop potential

2.7.1 The perturbative effective potential for the gauge fields

The order parameter potential, i.e. the effective potential, for a pure $SU(N_c)$ gauge theory is given in one-loop perturbation theory by the Weiss potential [143, 144] which is valid at high temperatures[4]. It shows that the Z_{N_c} symmetry is broken and indicates that it is restored at low temperatures. A simple description of the potential is given in Polyakov gauge, where the zero-component of the gauge field is rotated into the Cartan subalgebra and the time derivative of A_0 vanishes, $\partial_0 A_0 = 0$. The potential is given for a $SU(N)$ gauge theory in $d = 4$ dimensions by

$$\frac{V_{\text{Weiss}}^{SU(N)}(\varphi_m)}{T^4} = -\sum_{m=1}^{N_c^2-1}\sum_{n=1}^{\infty}\frac{2\,\cos(n\,\varphi_m)}{n^4\pi^2}, \tag{2.20}$$

where the φ_m denote the eigenvalues of the Hermitian matrix $\phi^a T^a = g\,\beta\,A_0^a T^a$ in the adjoint representation and $\beta = 1/T$ is the inverse temperature[5]. The components of ϕ^a lie only in the Cartan directions. E.g. for $SU(3)$ a convenient choice is

$$g\,\beta\,A_0 = \varphi_3\frac{\lambda^3}{2} + \varphi_8\frac{\lambda^8}{2}, \tag{2.21}$$

where the λ^j are the Gell-Mann matrices and are given in App. A.3 and the eigenvalues then are the φ_m. E.g. the $SU(3)$ Weiss potential only depends on the two directions φ_3 and φ_8 and it is given as the sum over the potential in the φ_3-direction and the φ_8-direction. For $SU(2)$ Eqn. (2.7.1) simplifies to [143]

$$\frac{V_{\text{Weiss}}^{SU(2)}(\varphi)}{T^4} = -\sum_{n=1}^{\infty}\frac{4\,\cos(n\,\varphi)}{n^4\pi^2}, \tag{2.22}$$

where $\varphi = g\beta A_0$ and $\varphi \in [0, 2\pi]$. Here, the minima are located at $\varphi = 2\pi n$ with $n \in \mathbb{Z}$ and the potential is invariant under $\varphi \to 2\pi - \varphi$, so obeys Z_2 symmetry, see Fig. 2.5.

The order parameter, the Polyakov loop, is given in Polyakov gauge by

$$L(\vec{x}) = \cos\left(\frac{g\beta A_0(\vec{x})}{2}\right), \tag{2.23}$$

so that for $\varphi = 2\pi n$ its expectation value is finite and thus breaks the Z_2 symmetry spontaneously. Remember that also $\varphi = g\beta A_0$, which means that at high temperatures, where

[4] Although it is commonly called Weiss potential it was also computed in [144] and hence should be called Gross–Pisarski–Yaffe–Weiss potential. Despite this we stick to the convention and call it Weiss potential in the following.

[5] In the following we use the abbreviation $A_0^a T^a = A_0$.

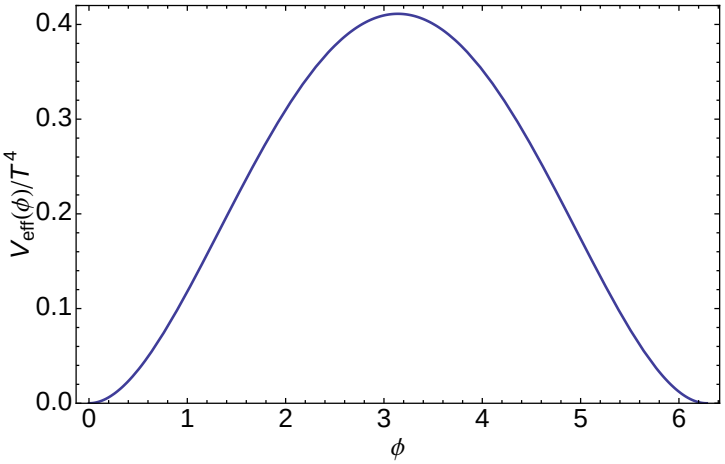

Figure 2.5: The $SU(2)$ Weiss potential [143]. Here we plot one period. The minima are located at 0 and 2π. The potential is valid at high temperatures in the perturbative regime for small coupling g.

g is small, the potential is deconfining as the symmetry is broken. For $T \to 0$ and large coupling strength the separation between the minima decreases until both minima are at the same point $\varphi = \pi$ and the Polyakov loop vanishes and the symmetry is restored. Because the derivation of the Weiss potential is based on perturbation theory, one can only deduct the potential at high temperatures and for small coupling strength. The full potential has to be derived in a non-perturbative ansatz where one can then make a statement about the form of the potential for all temperatures and couplings.

2.7.2 The non-perturbative Polyakov loop potential

The non-perturbative effective potential, the Polyakov loop potential, was derived with the FRG in [145, 146] and the studies of the YM potential were extended to higher $SU(N)$ groups and also included $Sp(2)$ and $E(7)$ [147]. At high temperatures the non-perturbative Polyakov loop potential agrees with the Weiss potential and it is also valid at low temperatures, where it shows the symmetry restoration of the $SU(N)$ gauge theory. It is directly derived from the effective action [146]

$$V[L(A_0)] = \frac{\Gamma[A_0]}{\Omega}, \tag{2.24}$$

where Ω is the space-time volume and $V[L(A_0)]$ is evaluated with a constant background field A_0. Note that we compute $V[L(\langle A_0 \rangle)]$, see Sec. 2.5. The input for the potential are the ghost and gluon propagators, which in QCD have contributions from the matter sector, see Fig. 4.3. This changes (lowers) the phase transition temperature compared to pure Yang–Mills theory. From the minima of the Polyakov loop potential the Polyakov loop is calculated.

In QCD the effective potential contains contributions from the glue sector and the matter

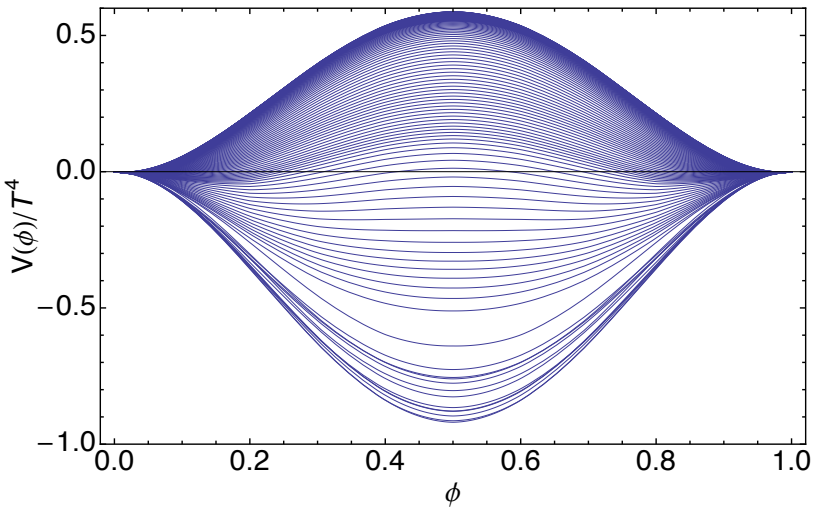

Figure 2.6: The non-perturbative $SU(2)$ Polyakov loop potential from Yang–Mills theory for various temperatures.

sector

$$V[L(A_0)] = V_{\text{glue}}[L(A_0)] + V_{\text{ferm}}[L(A_0)], \tag{2.25}$$

which couple back to another. Note also that they do not exhibit the same periodicity, due to the properties of the fermionic fields, the fermionic potential has double the period of the glue potential.

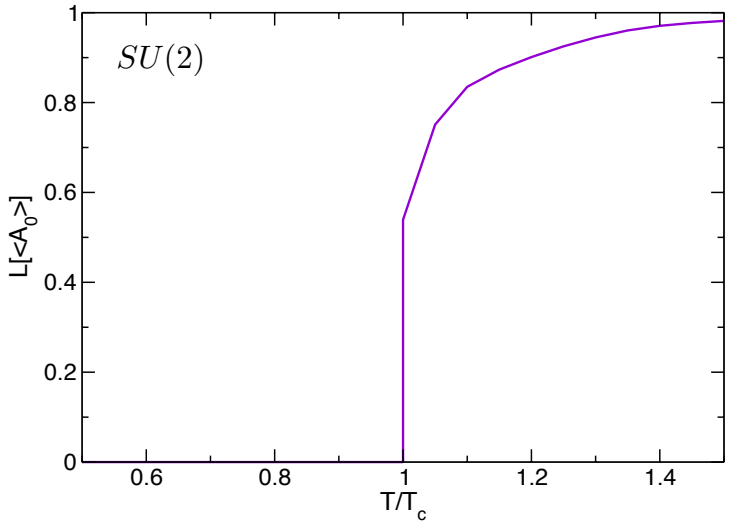

Figure 2.7: The $SU(2)$ Polyakov loop in Yang–Mills theory. The Polyakov loop was obtained from the minima of the Polyakov loop potential given in Fig. 2.6, where we show here only the temperature range around the phase transition.

In Fig. 2.6 we show the non-perturbative Polyakov loop potential for various temperatures for Yang–Mills theory. Low temperatures correspond to the lower curves, the IR regime, high temperatures to the upper curves, where it approaches its asymptotic form, the Weiss potential in the UV. In between the phase transition occurs. There the potential is flat. One can follow the continuous deformation by looking at the minima. The phase transition occurs, when both minima are together in the center. Fig. 2.7 shows the corresponding Polyakov loop around the critical temperature. Because we consider $SU(2)$ YM theory, the phase transition is of second order.

Chapter 3

The Functional Renormalisation Group

We want to deduce the physical behaviour of macroscopic objects such as hadrons from the interactions of fundamental microscopic degrees of freedom such as quarks and gluons. The key idea originates in the block-spin transformation of Kadanoff [34], where only the relevant information at a (momentum) scale is kept and transported to the next. Therefore consider a lattice of many spins and split them into smaller lattices, then average over the spins contained in the smaller lattices. One obtains again a lattice of spins, now the effective spins, which can again be split into sub-lattices and averaged over and so on. This means that starting at microscopic scales one step-wise approaches macroscopic scales, keeping only information that is relevant at the scale considered. This idea of integrating out degrees of freedom was adapted by Wegner and Houghton [35] and Wilson [36, 37], where they applied this to the Hamiltonian of the theory. So instead of integrating over all momenta at the same time one only integrates out one momentum shell after the other. Therefore one can include all fluctuations up to this scale and also carry only the relevant information to the next. Hence a large coupling strength does not cause problems. The concept was formulated in a functional approach by Wetterich [38] and this is the form we apply in this thesis. For reviews on the FRG see [31, 39–44]. In this chapter we follow the ideas of [39] in the derivation of the flow equation.

3.1 The effective action

A Quantum Field Theory (QFT) is uniquely defined by the set of all n-point correlation functions. These can be obtained by taking the variation of the generating functional $Z[J]$ with respect to the fields. The generating functional $Z[J]$ of a field $\varphi(x)$ in the path integral formulation, here in Euclidean space-time, is given by

$$Z[J] = \int \mathcal{D}\varphi \, e^{-S[J]+\int J\cdot\varphi} \tag{3.1}$$

where the integral is regularised in the UV with a cutoff Λ_{UV} and $S[\varphi]$ is the classical action and $J(x)$ the source. The n-point correlation functions determine the behaviour of the theory at any given point in space-time. The Schwinger functional $W[J]$ is the logarithm of $Z[J]$ and contains only the connected n-point correlation functions of the theory. A Legendre transform yields the effective action $\Gamma[\phi]$, the generating functional of all one particle irreductible correlation functions. The field $\phi(x) = \langle\varphi(x)\rangle_J$ stands for the classical field around which the quantum fields fluctuate, this means that all quantum fluctuations are included. The effective action reads

$$\Gamma[\phi] = \sup_J \left(\int J \cdot \phi - W[J] \right). \tag{3.2}$$

For any ϕ there exists a $J = J_{sup} = J[\phi]$ for which $\int J \cdot \phi - W[J]$ approaches its supremum. This definition of $\Gamma[\phi]$ guarantees that it is convex, i.e. the second derivative with respect to the field is positive, $\frac{\delta^2\Gamma}{\delta\phi^2} \equiv \Gamma^{(2)} \geq 0$. Note that Γ contains all quantum fluctuations, it's the quantum effective action. To obtain the quantum equation of motion, one has to take the variation of Γ with respect to the field $\phi(x)$, so $\frac{\delta\Gamma}{\delta\phi(x)} = J(x)$. The effective action is the starting point for the derivation of the one particle irreducible n-point correlation functions such as the propagator or the vertices to which we come back later.

3.2 The Wetterich equation

We can study how a theory, specified by the effective action Γ, behaves at a certain (momentum) scale. The interesting facets of a theory like QCD are not its static properties but its characteristics at changing scales. In the case of QCD it is the transition from the fundamental degrees of freedom, the quarks and gluons to the composite hadronic bound states. Therefore we need a technique that enables us to capture the transition when we 'zoom-out' of the considered theory and study it at various scales.

A QFT is described by the effective action $\Gamma[\phi]$ and can be expanded in terms of basis functionals $F_n[\phi]$ with coefficients g_n

$$\Gamma[\phi] = \sum_n g_n F_n[\phi]. \tag{3.3}$$

There are infinitely many coefficients g_n which are all orthogonal to each other and they constitute all possible couplings of a theory. The couplings themselves are not static but depend on (momentum) scale k. One can therefore imagine a space that is spanned by all infinitely many scale dependent couplings of a theory. One point in this space then describes an effective action at a certain scale. We can then imagine further that a line in this space corresponds to the change of the theory with respect to the momentum scale. We can draw a trajectory starting in the UV with the microscopic action, the bare action, to the IR where we recover the full quantum effective action, see Fig. 3.1.

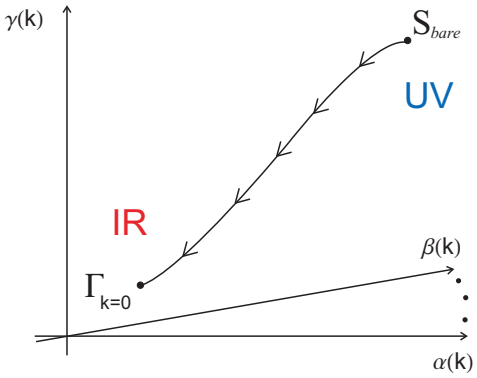

Figure 3.1: Example of a flow of a theory in theory space. Theory space is spanned by all (infinitely many) scale dependent couplings of a theory. In the UV the theory is described by the bare action, in the IR it is given by the full quantum effective action.

A language of describing QCD at all momentum scales is provided by the flow equation of the effective action describing the trajectory in theory space. This equation describes, how a theory, e.g. QCD, changes if one changes the momentum scale. The restrictions we impose on such an equation is that in the UV, where we start the flow, the bare action $S_{\rm bare}$ describes the microscopic physics, and in the IR we approach the full quantum action Γ

$$\Gamma_{k\to\Lambda_{UV}} \simeq S_{\rm bare}, \quad \Gamma_{k\to 0} = \Gamma. \tag{3.4}$$

Here we introduced the effective average action Γ_k it depends on the momentum scale k.

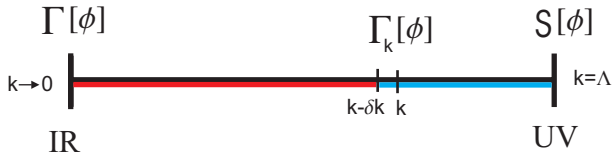

Figure 3.2: Γ_k interpolates between S at microscopic scales and $\Gamma[\phi]$ at macroscopic scales. The red regime is suppressed by the regulator.

To derive the flow equation we have to ensure that we only integrate out momentum modes that are higher than the momentum scale k, such that the underlying microscopic physics are decoupled from the macroscopic physics, see Fig. 3.2. For example in QCD the exact information about quark-gluon interactions in the UV is not relevant for IR QCD since the latter is governed by hadronic degrees of freedom. We only need to take the relevant information to the next scale. To ensure this, we need to introduce a regulator function into the path integral which cuts off the momentum modes below the scale k. Instead of integrating over the whole space (over all momentum modes) at once, like e.g. in perturbation theory, we only integrate out small momentum shells.

To derive the flow equation, first we consider the scale dependent generating functional Z_k[1]

$$Z_k[J] = \int \mathcal{D}\varphi \, e^{-S[\varphi]-\Delta S_k[\varphi]+\int J\varphi}, \tag{3.5}$$

where

$$\Delta S_k[\varphi] = \frac{1}{2}\int \frac{d^dq}{(2\pi)^d}\varphi(-q)R_k(q)\varphi(q) \tag{3.6}$$

is the regulator term that suppresses momenta lower than k and R_k is the regulator function and also the source now depends on momentum scale, compare with Eqn. (3.1). We can then perform a modified Legendre transformation and obtain the effective average action

$$\Gamma_k[\phi] = \sup_J \left(\int J\phi - W_k[J] \right) - \Delta S_k[\phi]. \tag{3.7}$$

The regulator function R_k must satisfy a number of criteria to guarantee that the constraints given in (3.4) are fulfilled. So R_k must ensure IR regularisation, meaning that the effective propagator which we define in the following remains finite at macroscopic scales, so that no divergencies occur. This means that

$$\lim_{q^2/k^2\to 0} R_k(q) > 0. \tag{3.8}$$

Second, R_k must vanish as k goes to zero, as the full quantum effective action must be obtained in the IR, hence

$$\lim_{k^2/q^2\to 0} R_k(q) = 0. \tag{3.9}$$

And last as k approaches the UV cutoff Λ_{UV}, the initial boundary condition, the classical field configurations and the bare action must be given. This means that the regulator term must vanish from the scale dependent generating functional (3.5), as the scale dependent effective action approaches with $k \to \Lambda_{\mathrm{UV}}$ the bare action S_{bare}. For this we need

$$R_k \to \infty \quad \text{for} \quad k \to \Lambda. \tag{3.10}$$

In the following we abbreviate the scale derivative $k\frac{d}{dk}$ with ∂_t so that $t = \ln \frac{k}{\Lambda_{UV}}$. Taking the scale derivative of Γ_k we find that $\partial_t\Gamma_k[\phi]$ is proportional to the integral over all momenta, the scale derivative of the regulator function $\partial_t R_k(q)$ and the full connected propagator. To work out what the full connected propagator is, we look at the modified equation of motion, including the regulator term, and we find that the regulator term changes the original equation of motion by an additional term proportional to the regulator function times the field ϕ

$$\frac{\delta\Gamma_k[\phi]}{\delta\phi(x)} = J(x) - (R_k\phi)(x). \tag{3.11}$$

Then the full propagator is the second variation of $\Gamma_k[\phi]$ with respect to the fields, which is then the original solution changed by an additional term proportional to the regulator

[1] In the following derivation we consider only scalar fields, see [31] for arbitrary fields.

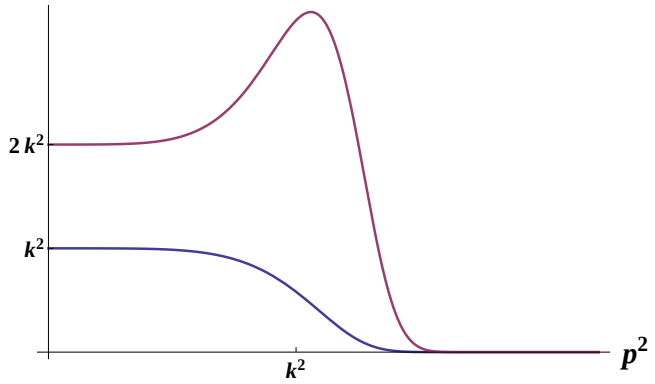

Figure 3.3: Example of a regulator function $R_k(p^2)$ (blue) and its scale derivative $\partial_t R_k(p^2)$ (red). The regulator shown here is $R_k(p^2) = p^2 \frac{(p^2/k^2)^{m-1}}{e^{(p^2/k^2)^m}-1}$.

function. This we can rearrange such that we can see immediately the full propagator, which is given by the variation of the field with respect to the source

$$\frac{\delta J(x)}{\delta \phi(y)} = \frac{\delta^2 \Gamma_k[\phi]}{\delta\phi(x)\delta\phi(y)} + R_k(x,y) \equiv \left(\Gamma_k^{(2)}[\phi] + R_k\right)(x,y). \tag{3.12}$$

An example of the regulator function and its scale derivative is shown in Fig. 3.3. It is peaked around $p^2 = k^2$, meaning that these are the important contributions weighted by $\partial_t R_k$ in the flow. Furthermore it has a finite value for $p^2/k^2 \to 0$ and it vanishes for $k^2/p^2 \to 0$ while for $k \to \Lambda_{\mathrm{UV}}$ the bare action is retrieved as both R_k and $\partial_t R_k$ vanish.

Eqn. (3.12) also leads to the following identity [2]

$$\mathbb{1} = (\Gamma_k^{(2)}[\phi] + R_k)(x,y) \cdot G_{k,c}^{(2)}(x,y). \tag{3.13}$$

Then we can take the scale derivative of the effective average action, see Eqn. (3.11), and insert the propagator given in Eqn. (3.12) and the identity of Eqn. (3.13) and obtain the flow equation for the effective average action, the Wetterich equation [38]

$$\partial_t \Gamma_k[\phi] = \frac{1}{2} \int \frac{d^d q}{(2\pi)^d}\, \partial_t R_k(q) \left(\Gamma_k^{(2)}[\phi] + R_k\right)^{-1}. \tag{3.14}$$

It can be rewritten in terms of operator traces such that its one-loop structure becomes clear

$$\partial_t \Gamma_k[\phi] = \frac{1}{2}\, \mathrm{STr} \frac{1}{\Gamma_k^{(2)}[\phi] + R_k} \partial_t R_k \tag{3.15}$$

We can also express it in terms of diagrams, where the propagator is represented by the line and the regulator insertion is symbolised with the crossed circle

[2] Remember that $\frac{\delta\phi(x)}{\delta J(y)} = \frac{\delta^2 W_k[J]}{\delta J(x)\delta J(y)} = G_{k,c}^{(2)}(x,y)$.

$\partial_t \Gamma_k[\phi] = \frac{1}{2}\,\mathrm{STr}$ 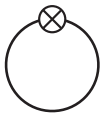

This is an exact equation which describes the complete QFT and solving the flow equation is equivalent to solving the path integral. However, all operators respecting the symmetry of the Lagrangian are generically included by quantum fluctuations and have therefore running couplings. This means that the Wetterich equation describes infinitely many coupled differential equations. Of course only few theories exist which can be solved exactly. For all other cases one must choose a subset of equations that includes all relevant physical information in a systematic way. This will be discussed in the next subsection. The solution to the Wetterich equation also corresponds to one trajectory in theory space. Using different regulator functions simply means that the trajectory is changed, however the initial and the final state, the bare action in the UV and the full quantum effective action in the IR do not change.

The one-loop form has great advantages, one 'only' has to calculate one-loop diagrams to obtain the flow equations of the scale dependent couplings of the theory, no further loops are required. But remember that all propagators and vertices are scale and momentum dependent, so this is already a challenge. The one-loop structure is a consequence of ΔS_k being quadratic in the field ϕ coupled to the source. It is also possible to recover perturbation theory if one expands Γ_k in a one-loop expansion

$$\Gamma_k = S + \hbar\,\Gamma_k^{\text{1-loop}} + \mathcal{O}(\hbar^2) \tag{3.16}$$

and sets $\Gamma_k^{(2)} = S^{(2)}$ such that the flow equation is

$$\partial_t \Gamma_k^{\text{1-loop}} = \frac{1}{2}\,\mathrm{STr}\,\left(\partial_t R_k (S^{(2)} + R_k)^{-1}\right). \tag{3.17}$$

The procedure to derive the flow equations is mostly straightforward, however subtleties like the Grassmanian nature of fermions can difficult the derivation. First, one chooses a suitable truncation, see Subsec. 3.2.1. Then one needs to determine all flow equations of the scale dependent quantities within the truncation, like couplings, wave function renormalisations, etc. The left hand side of the flow equation (3.15) is specified by the scale derivative of the theory, e.g. for QCD this is Eqn. (2.1) in a vertex expansion (3.21). Then one needs to project onto the desired coupling or wave function renormalisation by applying derivatives with respect to momenta, fields or projection operators. The same is done with the right hand side of the flow equation (3.15), where the derivatives act on the loops, e.g. a derivative with respect to a field adds an external leg to a diagram connected to the loop by a vertex. This means that taking two derivatives with respect to a field, one obtains a loop with two external legs. Equating the left hand side and the right hand side we find the flow equation.

In calculating the derivatives with respect to the fields, one needs to treat bosonic and fermionic fields differently due to the Grassmanian nature of the fermions. The general

description for taking a derivative is

$$\frac{\delta}{\delta\phi_c}G_{ab} = -\eta_a^c\, G_{ai}\, \eta_i^c\, \Gamma_{cij}\, \eta_{jk}\, G_{kb} + \eta_a^c\, G_{ab}\, \eta_a^c \frac{\delta}{\delta\phi_c}, \tag{3.18}$$

where a 'metric' appears every time two fields are commuted, which accounts for minus signs appearing when two fermions are interchanged. The 'metric' is given by

$$(\eta_b^a)_{ij} = (-1)^{ab}\delta_{ij}, \tag{3.19}$$

where a and b stand for the fermion number. If a and b are fermionic fields, η is equal to -1, and if both or one of them is bosonic, η is equal to 1. Then we only need to take care when we commute a field or a derivative through a vertex

$$\frac{\delta}{\delta\phi_c}\Gamma_{a_1\ldots a_n} = \Gamma_{ca_1\ldots a_n} + \Gamma_{a_1\ldots a_n}\left(\prod_{i=1}^{n}\eta_{a_i}^c\right)\frac{\delta}{\delta\phi_c}. \tag{3.20}$$

3.2.1 Truncation

Eqn. (3.15) describes infinitely many coupled partial differential equations, which means that apart from some special cases, there is no exact solution. One therefore has to find a systematic non-perturbative approximation. One way to do this is to restrict the space of operators to a finite dimensional subspace. This is called the method of truncations. Therefore the truncation should capture all relevant physical information about the considered system. There are several ways to choose a sensible truncation, however there are next to no ways to prove that the neglected equations give only small errors. It is therefore of great importance to compare objects such as the propagators with other methods. E.g. in QCD it is sensible to compare the thermodynamics and propagators at imaginary and vanishing chemical potential with lattice QCD studies. One can then estimate the quality of the truncation and perform calculations at real chemical potential, where lattice QCD cannot be applied. It would be very beneficial to compare results obtained from two different truncations, however this is in most cases very time consuming. The guideline of a truncation should be that it is chosen in a systematic and physically sensible way where one incorporates the general information one has about the relevant interactions.

One example of a truncation is the vertex expansion, which we also utilise in this thesis. In this case one expands the scale dependent effective action in powers of the fields

$$\Gamma_k[\phi] = \sum_{n=0}^{\infty}\frac{1}{n!}\int d^dx_1\ldots d^dx_n\,\Gamma_k^{(n)}(x_1,\ldots,x_n)\,\phi(x_1)\ldots\phi(x_n). \tag{3.21}$$

where the expansion coefficients $\Gamma_k^{(n)}$ are the full vertices.

Another example is the operator or derivative expansion, where one expands in powers of the derivative of the fields, i.e. their mass dimension. E.g. if we have a scalar field theory we obtain

$$\Gamma_k[\phi] = \int d^dx\left\{U_k(\phi) + \frac{1}{2}Z_k(\phi)\,(\partial_\mu\phi)^2 + \mathcal{O}\left((\partial_\mu\phi)^4\right)\right\}, \tag{3.22}$$

where the first term gives the effective potential $U_k(\phi)$. All terms which do not vanish for constant fields are included in the effective potential. The coefficient of the second term is the scale dependent wave function renormalisation.

3.3 Dyson–Schwinger equations

Here we briefly introduce the Dyson–Schwinger equations (DSE), as some results for the Yang–Mills propagators we utilise later on were obtained with a combination of FRG and DSE equations. The DSE are the equations of motion of the Greens functions of a theory. They are also exact and are derived from

$$e^{-\Gamma[\phi]} = \int \mathcal{D}\varphi \, e^{(-S[\phi+\varphi])+\int \frac{\delta\Gamma[\phi]}{\delta\phi}\varphi}, \tag{3.23}$$

where we used that the expectation value of φ vanishes and that the measure is translational invariant. Now we can take a derivative with respect to ϕ so that we find

$$\frac{\delta\Gamma}{\delta\phi} = \left\langle \frac{\delta S}{\delta\varphi} \right\rangle. \tag{3.24}$$

These are the Dyson–Schwinger equations. Further derivatives amount to an infinite tower of coupled integro-differential equations for the vertices. Like the Wetterich equation, the DSE describe physics at all scales and hence are a non-perturbative way of solving the path integral. However finding a suitable truncation, especially a closed set of equations that captures all relevant physical information proves more difficult than with the FRG approach as they also contain more than one-loop diagrams which additionally difficults the derivations. For a review on the DSE see e.g. [148].

3.4 Dynamical hadronisation

In QCD, the microscopic degrees of freedom are distinctively different from the macroscopic degrees of freedom. In the UV they are given by the quarks and gluons whereas in the IR these are the hadrons. The bound state formation occurs due to the strong interaction of the quarks induced by the gluons. The transition happens smoothly when changing the momentum scale. Therefore it is not sensible to use a description in terms of quarks and gluons when looking at IR scales or a description in terms of hadrons when considering microscopic physics. We can incorporate the transition to hadrons naturally by using rebosonisation or also called dynamical hadronisation [27–33]. It has been successfully applied in e.g. [28, 29, 50, 68, 89].

3.4.1 Partial bosonisation

To explain partial bosonisation, we follow the line of arguments of Ref. [39]. The bosons we are considering in the following are mesons and hence built from quark–anti-quark pairs. Therefore we need to find a transformation description that tells us how to transform two

fermions into a boson. This is achieved by applying a Hubbard–Stratonovich transformation [128, 129], where in the case of QCD the mass of the meson is related to the Yukawa coupling and the four-fermion interaction of the quarks. The four-fermion interactions are created by exchange of gluons at the leading one loop order

$$\int_x \frac{\lambda_\psi}{2}\left[(\bar{\psi}\psi)^2 + (\bar{\psi}i\gamma_5\vec{\tau}\psi)^2\right], \tag{3.25}$$

where the four-fermion coupling is proportional to α_s^2, see the last diagram in Fig. 3.4. The two terms in Eqn. (3.25) have the same quantum numbers as the sigma-meson and the pions. So in principle we can write down a mixed fermionic-bosonic action by introducing a scalar field interacting with the quarks through a Yukawa coupling and including in the original purely fermionic action an four-quark interaction term. The translation amounts to

$$\int_x \frac{\lambda_\psi}{2}\left[(\bar{\psi}\psi)^2 + (\bar{\psi}i\gamma_5\vec{\tau}\psi)^2\right] = \int_x \frac{m_\sigma^2}{2}\left(\phi^2\right) + \int_x ih\left(\bar{\psi}(\tau\cdot\phi)\psi\right), \tag{3.26}$$

where $\tau\cdot\phi = \sigma + i\gamma_5\vec{\tau}\vec{\pi}$ and $\phi = (\sigma, \vec{\pi})$ and the τ^j are the Pauli matrices, see App. A.2. The Hubbard–Stratonovich transformation then relates the mass of the scalar field to the Yukawa and the four-fermion coupling

$$\lambda_\psi = \frac{h^2}{m_\sigma^2}. \tag{3.27}$$

For a four-fermion coupling λ_ψ greater than the critical coupling $\lambda_{\psi,\mathrm{cr}}$, the effective potential of the bosons acquires a non-zero minimum with a non-vanishing vacuum expectation value for the scalar field $\langle\phi\rangle$. One can then relate $\langle\phi\rangle$ again to a description in terms of fermions so that it is proportional to the chiral condensate $\langle\bar{\psi}\psi\rangle$

$$\sigma = -\frac{ih}{m_\sigma^2}\bar{\psi}\psi \quad \text{and} \quad \pi = \frac{h}{m_\sigma^2}\bar{\psi}\gamma_5\tau\psi. \tag{3.28}$$

A non-vanishing expectation value for $\langle\bar{\psi}\psi\rangle$ means that the chiral symmetry is broken and a fermion mass is dynamically generated $m_\psi \sim h\langle\phi\rangle$. For $\lambda_\psi < \lambda_{\psi,\mathrm{cr}}$ the vacuum expectation value of the bosonic field is zero $\langle\phi\rangle = 0$ and there is no generation of fermion mass and hence no spontaneous breaking of chiral symmetry.

QCD does not contain four-fermion self-interactions at a microscopic level as it is perturbatively non-renormalisable and hence $\lambda_\psi|_{k=\Lambda} = 0$, however contributions to the flow of λ_ψ are created through gluon exchange between the quarks, so that a flow of the four-fermion coupling is generated, see Fig. 3.4 for the diagrams. As in our case only the last diagram of Fig. 3.4 contributes, the scale beyond which chiral symmetry breaking sets in is controlled by the strength of the strong coupling α_s. After performing the Hubbard–Stratonovich transformation at the scale k, our microscopic degrees of freedom are transformed into macroscopic degrees of freedom and all λ_ψ interactions are transformed to Yukawa interactions. Unfortunately, performing the next RG step, new gluon-induced quark interactions are produced which cannot be neglected. One has to apply the bosonisation at each RG step to obtain consistent solutions, this means that we have to bosonise the theory on all scales, this is called rebosonisation.

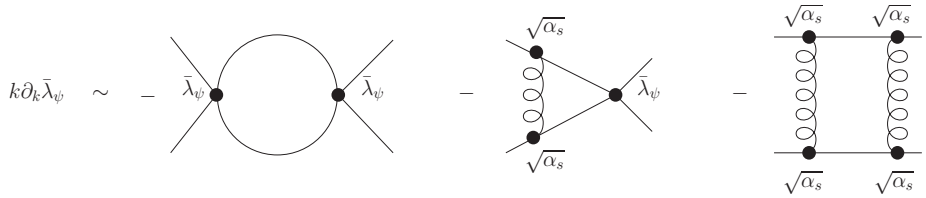

Figure 3.4: Contributions to the flow of the four-fermion coupling $\partial_t\lambda_\psi$. All diagrams but the last, the box diagrams, do not contribute for $\lambda_\psi = 0$, however they are generated during the flow.

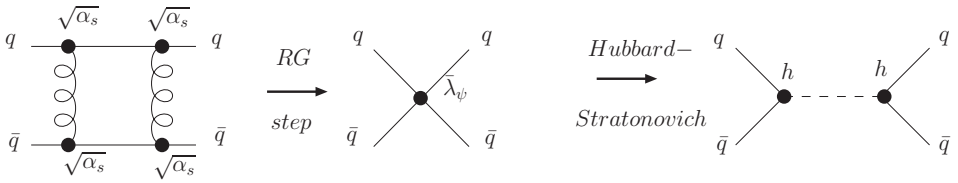

Figure 3.5: Bosonisation. The fundamental interactions generate these box-digram contributions which contribute to the flow of the four-fermion coupling. The first arrow symbolises one RG step, i.e. 'zooming out'. Then the Hubbard–Stratonovich transformation is performed, where the contribution from the four-fermion coupling is transformed to an exchange of a scalar coupled via two Yukawa-type interactions to the fermions.

3.4.2 Rebosonisation

A way to resolve our problem that contributions proportional to $\partial_t\lambda_k$ are generated, is to introduce a scale dependence for the bosonising field which is a scalar boson. Its flow can in principle depend on all fields of the system. What we want in the end is the flow of the effective average action depending on the new scale dependent field, but evaluated such that further field dependencies are suppressed (which we denote here with $|_\phi$)

$$\partial_t\Gamma_k[\phi]\big|_\phi, \tag{3.29}$$

where the rebosonised field is $\hat{\phi}_k[\hat{\varphi}]$ and we have $\phi = \langle\hat{\phi}_k\rangle$. Later on we want a description in terms of a scalar σ and a pseudo-scalar field $\vec{\pi}$ where $\phi = (\sigma, \vec{\pi})$. The generating functional is then given by

$$e^{-\Gamma_k[\phi]} = \int \mathcal{D}\hat{\varphi}\, e^{-S[\hat{\varphi},\hat{\bar{\psi}},\hat{\psi}]-\Delta S_k[\hat{\phi}_k,\hat{\bar{\psi}},\hat{\psi}]+\frac{\delta(\Gamma_k+\Delta S_k)}{\delta\phi}(\hat{\phi}_k-\phi)+\Delta S_k[\phi]}, \tag{3.30}$$

where we integrate over the field $\hat{\varphi}$ and include the source J and the regulator term $\Delta S_k[\phi]$

$$J = \frac{\delta\left(\Gamma_k + \Delta S_k\right)}{\delta\phi} \qquad \text{and} \qquad \Delta S_k[\phi] = \frac{1}{2}\phi\hat{R}_k\phi. \tag{3.31}$$

Lets have a closer look at Eqn. (3.30). The last term on the rhs is the regulator term which actually stems from the lhs, depending only on ϕ. The first term on the rhs is the standard

action depending on the field of integration and all other scale dependent fields. The second term on the rhs is the standard regulator term matching the action. In the third term we coupled the regulator to the scale dependent fields and the fourth term is simply the source term which also couples to scale dependent fields. In the end we want a description in terms of the σ and the $\vec{\pi}$ fields and we know that $\phi = (\sigma, \vec{\pi})$, hence the flow of the field $\hat{\phi}_k$ can be expressed in terms of the fields $\bar{\psi}\psi$ and $\hat{\phi}_k$, with some functions $\dot{A}_k$ and $\dot{B}_k$ which we still need to determine

$$\dot{\hat{\phi}}_k = \dot{B}_k \hat{\phi}_k + \dot{A}_k \bar{\psi}\psi. \tag{3.32}$$

In the last term only the expectation values $\psi = \langle\hat{\psi}\rangle$ and $\bar{\psi} = \langle\hat{\bar{\psi}}\rangle$ appear. The field $\hat{\phi}_k$ depends on $\hat{\varphi}$: $\hat{\phi}_k = \hat{\phi}_k[\hat{\varphi}]$ with the initial condition that $\hat{\phi}_{\Lambda_{UV}} = \hat{\varphi}$ at the UV scale Λ_{UV}. Now we can derive the scale derivative of the effective average action

$$\frac{\partial}{\partial t}\Big|_\phi \Gamma_k[\phi] = \frac{1}{2}\dot{\hat{R}}_k \langle\hat{\phi}_k^2\rangle + \hat{R}_k \langle\dot{\hat{\phi}}_k \hat{\phi}_k\rangle - \frac{\delta\Gamma}{\delta\phi}\langle\dot{\hat{\phi}}_k\rangle - \frac{\delta\Delta S_k[\phi]}{\delta\phi}\langle\dot{\hat{\phi}}_k\rangle - \partial_t \Delta S[\phi], \tag{3.33}$$

where the first and the second term are the standard flow and the third and fourth term stems from Eqn. (3.31). The last term is obtained from the lhs. Now we use the full propagator given by $\hat{G}_k = \left[\frac{\delta^2\Gamma}{\delta\phi^2} + \hat{R}_k\right]^{-1}$ and we define

$$\langle\dot{\hat{\phi}}_k\rangle \equiv \dot{\phi}_k, \tag{3.34}$$

which is motivated by the relation that $\phi = \langle\hat{\phi}_k\rangle$ and the scale derivative of the expectation value of $\dot{\hat{\phi}}_k$ which is

$$\begin{aligned} \langle\dot{\hat{\phi}}_k\rangle &= \dot{B}_k \langle\hat{\phi}_k\rangle + \dot{A}_k \bar{\psi}\psi \\ &= \dot{B}_k \phi_k + \dot{A}_k \bar{\psi}\psi \\ &\equiv \dot{\phi}_k. \end{aligned} \tag{3.35}$$

We also make use of

$$\begin{aligned} \langle\dot{\hat{\phi}}_k \hat{R}_k \hat{\phi}_k\rangle &= \left(\hat{G}\frac{\delta}{\delta\phi}\Big|_\psi + \phi\right)\hat{R}_k\langle\dot{\hat{\phi}}_k\rangle \\ &= \left(\hat{G}\frac{\delta}{\delta\phi}\Big|_\psi + \phi\right)\hat{R}_k\dot{\phi}_k \\ &= \hat{G}\hat{R}_k\dot{B}_k + \phi\hat{R}_k\dot{\phi}_k, \end{aligned} \tag{3.36}$$

where we can remove one field from the expectation value by employing

$$\langle\varphi_1 \dots \varphi_n\rangle_J = \left(\frac{\delta}{\delta J_1} + \phi_1\right)\langle\varphi_2 \dots \varphi_n\rangle_J \tag{3.37}$$

and we use that a variation with respect to the source J is given by the propagator and a variation with respect to the field ϕ, $\frac{\delta}{\delta J} = G\frac{\delta}{\delta\phi}$. The last term of Eqn. (3.36) cancels the

term $-\phi\hat{R}_k\dot{\phi}_k$ appearing in the flow of the effective action. Then we find for the rebosonised flow

$$\frac{\partial}{\partial t}\Big|_\phi \Gamma_k[\phi] = \frac{1}{2}\dot{\hat{R}}_k\left(\hat{G}_k + \phi^2\right) + \hat{R}_k\left\langle(\dot{B}_k\hat{\phi}_k + \dot{A}_k\bar{\psi}\psi)\hat{\phi}_k\right\rangle - \frac{\delta\Gamma}{\delta\phi}\left(\dot{B}_k\phi + \dot{A}_k\bar{\psi}\psi\right) \quad (3.38)$$

$$-\hat{R}_k\phi\left(\dot{B}_k\phi + \dot{A}_k\bar{\psi}\psi\right) - \frac{1}{2}\dot{\hat{R}}_k\phi^2, \quad (3.39)$$

which can be simplified by using the relations above to

$$\frac{\partial}{\partial t}\Big|_\phi \Gamma_k[\phi] = \frac{1}{2}\left(\dot{\hat{R}}_k + 2\hat{R}_k\dot{B}_k\right)\hat{G}_k - \frac{\delta\Gamma}{\delta\phi}\left(\dot{B}_k\phi + \dot{A}_k\bar{\psi}\psi\right). \quad (3.40)$$

Because we want to adapt the non-rebosonised flow equations, Eqn. (3.40) tells us how we have to change them. In detail this means that we have to modify the regulator terms of the scalar part of our flows, i.e. we have to translate $\eta_\phi \to \eta_\phi - 2\dot{B}_k(p)$ so that the standard scale derivative of the scalar regulator appearing on the rhs of the flow equation receives an additional contribution. Indeed, the additional term proportional to $\dot{B}_k(p)$ is very small as it is multiplied with R_k and hence suppressed in the flow. However, neglecting the latter could cause errors and it is not expensive to include it. Eqn. (3.40) also tells us that we have to add the last term to receive the rebosonised equations. An example is given in Sec. 4.3, where we study QCD at vanishing temperature and vanishing chemical potential in a vertex expansion up to third order utilising rebosonisation. The results are given in Sec. 6.1.

Chapter 4

Setting the stage

In this chapter we explain our approximation to QCD using RG techniques. It contains all technical details specific to our setup. The results are presented in the following chapters.

4.1 Truncation

In the following sections we derive the propagators, regulators, vertices and the flow equations for the couplings and anomalous dimensions within a FRG truncation. We use a vertex-expansion in the matter sector and include vertices up to order three. In the gauge sector we also apply a vertex expansion but up to fourth order and we work in Landau gauge.

The two flavour $N_f = 2$ QCD effective average action for 4-dimensional Euclidean space-time with three colours $N_c = 3$ at finite temperature T and quark chemical potential μ in our truncation is

$$\begin{aligned}\Gamma_k &= \int d^4x \left\{\frac{1}{4}F^a_{\mu\nu}F^a_{\mu\nu}\right\} + \int d^4x \Bigg\{ Z_\psi\, \bar\psi \left(i\not{D} + i\frac{m_\psi}{Z_\psi} + i\mu\gamma_0 \right)\psi + ih\left(\bar\psi(\tau\cdot\Phi)\psi\right) \\ &\qquad + \frac{\lambda_\psi}{2}\left[(\bar\psi\psi)^2 - (\bar\psi\gamma_5\vec\tau\psi)^2\right] + \frac{1}{2}Z_\sigma(\partial_\mu\Phi)^2 + U(\Phi^2)\Bigg\}. \end{aligned} \tag{4.1}$$

We include mesonic degrees of freedom through the scalar field $\Phi = (\sigma, \vec\pi)^T$. It contains the sigma-meson σ and the three pion fields π^j. In the effective average action we have used the short hand notation for

$$\tau\cdot\Phi = \sigma + i\gamma_5\vec\tau\vec\pi, \tag{4.2}$$

where the τ^j are the Pauli matrices, see App. A.2. Here, the Dirac operator in momentum space and the field strength tensor are

$$i\not{D} = \gamma_\mu(p_\mu + gA^a_\mu t^a) \tag{4.3}$$

$$F^a_{\mu\nu} = \partial_\mu A^a_\nu - \partial_\nu A^a_\mu + g f^{abc} A^b_\mu A^c_\nu. \tag{4.4}$$

Furthermore we include an effective potential for the scalar field $U(\Phi^2)$ from which we derive the order parameter for the chiral phase transition, the minimum of the effective potential

σ_0. The matter sector also contains a kinetic term with a wave function renormalisation for the scalar field Z_σ. We couple the quark fields ψ and $\bar{\psi}$ to the mesons through a Yukawa coupling h and include a four-fermion interaction term which we utilise later when applying the rebosonisation technique. Note that at the UV scale, λ_ψ and h vanish[1]. The quark fields themselves couple through the strong coupling $g = \sqrt{4\pi\alpha_s}$ to the gluons, the gauge fields. We also incorporate a non-vanishing quark chemical potential μ. The glue dynamics are captured in the first term of the effective average action which includes also the ghost fields which are obtained after using the Faddeev–Popov method in deriving the gauge field propagators, see Subsec. 4.2.2.

Given the diagrammatic expression of the Wetterich equation (3.2), we can now express our truncation (4.1) in terms of 1-loop digrams containing the full propagators, see Fig. 4.1. The first two loops make up the glue sector, the last two the matter sector. In principle, one can study the two sectors separately, which is done in model calculations for the pure matter sector for small temperatures and larger chemical potentials. Cutting off the matter sector, one is left with pure Yang–Mills theory (only gluon and ghost degrees of freedom, so a pure $SU(3)$ gauge theory) which has been studied thoroughly on the lattice and with the RG. This plays the dominant role at vanishing chemical potential, however, already the coupling of the quarks to the gluons via the vacuum polarisation of the gluon and its feedback to the full glue sector changes characteristics such as the critical temperature of the phase transition. The full coupling of the matter sector to the glue sector plays also a significant role at non-zero chemical potential.

Here we couple both sectors such that each propagator feeds-back either directly, like the quark to the gluon, or indirectly, like the quark to the ghost, see Fig. 4.1. The type of back-coupling is only determined through the allowed interactions, i.e. there is no 3-point quark–ghost interaction but there is a 3-point quark–gluon and a 3-point ghost–gluon interaction. This becomes more clear when we derive the propagators and show the connection, see Figs. 4.3 and 4.6. We want to emphasise that it is important to include the back-coupling of the two sectors as it changes the propagators and hence determines the scale of the phase transition and the strength of the coupling α_s. Also the temperature scale of the effective potential of the glue sector is changed, see Sec. 6.3.

The effective potential of the matter sector in our truncation is given by

$$U(\Phi^2) = \frac{m_\sigma^2}{2}\left(\Phi^2 - \sigma_0^2\right) + \frac{\lambda_\sigma}{8}\left(\Phi^2 - \sigma_0^2\right)^2, \tag{4.5}$$

where we use a Taylor expansion up to fourth order in the fields Φ. The potential includes a scalar coupling λ_σ and a scale dependent mass m_σ. σ_0 stands for the minimum of the effective potential and vanishes in the symmetric phase. The general form of the potential in the symmetric and the broken phase are given in Fig. 2.2. The masses for the scalar fields are

[1]Indeed our initial conditions have non-vanishing but very small values for the Yukawa coupling and the four-fermion coupling for numerical reasons, see App. C.3.

Figure 4.1: Diagrammatic representation of the flow of Eqn. (4.1). The flow contains a glue part (first two loops), the full gluon and the full ghost propagators, and a matter part (the last two loops), the quark and the meson propagators. The circle with the cross denotes the flow of the regulator, which ensures that modes below the momentum scale k are cut off. The system is highly coupled as fluctuations feed back into each other. In the following section this is shown explicitly.

then given by the eigenvalues of the second derivative matrix of the potential. It is useful to write down the potential in the symmetric and the broken phase separately for the derivation of the masses

$$U_{\mathrm{sym}}(\Phi^2) = \frac{m_\sigma^2}{2}\Phi^2 + \frac{\lambda_\sigma}{8}\Phi^4 \tag{4.6}$$

$$U_{\mathrm{bro}}(\Phi^2) = \frac{\lambda_\sigma}{8}(\Phi^2 - \sigma_0^2)^2, \tag{4.7}$$

where we can now read-off the pion and the sigma masses in the symmetric phase

$$M_\pi^2 = 2\frac{\partial U_{\mathrm{sym}}}{\partial \Phi^2}\big|_{\Phi^2=0} = m_\sigma^2 \tag{4.8}$$

$$M_\sigma^2 = (\frac{\partial U_{\mathrm{sym}}}{\partial \Phi^2} + 4\Phi^2\frac{\partial^2 U_{\mathrm{sym}}}{\partial \Phi^2 \partial \Phi^2})\big|_{\Phi^2=0} = m_\sigma^2, \tag{4.9}$$

from symmetry arguments it is clear that the masses for the scalars are degenerate in the symmetric phase as the symmetry has not been broken. In the broken phase the masses are no longer degenerate as the radial and the tangential direction are no longer symmetric to each other and we find for the chiral limit

$$M_\pi^2 = 2\frac{\partial U_{\mathrm{bro}}}{\partial \Phi^2}\big|_{\Phi^2=\sigma_0^2} = 0 \tag{4.10}$$

$$M_\sigma^2 = (\frac{\partial U_{\mathrm{bro}}}{\partial \Phi^2} + 4\Phi^2\frac{\partial^2 U_{\mathrm{bro}}}{\partial \Phi^2 \partial \Phi^2})\big|_{\Phi^2=\sigma_0^2} = \lambda_\sigma \sigma_0^2. \tag{4.11}$$

The quark masses obtain a dynamical mass through the Yukawa interactions, so that in the chirally broken phase the total mass is given by the sum of the Higgs and the dynamical mass. Due to chiral symmetry breaking the sigma obtains a mass. In the chiral limit, i.e. for vanishing quark mass m_ψ, the pions are massless. In summary we find the following masses for the matter sector within our truncation of QCD

symmetric	broken
$M_\psi^2 = m_\psi^2$	$M_\psi^2 = (m_\psi + \sigma_0 h)^2$
$M_\sigma^2 = m_\sigma^2$	$M_\sigma^2 = \lambda_\sigma \sigma_0^2$
$M_\pi^2 = m_\sigma^2$	$M_\pi^2 = 0.$

For practical use we introduce dimensionless and RG invariant quantities, which are denoted with a bar (except for κ)

$$\kappa = \frac{\sigma_0^2 Z_\sigma}{2k^2}, \quad \bar{m}^2 = \frac{m^2}{Zk^2}, \quad \bar{h}^2 = \frac{h^2}{Z_\sigma Z_\psi^2}, \quad \bar{\lambda}_\sigma = \frac{\lambda_\sigma}{Z_\sigma^2}, \quad \bar{\lambda}_\psi = \frac{\lambda_\psi}{Z_\psi^2} k^2, \quad \bar{T} = \frac{T}{k}, \quad \bar{\mu} = \frac{\mu}{k}, \tag{4.12}$$

where the corresponding wave function renormalisations for the masses have to be chosen accordingly. We use this notation in the flow equations.

4.2 Propagators, regulators, vertices and other tools

Now we derive the tools we need to find the flow of the couplings and wave function renormalisations, that is we need the two- and three-point correlation functions, i.e. the propagators and vertices.

As shown in section 3.2, the propagator $G_k[\phi]$ is a matrix depending on all fields specified in the effective average action

$$G_k[\phi] = \left(\Gamma_k^{(2)}[\phi] + R_k\right)^{-1}, \tag{4.13}$$

where the explicit expression of $\Gamma_k^{(2)}$ – and of course also the corresponding regulator – depends on the fields. We do not need to calculate all entries of G_k, as we set the remaining fields after two field derivatives to zero. Only the quark–anti-quark, the gluon and the ghost propagator are left over and all other 'mixed' propagators vanish as they do not reflect our particle spectrum. In the following we determine the quark–anti-quark propagator $G_{\psi\bar{\psi}}$ and the gluon and ghost propagators G_{AA} and $G_{c\bar{c}}$.

4.2.1 The quark propagator and the quark-gluon vertex

The quark propagator

For the propagator of the quarks we only need to know the second derivative of the effective action with respect to $\bar{\psi}$ and ψ and the regulator function we wish to use. The quarks carry flavour, spinor and colour degrees of freedom, but are diagonal in colour space and are given in the fundamental representation.

First, we need to determine $\Gamma^{(2)}_{\psi\bar{\psi},k}$, which is directly determined from the effective action (4.1)

$$\Gamma^{(2)}_{\psi\bar{\psi},k} = \frac{\delta^2\Gamma_k}{\delta\psi^g_{j\beta}\delta\bar{\psi}^f_{i\alpha}} = \left[Z^{\perp}_{\psi}(\not{q})_{\alpha\beta} + i\,m_\psi\delta_{\alpha\beta} + i\,\mu(\gamma_0)_{\alpha\beta}\right]\delta_{ij}\delta_{fg} + ih\,(\tau\cdot\Phi)^{fg}_{\alpha\beta}\,\delta_{ij}, \tag{4.14}$$

where i, j are the group indices (colour), f, g are the flavour indices and the greek letters stand for the spinor degrees of freedom. Here we can also distinguish between the momentum components parallel and perpendicular to the heat bath, if we introduce the four momentum

$$q_\mu = \left(\frac{Z^{\parallel}_{\psi}}{Z^{\perp}_{\psi}}q_0, \vec{q}\right). \tag{4.15}$$

For vanishing temperature and chemical potential, there is no heat bath, so $Z^{\parallel}_{\psi} = Z^{\perp}_{\psi} = Z_\psi$, and this is also reflected in the four momentum.

Then we have to choose the regulator $R_{\psi\bar{\psi}}$. Within the restrictions of R_k given in Eqns. (3.8)-(3.10), it is up to our liking to choose it such that it simplifies our numerics. There are several ways to implement the regulator function: non-zero temperature and also non-zero chemical potential break the $O(4)$ symmetry, in this case the calculations simplify when using a regulator function that also distinguishes between the zero component and the vector component of the momentum. Likewise for vanishing temperature and also vanishing chemical potential it seems wise to implement a $4d$ regulator, respecting the $O(4)$ symmetry. Note that vanishing temperature but non-vanishing chemical potential also breaks the $O(4)$ symmetry, there it is not so clear what the smartest choice of a regulator function is.

At non-zero temperature and chemical potential we use a $3d$ regulator

$$R^{3d}_{\psi\bar{\psi}}(\vec{q}) = Z^{\perp}_{\psi}(\not{\vec{q}})_{\alpha\beta}\; r_\psi\left(\frac{\vec{q}^2}{k^2}\right)\delta_{fg}\delta_{ij} \tag{4.16}$$

and hence the scale derivative is

$$\partial_t R^{3d}_{\psi\bar{\psi}}(\vec{q}) = Z^{\perp}_{\psi}(\not{\vec{q}})_{\alpha\beta}\left(\partial_t r_\psi - \eta^{\perp}_{\psi} r_\psi\right)\delta_{fg}\delta_{ij}. \tag{4.17}$$

From now on we drop the flavour and colour indices except where needed for an improved readability. One can again choose the shape function r_ψ such that it suits best the calculations. It determines the rapidity, i.e. the shape of the cutoff function, of the momentum modes. In some cases it is convenient to implement an exponential cutoff, as it falls off very quickly, sometimes it is more beneficial to use an optimised regulator as it amounts to the shortest path in theory space [149]. We chose the optimised regulator with

$$r_\psi(x) = \left(\frac{1}{\sqrt{x}} - 1\right)\theta(1-x), \tag{4.18}$$

where $x = \vec{q}^2/k^2$ and we find for the scale derivative

$$\partial_t r_\psi(x) = \frac{1}{\sqrt{x}}\theta(1-x). \tag{4.19}$$

Then we add both, $\Gamma^{(2)}$ and R_k and invert them to obtain the propagator $G_{\psi\bar{\psi}}$. In doing so we want to keep all dependence on the γ-matrices in the numerator (remember that we have to take the trace later on in the flow equation). We then find for the $3d$ propagator

$$\begin{aligned} G^{3d}_{\psi\bar{\psi}} &= \left(Z^{\parallel}_{\psi}\gamma_0(q_0+i\mu) + Z^{\perp}_{\psi}\not{\vec{q}}(1+r_\psi) + iM_{\psi,k}\right)\cdot \\ &\quad \left[(Z^{\parallel}_{\psi})^2(q_0+i\mu)^2 + (Z^{\perp}_{\psi})^2\vec{q}^2(1+r_\psi)^2 + M^2_{\psi,k}\right]^{-1}. \end{aligned} \tag{4.20}$$

The $4d$ regulator and its scale derivative we implement at vanishing temperature and non-vanishing chemical potential are

$$R^{4d}_{\psi\bar{\psi}}(q) = Z^{\perp}_{\psi}\not{q}\, r_\psi\left(\frac{q^2}{k^2}\right), \tag{4.21}$$

$$\partial_t R^{4d}_{\psi\bar{\psi}} = Z^{\perp}_{\psi}\not{q}\left(\partial_t r_\psi - \eta^{\perp}_{\psi} r_\psi\right), \tag{4.22}$$

and the resulting propagator is

$$\begin{aligned} G^{4d}_{\psi\bar{\psi}} &= \left(Z^{\perp}_{\psi}\not{\vec{q}}(1+r_\psi) + Z^{\parallel}_{\psi}\gamma_0 i\mu - iM_{\psi,k}\right)\cdot \\ &\quad \left[(Z^{\parallel}_{\psi})^2(q_0(1+r_\psi)+i\mu)^2 + (Z^{\perp}_{\psi})^2\vec{q}^2(1+r_\psi)^2 + M^2_{\psi,k}\right]^{-1}. \end{aligned} \tag{4.23}$$

Note that there are different ways of including the chemical potential in the regulator, see App. C.1 for more details.

Also at non-zero temperature and chemical potential it can be of advantage to implement a $4d$ regulator, see e.g. [150, 151]. As a $4d$ exponential regulator falls off very quickly and hence can simplify full momentum dependent numerical computations drastically. In general, $\Gamma^{(2)}_{\psi\bar{\psi}}$ obtains flow contributions from the glue sector of QCD, where the ghost contributions enter through the gluon propagator, see Fig. 4.2. In the next subsection we discuss the gauge field propagators. The flow of $\Gamma^{(2)}_{\psi\bar{\psi}}$ is important as it is directly related to the anomalous dimension η_ψ which is given by

$$\eta_\psi = -\frac{\partial_t Z_\psi}{Z_\psi}, \tag{4.24}$$

which, of course, can be parallel or perpendicular to the heat bath. The full flow of $\Gamma^{(2)}_{\psi\bar{\psi}}$ in our truncation is given by Fig. 4.2, although we did not compute if with the full momentum dependence.

The quark-gluon vertex

For the quark-gluon interactions we include a simple ansatz for the vertex, the quark-gluon vertex. It can be determined straight forward from the effective action

$$\Gamma^{(3)}_{A\psi\bar{\psi}} = \frac{\delta^3\Gamma_k}{\delta A^a_\mu \delta\psi^g_{j\beta}\delta\bar{\psi}^f_{i\alpha}} = +g\, Z_A^{1/2}\,(t^a)_{ij}\begin{pmatrix} Z^{\parallel}_{\psi}\gamma_0 \\ Z^{\perp}_{\psi}\vec{\gamma}\end{pmatrix}_{\alpha\beta}\delta_{fg}. \tag{4.25}$$

The vertex contains in contradistinction to perturbation theory the field strength renormalisations of the gluon and the quark and the coupling g is scale dependent and related to the

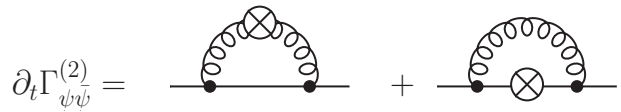

Figure 4.2: Flow of $\Gamma^{(2)}_{\psi\bar{\psi}}$. The quark propagator is given by the solid lines, the gluon propagator is symbolised with the curly lines and the black dots stand for the quark-gluon vertex. The circle with the cross symbolises the flow of the regulator. At the level of our truncation only the gluon fluctuations contribute. One can see how the glue sector feeds back to the matter sector by the gluon propagator.

strong coupling via $g = \sqrt{4\pi\alpha_s}$. We neglect any further contributions from the running of the vertex, see e.g. [152, 153].

4.2.2 Propagators from the glue sector

The propagators of the glue sector are not as easily determined as the quark propagator. One needs to be very careful already at the level of quantising the gauge fields. For vanishing temperature the fully momentum dependent propagators [150, 151] including the vacuum polarisation of the gluon propagator through the quarks is used. At non-zero temperature we utilise the Yang–Mills propagators from [154] where we add to and back-couple the vacuum polarisation of the gluon [89, 155]. The implicit temperature dependence is neglected, however it is to a first approximation negligible compared to the explicit temperature dependence through the Matsubara frequencies [146].

The gauge field propagator

Here, we briefly describe the general derivation of the gauge field propagators, see [150–152] for a complete derivation and also e.g. [156, 157] for introductory books on the quantisation of the gauge fields.

The problem that arises when deriving the gluon propagator is that the Lagrangian of the gauge sector of QCD is unchanged under certain local gauge transformations in configuration space, so an infinite amount of physically equivalent configurations is integrated over in the integration measure of the Lagrangian giving rise to a diverging integral. What is needed are those configurations, that correspond to the physically non-equivalent ones and are hence only given once. Therefore one fixes the gauge at each point in space and inserts in a smart way a 1 into the path integral that singles out the desired configurations. One can then perform the integration and obtains a bosonic gauge propagator that now depends on the gauge parameter ξ, which is up to our liking to choose. In this work we set $\xi = 0$, which is called Landau gauge. The advantage is that the gauge field then only contains a transverse part. At the same time the insertion of the 1, which is called the Faddeev–Popov [158] trick,

introduces new fields with interesting properties, as they are anti-commuting scalar fields in the adjoint representation, meaning that they are fermions but obey the wrong spin-statistics, which has the consequence that they are not physical particles and that's why they are called ghosts. Hence they do not appear as external legs in Feynman diagrams and do not correspond to physical particles but their fluctuation contributions are very important to the other propagators. E.g. in our ansatz for the running of the strong coupling α_s they play a crucial role, see Subsec. 4.2.3.

The gluon propagator is given by

$$G_{AA} = \left[Z_A^{\parallel} q_0^2 + Z_A^{\perp} \vec{q}^2 (1 + r_A)\right]^{-1} \Pi_{\mu\nu}^{\perp} + \xi \left[q_0^2 + \vec{q}^2 (1 + r_A)\right]^{-1} \Pi_{\mu\nu}^{\parallel}, \tag{4.26}$$

where in Landau gauge, $\xi = 0$, the longitudinal part vanishes. Additionally it is diagonal in colour space. The zero component of the momentum at finite temperature is given by the bosonic Matsubara frequencies, see Sec. 2.6. Although the propagator in Landau gauge is purely transversal, at finite temperature it splits into a part that is longitudinal and one that is transversal to the heat bath. So if $\xi \neq 0$ this means that it has a transversal and a longitudinal part that themselves have at non-vanishing temperature also a longitudinal and a transversal part with respect to the heat bath. The regulator shape function introduced here is a $3d$ optimised cutoff function given by

$$r_A(x) = \left(\frac{1}{x} - 1\right) \theta(1 - x) \tag{4.27}$$

with $x = \vec{q}^2/k^2$ and the complete regulator then reads

$$R_A = Z_A^{\perp} \vec{q}^2 r_A \left(\frac{\vec{q}^2}{k^2}\right) \Pi_{\mu\nu}^{\perp} + \frac{1}{\xi} \vec{q}^2 r_A \left(\frac{\vec{q}^2}{k^2}\right) \Pi_{\mu\nu}^{\parallel}, \tag{4.28}$$

with the transverse and longitudinal projectors

$$\Pi_{\mu\nu}^{\perp} = \delta_{\mu\nu} - \frac{p_\mu p_\nu}{p^2} \tag{4.29}$$

$$\Pi_{\mu\nu}^{\parallel} = \mathbb{1}\delta_{\mu\nu} - \Pi_{\mu\nu}^{\perp} = \frac{p_\mu p_\nu}{p^2}. \tag{4.30}$$

For later use we specify here the $3d$ projectors which can be directly read off the $4d$ projectors

$$\Pi_{\mu\nu}^{\perp,3d} = \left(\delta_{\mu\nu} - \frac{p_\mu p_\nu}{p^2}\right)(1 - \delta_{\mu 0})(1 - \delta_{\nu 0}) \tag{4.31}$$

$$\Pi_{\mu\nu}^{\parallel,3d} = \mathbb{1}\delta_{\mu\nu} - \Pi_{\mu\nu}^{\perp,3d}. \tag{4.32}$$

We can ask now how the wave function renormalisation Z_A, which is closely connected to the gluon propagator, changes with momentum scale k. The gluon self-interacts and hence there are many diagrams one has to take into account when calculating the flow of the gluon propagator, see Fig. 4.3 for the contributions within our truncation. The dressing function $p^2/\Gamma_{AA}^{(2)}$ as a function of momentum is shown in Fig. 4.4. The result agrees well with the lattice results.

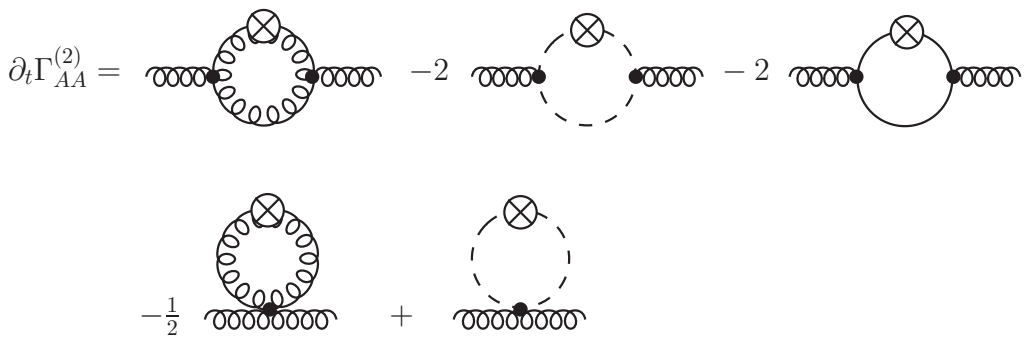

Figure 4.3: Flow of $\Gamma^{(2)}_{AA}$. The gluon propagator is given by the curly lines, the ghost by the dashed and the quark propagator is symbolised by the solid line. All propagators are the full propagators and the circle with the cross stands for the flow of the scale dependent regulator ensuring that only modes above k are integrated over. The matter sector of QCD couples back to the glue sector through the vacuum polarisation of the gluon through the quark. This contribution is derived in the next subsection and plays a major role for QCD as this is the link between the two sectors.

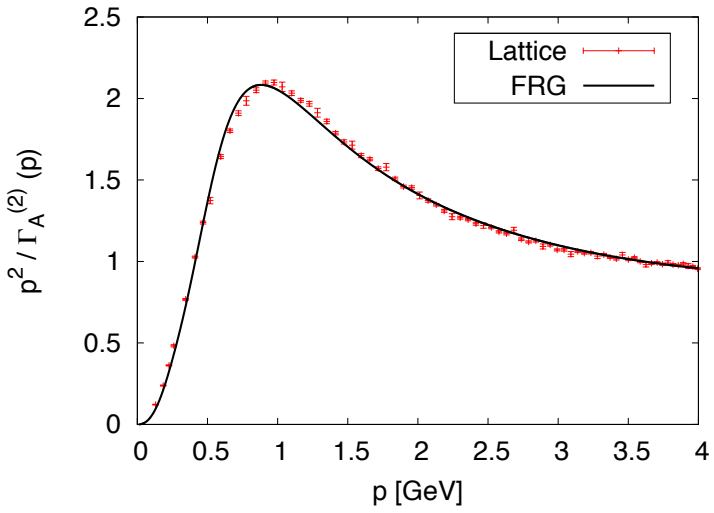

Figure 4.4: The gluon dressing function at vanishing temperature and chemical potential. The plot is taken from [146], FRG data from [154] and lattice data from [159]. The plot shows that the results for the pure Yang–Mills FRG gluon dressing function agrees very well with the lattice results.

Vacuum polarisation of the gluon

The vacuum polarisation of the gluon has already been calculated in Ref. [89] in a one-loop RG improved approximation and is given by

$$\Delta\eta_{A_q} = \frac{N_f}{\sqrt{1+\bar{M}_\psi^2}}\frac{4}{3}\frac{1}{4\pi}\alpha_s\left(1 - \frac{1}{1+e^{\frac{-2\pi i\theta+\sqrt{1+\bar{M}_\psi^2}-\bar{\mu}}{\bar{T}}}} - \frac{1}{1+e^{\frac{2\pi i\theta+\sqrt{1+\bar{M}_\psi^2}+\bar{\mu}}{\bar{T}}}}\right). \tag{4.33}$$

The equation we derive here has been studied simultaneously in the same truncation by F. Rennecke, see [160]. Here we give the full results within our truncation and at finite chemical potential and temperature and also include wave function renormalisations parallel $Z_\psi^{\parallel}$ and perpendicular $Z_\psi^{\perp}$ to the heat bath, renormalising the zero and the vector component of the momentum.

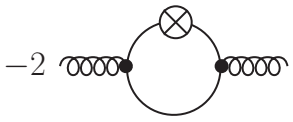

Figure 4.5: The vacuum polarisation of the gluon through the quark.

We implement the $3d$ regulator given by Eqn. (4.16). To determine the vacuum polarisation of the gluon, i.e. $\Delta\eta_{A_q}^{\perp}$, we must project onto the lhs of the flow of $\Gamma_{AA}^{(2)}$

$$\partial_t\Gamma_{AA}^{(2)} = \left(\dot{Z}_A^{\parallel}\omega_n^2 + \dot{Z}_A^{\perp}\vec{p}^2\right)\Pi_{\mu\nu}^{\perp,3d}\,\delta^{ab} + \frac{1}{\xi}\,\Pi_{\mu\nu}^{\parallel,3d}\,\delta^{ab}p^2, \tag{4.34}$$

where the ω_n are the bosonic Matsubara frequencies and we want to project onto the transverse component relative to the heat bath (as we are in Landau gauge there is only the standard transverse part of the propagator but there is a transverse and a longitudinal component with respect to the heat bath) and there we want the flow of the wave function renormalisation proportional to the vector component of the momentum. So we have to perform two derivatives with respect to the momentum p at vanishing momentum. Dividing by the negative of the wave function renormalisation we are left with the desired contribution to the anomalous dimension, i.e. the vacuum polarisation of the gluon by the quarks. The rhs is simply given by the same manipulations we have just performed on the lhs and which we then apply to the diagram given in Fig. 4.5.

So we have to derive the rhs of

$$\Delta\eta_{A_q}^{\perp} = -\frac{1}{4(N_c^2-1)}\frac{1}{Z_A^{\perp}}\left\{\partial_p^2\left(\Pi_{\mu\nu}^{\perp,3d}\delta^{ab}\Big[\ -2\ \Big]\right)\Big|_{p=0}\right\}. \tag{4.35}$$

and actually all we have to do is to calculate the quantity in the curly brackets. The trace

over the group indices gives a factor $\mathrm{Tr}(t^a t^a) = C_2(N_c)\, N_c$ and in flavour space we have $\mathrm{Tr}(\mathbb{1}_f) = N_f$. More details of the calculation are given in App. C.2. The result for $Z_\psi^{\parallel} = Z_\psi^{\perp} = Z_\psi$ is given by

$$\Delta\eta_{A_q} = \frac{2}{15}\frac{1}{(2\pi)^2} N_f\, g^2\, \bar{T} \sum_n \left(3\bar{G}^2_{\psi\bar{\psi}}(2\eta_\psi - 3) - 4\bar{G}^3_{\psi\bar{\psi}}(3\eta_\psi - 8) - 8\bar{G}^4_{\psi\bar{\psi}} \right), \tag{4.36}$$

where $\bar{G}^{-1}_{\psi\bar{\psi}} = \bar{q}_0^2 + 1 + \bar{M}_\psi^2$ and $\bar{q}_0$ is given by the dimensionless fermionic Matsubara frequencies. We have checked that our result agrees with perturbation theory in the limit of $k \to \Lambda_{UV}$ and with the result of [89] also for intermediate momenta for $\eta_\psi = 0$. Note that Eqn. (4.36) contains only dimensionless and RG invariant quantities.

The ghost propagator

For the ghost propagator one derives the standard Feynman rules, see e.g. [156]. For the RG propagator see e.g. [153]

$$G_{c\bar{c}} = -\frac{1}{Z_C\, p^2}\delta^{ab}. \tag{4.37}$$

The flow of $\Gamma^{(2)}_{c\bar{c}}$ is given in our truncation by Fig. 4.6, where the gluon quantum fluctuations couple to the ghost propagator. Indirectly, in QCD, the quark couples via the gluon propagator to the ghost propagator. The result for the dressing function of the ghost $p^2/\Gamma^{(2)}_C$ is shown in Fig. 4.7. It agrees for intermediate and large momenta with the lattice results. We discuss the discrepancy at very low momenta in Subsec. 4.2.2, however they are not relevant for physical observables as at these scales all relevant information has already been integrated out.

Figure 4.6: Flow of $\Gamma^{(2)}_{c\bar{c}}$. Here, the gluon (curly lines) and ghost (dashed lines) fluctuations contribute to the flow and the quark dynamics enter through the full gluon propagator, see Fig. 4.3. The lines are the full propagators and the circle with the cross symbolises the flow of the regulator function and cuts off momentum modes below the scale k.

The IR behaviour of the propagators

We briefly explain the discrepancy of the RG and the lattice propagators in the IR. At the moment there is a lively discussion [161], whether or not the gluon and ghost propagators exhibit a scaling (the gluon propagator vanishes and the ghost propagator is enhanced in the IR) [154, 162–167] or decoupling (ghost and gluon propagators are finite and behave mass-like in the IR) [154, 166, 168–171] behaviour at momentum scales that actually are not relevant

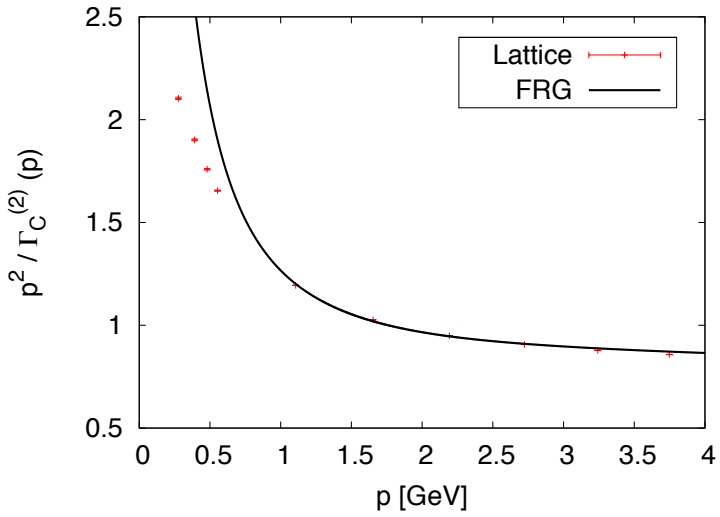

Figure 4.7: The ghost dressing function. Plot taken from [146], FRG data from [154] and lattice data from [159]. The result agrees very well with the lattice calculations, the deviations in the IR are under strong debate but do not influence the physics at hand.

for physical objects. The debate ranks around the question whether only one solution is valid or whether both are as they may correspond to different types of completions of Landau gauge in the IR, see [172] for an overview. We emphasise that this dispute does not influence the results of any observable presented here or elsewhere. However it influences the understanding of the confinement mechanism [154, 173]. For more details see e.g. [152, 153, 174, 175] and references therein.

4.2.3 The running coupling α_s

There are several ways to implement a non-perturbative running of the strong coupling α_s. In general it receives non-perturbative contributions from the wave function renormalisations of the ghost or the quark and the gluon. Its behaviour in the IR then depends on the behaviour of the propagators in the IR. In our case we implement the coupling defined in [162, 163] for our calculations at finite temperature and chemical potential and we include the propagators that exhibit scaling behaviour.

The strong running coupling α_s receives contributions from the ghost and gluon wave function renormalisation as a result of the non-renormalisation theorem of the ghost-gluon vertex in Landau gauge [162, 163] and can therefore be expressed as the bare coupling at some UV scale and a factor proportional to the wave function renormalisations of the ghost and the gluon

$$\alpha_s(k) = \frac{g^2}{4\pi} \frac{1}{Z_{A_k}(p=k)\, Z^2_{C_k}(p=k)}, \tag{4.38}$$

where the fully coupled wave function renormalisations of the glue sector enter. For pure

Yang–Mills theory, cf. Figs. 4.3, 4.6 without the vacuum polarisation of the gluon through the quark, Fig. 4.8 shows the behaviour of $\alpha_s(k)$. Including quark fluctuations, so having the full glue wave function renormalisations, α_s is smaller as Z_A is larger.

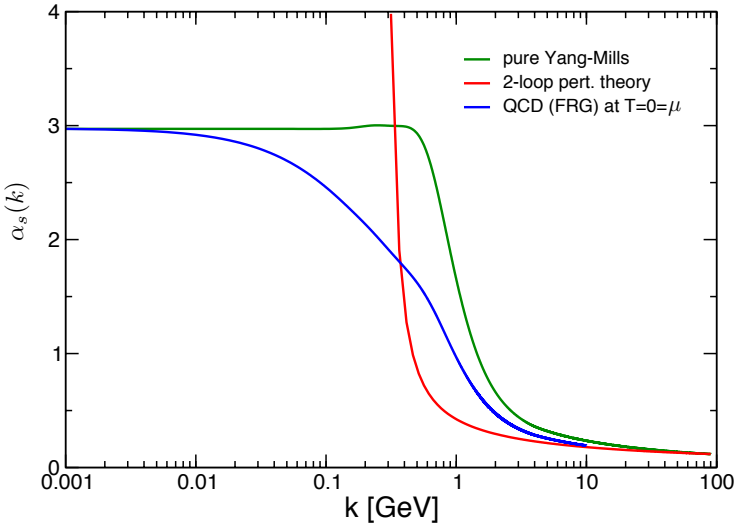

Figure 4.8: α_s as a function of momentum for perturbation theory, Yang–Mills theory and $N_f = 2$ QCD at vanishing temperature and chemical potential. The perturbative solution diverges at $\Lambda_{\rm QCD} \approx 200$ MeV.

Fig. 4.8 shows that the dynamical region is roughly around 300 MeV to 4 GeV, it runs into a fixed point in the IR [176–178] and it shows asymptotic freedom in the UV. The behaviour in the IR is determined solely by the scaling behaviour of the propagators and has no physical consequences. For comparison, if the decoupling propagators are implemented, the coupling goes to zero in the IR. Looking at α_s at all momentum regimes, the intermediate momentum region is of most importance for the dynamics of the interactions and physics. In the UV, quantum fluctuations do not play a role as perturbation theory is matched. The exact IR behaviour depends on the choice of propagators, but at this scales, all fluctuations have already been integrated out and all the relevant information is already included. This also means that the dynamical region of about 300 MeV-4 GeV is really crucial for QCD.

Including the back-coupling of the matter sector onto the gauge sector, we add the quark contribution of the anomalous dimension of the gluon to its glue contributions (this also includes the glue propagators which also receive contributions from the matter sector). We can now study the effects of an imaginary chemical potential θ, see Chap. 5, on the strong coupling. As imaginary chemical potential acts as a momentum shift in the quark propagator, its effects are small on α_s which therefore depends only indirectly on θ, see Fig. 4.9. We also show the dependence on real chemical potential μ which exhibits a mass-like behaviour, and hence has a bigger effect on the coupling, see Fig. 4.10.

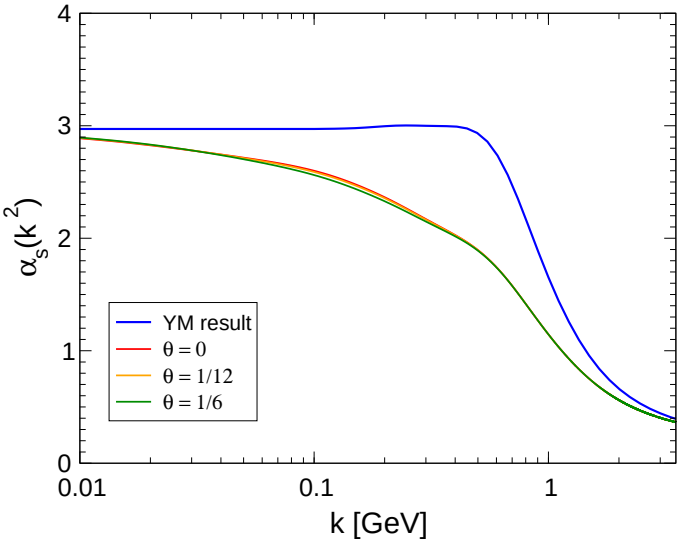

Figure 4.9: $\alpha_{s_k}(\theta)$ as a function of momentum and imaginary chemical potential for $N_f = 2$ QCD at vanishing temperature.

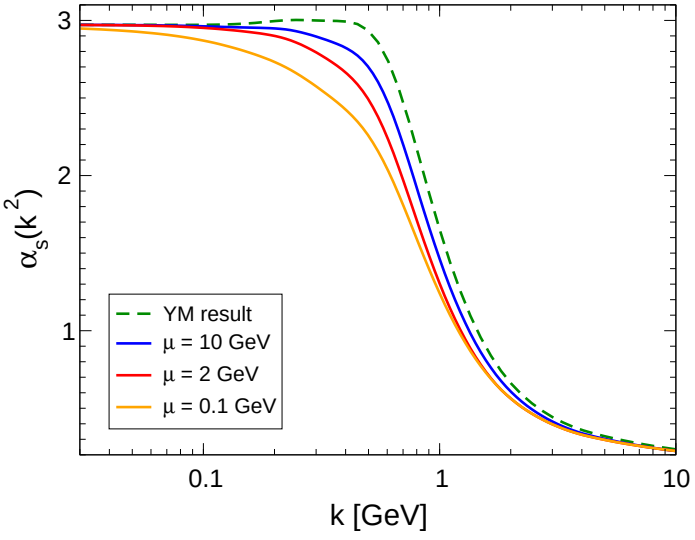

Figure 4.10: $\alpha_{s_k}(\mu)$ as a function of momentum and real chemical potential for $N_f = 1$ QCD at vanishing temperature. Figure taken from [155].

4.3 Flow equations for the couplings and anomalous dimensions

4.3.1 Flows for vanishing temperature and chemical potential

Now we can determine the flow equations of the couplings and wave function renormalisations. For non-zero temperature and quark chemical potential they were derived by J. Braun in [89]. Here we reprint them for vanishing temperature and zero chemical potential. The corresponding threshold functions can be found in App. B.1, where we used a $4d$ optimised regulator. In this subsection we specify only the flow equations, in the next section we derive then the fully rebosonised equations.

Flow of the Yukawa coupling

The beta function for the Yukawa coupling squared is proportional to the triangle diagrams with an incoming (pseudo) scalar and two outgoing quarks. Between the quarks a (pseudo) scalar, i.e. pion or sigma, or a gluon is exchanged. We find for the flow of the Yukawa coupling

$$\begin{aligned}\partial_t \bar{h}^2 &= (2\eta_\psi + \eta_\sigma)\bar{h}^2 - 4\, v(d)\, \bar{h}^4 \Big\{ (N_f^2 - 1)\, L_{1,1}^{(FB)}(\bar{M}_\psi^2, \bar{M}_\pi^2; \eta_\psi, \eta_\sigma) - L_{1,1}^{(FB)}(\bar{M}_\psi^2, \bar{M}_\sigma^2; \eta_\psi, \eta_\sigma) \Big\} \\ &\quad - 8(3+\xi)\, C_2(N_c)\, v(d)\, g^2\, \bar{h}^2\, L_{1,1}^{(FB)}(\bar{M}_\psi^2, 0; \eta_\psi, \eta_A) \end{aligned} \tag{4.39}$$

and the corresponding threshold functions can be found in App. B.1. The gauge coupling g is determined by $g^2 = \alpha_s\, 4\pi$. The dimensional prefactor $v(d)$ is given by

$$v(d) = \frac{1}{2^{d+1}\pi^{d/2}\Gamma(\frac{d}{2})}. \tag{4.40}$$

Flow of the four-quark coupling

The flow for the four-quark coupling is proportional to the box diagrams with two incoming and two outgoing quarks. Two gluons or two (pseudo) scalars are exchanged. The flow of the four fermion interaction reads

$$\begin{aligned}\partial_t \bar{\lambda}_\psi &= -6\, g^2\, (N_c+2)(N_c-1)\frac{C_2(N_c)}{N_c^2} v(d)\, L_{1,2}^{(FB)}(\bar{M}_\psi^2; \eta_\psi, \eta_A) \\ &\quad + \left(\frac{2}{N_c} + 1\right) v(d)\, L_{1,1,1}^{(FB)}(\bar{M}_\psi^2, \bar{M}_\pi^2, \bar{M}_\sigma^2; \eta_\psi, \eta_\sigma). \end{aligned} \tag{4.41}$$

Flow of the scalar coupling and mass

For the scalar coupling and mass we print the equations in the symmetric and in the broken phase separately. Then the correct description in terms of masses and other couplings can be read-off the equations. The flow equations were derived from the diagrams contributing to the effective potential of the matter sector.

In the symmetric regime, the flow of the scalar coupling $\bar{\lambda}_\sigma$ and the scalar mass $\bar{m}_\sigma$ are given by

$$\begin{aligned}\partial_t \bar{m}_\sigma^2 \equiv \partial_t \epsilon &= (\eta_\sigma - 2)\epsilon - (2(N_f^2-1)+6)\, v(d)\, \bar{\lambda}_\sigma\, l_1^B(\bar{M}_\sigma^2;\eta_\sigma) \\ &\quad +8\, N_c\, N_f\, v(d)\, \bar{h}^2\, l_1^F(\bar{M}_\psi^2;\eta_\psi) \qquad (4.42)\\ \partial_t \bar{\lambda}_\sigma &= 2\eta_\sigma\, \bar{\lambda}_\sigma + (2(N_f^2-1)+18)\, v(d)\, \bar{\lambda}_\sigma^2\, l_2^B(\bar{M}_\sigma^2;\eta_\sigma) \\ &\quad -8\, N_c\, N_f\, v(d)\, \bar{h}^4\, l_2^F(\bar{M}_\psi^2;\eta_\psi). \qquad (4.43)\end{aligned}$$

The threshold functions are the ones stemming from the effective potential, see App. B.1. In the broken regime the scalar couplings are

$$\begin{aligned}\partial_t \kappa &= -(\eta_\sigma+2)\kappa + 6\, v(d)\, l_1^B(\bar{M}_\sigma^2;\eta_\sigma) + 2\,(N_f^2-1)\, v(d)\, l_1^B(\bar{M}_\pi^2;\eta_\sigma) \\ &\quad -8\, N_c\, N_f\, v(d)\, \frac{\bar{h}^2}{\bar{\lambda}_\sigma} l_1^F(\bar{M}_\psi^2;\eta_\psi) \qquad (4.44)\\ \partial_t \bar{\lambda}_\sigma &= 2\eta_\sigma\, \bar{\lambda}_\sigma + 2(N_f^2-1)\, v(d)\, \bar{\lambda}_\sigma^2\, l_2^B(\bar{M}_\pi^2;\eta_\sigma) \\ &\quad +18\, v(d)\, \bar{\lambda}_\sigma^2\, l_2^B(\bar{M}_\sigma^2;\eta_\sigma) - 8\, N_c\, N_f\, v(d)\, \bar{h}^4\, l_2^F(\bar{M}_\psi^2;\eta_\psi). \qquad (4.45)\end{aligned}$$

Note that κ describes the dimensionless flow of the minimum of the effective potential.

Flow of the anomalous dimensions

The flow equations for the anomalous dimension of the scalars and the quarks are derived by expanding the rhs of the flow equation for the truncation up to second order in the fields and taking the limit of vanishing outer momentum, one can project onto the scalar and quark anomalous dimension, see [89] for the quark anomalous dimension η_ψ and [30, 89, 179, 180] for the scalar anomalous dimension η_ϕ.

The anomalous dimension for the mesons is

$$\begin{aligned}\eta_\sigma &= 4\, v(d)\, \kappa\, \bar{\lambda}_\sigma^2\, \mathcal{M}_{2,2}(\bar{M}_\pi^2, \bar{M}_\sigma^2;\eta_\sigma) + 4N_c\, N_f\, v(d)\, \bar{h}^2 \big\{ \mathcal{M}_4(\bar{M}_\psi^2;\eta_\psi) \\ &\quad +\kappa \bar{h}^2 \mathcal{M}_2(\bar{M}_\psi^2;\eta_\psi)\big\}, \qquad (4.46)\end{aligned}$$

and for the quarks we have

$$\begin{aligned}\eta_\psi &= 2\, v(d)\, C_2(N_c)\, g^2\, \big\{(3-\xi)\mathcal{M}_{1,2}(0,\bar{M}_\psi^2;\eta_\psi,\eta_A) - 3(1-\xi)\mathcal{M}_{1,2}(0,\bar{M}_\psi^2;\eta_\psi,\eta_A)\big\} \\ &\quad + 4\, v(d)\, \bar{h}^2 \big\{\mathcal{M}_{1,2}(\bar{M}_\psi^2, \bar{M}_\sigma^2;\eta_\psi,\eta_\sigma) + (N_f^2-1)\, \mathcal{M}_{1,2}(\bar{M}_\psi^2, \bar{M}_\pi^2;\eta_\psi,\eta_\sigma)\big\}, \qquad (4.47)\end{aligned}$$

where we use the convention that $\eta = -\frac{\partial_t Z}{Z}$.

From Eqn. (4.39)-(4.47) it is clear that they are a system of coupled partial differential equations, and they have to be solved simultaneously. Before we can study the results, we derive the rebosonised equations, using Eqn. (3.40) from Subsec. 3.4.2.

4.4 Rebosonised flow equations

The rebosonised equations to the flow equations above have been derived previously, see [30, 89], however in a different manner. Compare e.g. chapter E from Ref. [89]. Here we give a different derivation. Hence the rebosonised equations differ from the ones obtained in [30, 89].

To obtain the rebosonised equations for the couplings and the anomalous dimensions we express the flow of the field $\Phi = (\sigma, \vec{\pi})$ with the truncation given in (4.1)

$$\dot{\Phi}_k = \dot{A}_k \frac{Z_\psi}{k^2 Z_\sigma^{1/2}} \bar{\psi}\psi + \dot{B}_k \Phi_k, \tag{4.48}$$

where we normalised it such that it is dimensionless and RG invariant. The functions $\dot{A}_k$ and $\dot{B}_k$ are the first and the second transformation function which we need to determine in the following. To derive them, we use two approximations that are physically sensible, first we demand that the rebosonised flow of the four-fermion coupling vanishes, cf. section 3.4.2, and that it vanishes at the initial scale. This means also that it vanishes for all scales. Second we assume that the rebosonised flow of the Yukawa coupling does not depend explicitly on the outer momentum p. We incorporate these two conditions in the following.

We can express the rebosonised flow of the four fermion coupling as the standard flow and an additional term stemming from 4.48 inserted into the truncation given in 4.1. We find

$$\dot{\lambda}_\psi\big|_\phi = \partial_t \lambda_\psi - 2ih\dot{A} \frac{Z_\psi}{k^2 Z_\sigma^{1/2}}, \tag{4.49}$$

where we denote the standard flow for the four-fermion coupling derived earlier with $\partial_t \lambda_\psi$ and the final rebosonised flow is given by the full flow evaluated at fixed fields. Now we use the physical sensible constraint that $\dot{\bar{\lambda}}_\psi\big|_\phi = 0$ which also implies that $\bar{\lambda}_\psi = 0$ and we find for the dimensionless equation

$$\dot{\bar{\lambda}}_\psi\big|_\phi = \partial_t \bar{\lambda}_\psi - 2i\bar{h}\dot{A} + 2\bar{\lambda}_\psi(1 + \eta_\psi). \tag{4.50}$$

Now we can determine the first transformation function $\dot{A}_k$. We use that $\dot{\bar{\lambda}}_\psi\big|_\phi = 0$ and arrive at the equation for the first transformation function

$$\dot{A} = -i \frac{\partial_t \bar{\lambda}_\psi}{2\bar{h}}. \tag{4.51}$$

For the rebosonised flow of the dimensionful Yukawa coupling we find

$$i\dot{h}\big|_\phi = \partial_t(ih) - \left(m_\sigma^2 + \lambda_\sigma \sigma_0^2 + Z_\sigma p^2\right) \dot{A} \frac{Z_\psi}{k^2 Z_\sigma^{1/2}} - i\, h\dot{B}, \tag{4.52}$$

which is translated to the dimensionless rebosonised flow

$$\dot{\bar{h}}\big|_\phi = \partial_t \bar{h} + \bar{h}\left(\frac{1}{2}\eta_\sigma + \eta_\psi\right) + i\left(\bar{m}_\sigma^2 + 2\bar{\lambda}_\sigma \kappa + \frac{p^2}{k^2}\right)\dot{A} - \bar{h}\dot{B}. \tag{4.53}$$

We use a Taylor expansion in $\dot{B}$ so that $\dot{B}(p) = \dot{B}_0 + \dot{B}_1 p^2 + \dots$ and assume that h and $\dot{A}$ do not depend on the outer momentum p,

$$\partial_{p^2} \dot{\bar{h}}(p)\big|_\phi = 0, \quad \text{and} \quad \partial_{p^2} \dot{A}(p) \simeq 0 \tag{4.54}$$

and find for the first moment of the second transformation function

$$\dot{B}_1 = \frac{\partial_t \bar{\lambda}_\psi}{2\bar{h}^2} \frac{1}{k^2}, \tag{4.55}$$

as we choose $\dot{B}_0 = 0$, which seems to be the simplest case. Then we find for the flow of the Yukawa coupling (evaluated at $p^2 = 0$)

$$\dot{\bar{h}}\big|_\phi = \partial_t \bar{h} + \bar{h}\left(\frac{1}{2}\eta_\sigma + \eta_\psi\right) + \left(\bar{m}_\sigma^2 + 2\bar{\lambda}_\sigma \kappa\right) \underbrace{i\dot{A}}_{\partial_t \bar{\lambda}_\psi/(2\bar{h})}, \tag{4.56}$$

where the first and the second term of the rhs of Eqn. (4.56) are the standard flows and the third accounts for the rebosonisation.

With this we have determined both equations for the transformation functions and we can determine the rebosonised flow equations for the other couplings. The rebosonised flow of the wave function renormalisation of the meson is given by

$$\dot{Z}_\sigma\big|_\phi = \partial_t Z_\sigma - \left(m_\sigma^2 + \lambda_\sigma \sigma_0^2\right) \dot{B}_1, \tag{4.57}$$

and its anomalous dimension is

$$\eta_\sigma\big|_\phi = -\frac{\dot{Z}_\sigma}{Z_\sigma}\big|_\phi = -\eta_\sigma + \left(\bar{m}_\sigma^2 + 2\bar{\lambda}_\sigma \kappa\right) \dot{B}_1 k^2. \tag{4.58}$$

So it also receives a contribution to from the renormalised flow.

All other flow equations for the couplings do not change and are given by Eqns. (4.42), (4.43), (4.44), (4.45) and (4.47). Hence

$$\begin{aligned}
\eta_\psi\big|_\phi \equiv -\frac{\dot{Z}_\psi}{Z_\psi}\big|_\phi &= \eta_\psi, && (4.59)\\
\dot{\bar{\lambda}}_\sigma\big|_{\sigma=\sigma_0} &= \dot{\bar{\lambda}}_\sigma && (4.60)\\
\partial_t \bar{m}_\sigma^2\big|_\phi &= \dot{\bar{m}}_\sigma^2, && (4.61)\\
\partial_t \kappa\big|_\phi &= -\frac{1}{\lambda_\sigma \sigma_0^2} \partial_\sigma \dot{U}(\Phi^2)\big|_{\sigma=\sigma_0} = \partial_t \kappa. && (4.62)
\end{aligned}$$

4.5 Stability of the rebosonised flows

With the rebosonised flows derived in the last section, we also checked that they are stable against a variation of the initial scale Λ_{UV}, see Fig. 4.11, and for a fixed Λ_{UV} we varied the

initial conditions of the other couplings, see Fig. 4.12. We find stable flows for all couplings. Here we show exemplary the flow of the Yukawa coupling.

Fig. 4.11 shows that the system always drives the Yukawa coupling back to the stable solution, however it also shows that choosing Λ_{UV} somewhat smaller than 5 GeV also changes the results in the IR as there is not enough momentum left to relax to the stable solution. In this regime the dynamics of the system are influenced by the deviation of the flow. Similar behaviour is also found for the other couplings. One should therefore choose Λ_{UV} above or equal to 5 GeV.

Fig. 4.12 shows the variation of the other initial conditions at fixed UV scale. The flow of the Yukawa coupling and the other couplings is also stable. We varied the initial conditions over a wide range of orders of magnitude and always obtain the correct result. However one must be careful not to choose an initial value for the Yukawa coupling that is so large that it forces the system deeply into the broken phase at already at the UV scale Λ_{UV}.

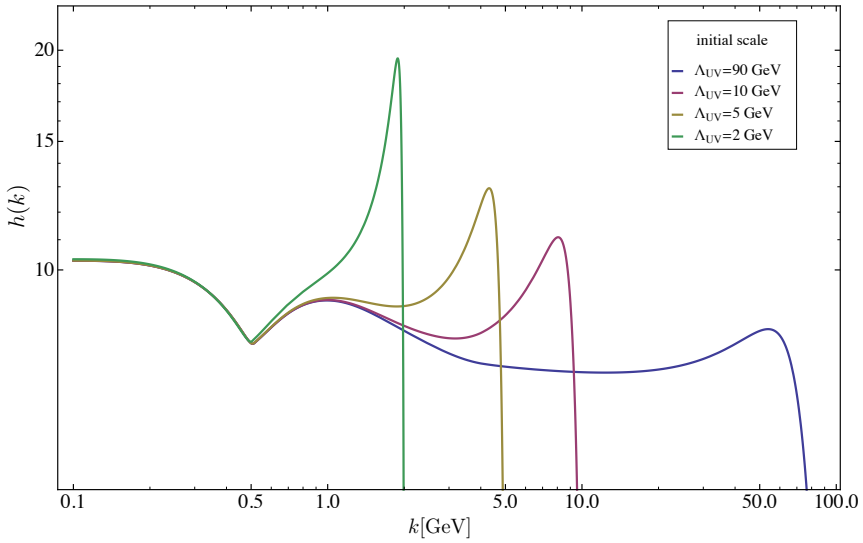

Figure 4.11: Flow of the Yukawa coupling with various initial scales. All parameters except for Λ_{UV} are specified as in Eqns. (C.11), (C.12), (C.13) and (C.14) in App. C.3.

4.6 Flow equations at non-vanishing temperature and chemical potential

At non-zero temperature and chemical potential we included the flow of the ground state of the effective potential of the matter sector, $\partial_t \kappa$, the scalar coupling $\partial_t \lambda_\sigma$ and the gauge field background A_0 as a function of temperature and imaginary chemical potential. We also calculated the scale dependent pressure. Their flow equations at non-zero temperature and

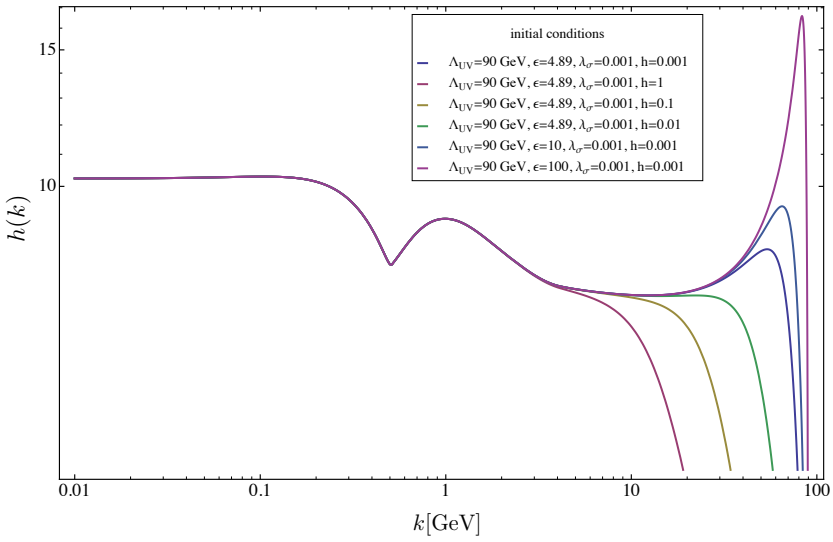

Figure 4.12: Flow of the Yukawa coupling with various initial conditions. The IR value of h does not change and the system is stable.

non-vanishing real and imaginary chemical potential are given by

$$\begin{aligned}\partial_t\kappa &= -2\,\kappa + 2\,\frac{\kappa}{\bar{M}_\sigma^2}\cdot \\ &\cdot\Big\{6\,v(d-1)\,\lambda_\sigma\,l_1^B(\bar{M}_\sigma^2,\bar{T};0,Z_\sigma) + 2(N_f^2-1)\,v(d-1)\lambda_\sigma\,l_1^B(\bar{M}_\pi^2,\bar{T};0,Z_\sigma) \\ &-8\,v(d-1)\,h^2\,N_f\left(\sum_{\mathrm{EV}_i} l_1^F(\bar{M}_\psi^2,\bar{T},\bar{\mu},\mathrm{EV}_i;0,Z_\psi)\right)\Big\} \qquad (4.63)\end{aligned}$$

$$\begin{aligned}\partial_t\lambda_\sigma &= 18\,v(d-1)\,\lambda_\sigma^2\,l_2^B(\bar{M}_\sigma^2,\bar{T};0,Z_\sigma) + 2\,(N_f^2-1)\,v(d-1)\,\lambda_\sigma^2\,l_2^B(\bar{M}_\pi^2,\bar{T};0,Z_\sigma) \\ &-8\,v(d-1)\,h^4\,N_f\left(\sum_{\mathrm{EV}_i} l_2^F(\bar{M}_\psi^2,\bar{T},\bar{\mu},\mathrm{EV}_i;0,Z_\psi)\right) \qquad (4.64)\end{aligned}$$

$$\partial_t c = -c\,3. \qquad (4.65)$$

Note that due to the gauge field background and imaginary chemical potential, we included here a sum over the eigenvalues, which are given in App. A.3.1. The flow equation for the pressure is given by

$$\begin{aligned}\partial_t p &= -\bar{T}^{-d}\Big(2\,v(d-1)\Big\{l_{\mathrm{therm}}^B(\bar{M}_\sigma^2,\bar{T};0,Z_\sigma) + (N_f^2-1)\,l_{\mathrm{therm}}^B(\bar{M}_\pi^2,\bar{T};0,Z_\sigma)\Big\} \\ &-8\,v(d-1)\,N_f\sum_{\mathrm{EV}_i} l_{\mathrm{therm}}^F(\bar{M}_\psi^2,\bar{T},\bar{\mu},\mathrm{EV}_i;0,Z_\psi)\Big). \qquad (4.66)\end{aligned}$$

The threshold function associated with its flow are also given in App. B.2.

4.7 Determining the QCD anomalous dimensions for the flow at $T \neq 0 \neq \mu$

In the next steps we want to calculate the contribution of $\Delta\eta_{A_q}$ to η_C from the propagators from [154]. In addition to the calculation at imaginary chemical potential we want to find the already fully coupled solutions for the anomalous dimensions of the ghost and the gluon. Therefore we determine the expressions for them in QCD given in terms of the YM and the quark contribution. We then have a set of coupled equations that is solved simultaneously with the other flow equations. The gluon anomalous dimension is given by

$$\eta_A(k^2) = \eta_{A_{QCD}}(p^2)\Big|_{YM,\, p^2=k^2} + \Delta\eta_{A_q}(k^2). \tag{4.67}$$

where

$$\eta_{A_{QCD}}\Big|_{YM} = \eta_{A_A} + \eta_{A_C}. \tag{4.68}$$

Her we denoted all contributions from gluon loops with the subscript A and the ghost contribution to the gluon anomalous dimension with the subscript C, see e.g. Figs. 4.6, 4.3. So actually the gluon propagator depends on the QCD gluon and ghost propagators. So we can rewrite α_s in terms of the pure YM and the full QCD contributions

$$\alpha_s = \alpha_{s_{YM}} \frac{Z_{A_{YM}} Z_{C_{YM}}^2}{Z_A Z_C^2}. \tag{4.69}$$

So then we can express the anomalous dimension of the ghost in this fashion

$$\eta_C = \eta_{C_{YM}} \cdot \frac{\alpha_s}{\alpha_{s_{YM}}} \cdot \frac{4 - \eta_A - \eta_C}{4 - \eta_{A_{YM}} - \eta_{C_{YM}}} \tag{4.70}$$

Now we need to determine η_{A_A} and η_{A_C} for the gluon and we find

$$\eta_{A_A} = \eta_{A_{A_{YM}}} \cdot \frac{2 - \eta_A}{2 - \eta_{A_{YM}}} \cdot \frac{\alpha_s}{\alpha_{s_{YM}}} \tag{4.71}$$

$$\eta_{A_C} = \eta_{A_{C_{YM}}} \cdot \frac{2 - \eta_C}{2 - \eta_{C_{YM}}} \cdot \frac{\alpha_s}{\alpha_{s_{YM}}}. \tag{4.72}$$

The flow equation for the coupling is then given by

$$\dot{\alpha}_s = \alpha_s \left(\eta_A + 2\eta_C\right). \tag{4.73}$$

In summary we find for the anomalous dimensions of the ghost and the gluon

$$\eta_C = \eta_{C_{YM}} \cdot \frac{\alpha_s}{\alpha_{s_{YM}}} \cdot \frac{4 - \eta_A - \eta_C}{4 - \eta_{A_{YM}} - \eta_{C_{YM}}} \tag{4.74}$$

$$\eta_A = \eta_{A_A} + \eta_{A_C} + \Delta\eta_{A_q}, \tag{4.75}$$

which depend solely on α_s and the YM input. This means that we can reorganise equations (4.74), (4.75) and (4.73) such that η_A and η_C are only functions of α_s.

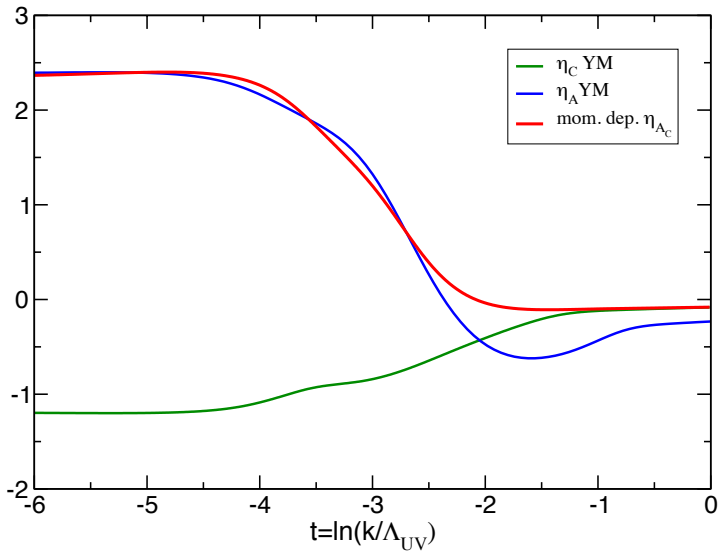

Figure 4.13: Matching the full momentum flow of η_{A_C} with $\Lambda_{\rm UV} = 10$ GeV.

Next we want to normalise the $\eta_{A_{QCD}}\big|_{YM}$ input given by the flow contributions f_{A_C} and f_{A_A} so that

$$f_{A_{QCD}}|_{YM} = f_{A_A} + f_{A_C} \quad \text{with} \quad \eta_{A_{QCD}}|_{YM} = -\frac{f_{A_{QCD}}|_{YM}}{Z_{A_{QCD}} k^2}. \tag{4.76}$$

where, of course the total flow is given by the individual contributions $p_A = \frac{f_{A_A}}{f_{A_{YM}}}$ and $p_C = \frac{f_{A_C}}{f_{A_{YM}}}$ yielding $p_A + p_C = 1$. This amounts to

$$\eta_{A_{A_{YM}}} = p_A \cdot \eta_{A_{YM}} \tag{4.77}$$

$$\eta_{A_{C_{YM}}} = p_C \cdot \eta_{A_{YM}}. \tag{4.78}$$

We then normalise the flow contributions such that in the IR f_{A_C} agrees with $\eta_{A_{YM}}$ and in the UV we find $\eta_{C_{YM}}$ and obtain

$$p_C \equiv \frac{\#f_{A_C} + \text{norm.}}{f_{A_{YM}}}, \tag{4.79}$$

where the factor # and the constant norm. is obtained by fitting to the functions. Further we find

$$p_C \cdot \eta_{A_{YM}} = \frac{\#f_{A_C} + \text{norm.}}{Z_{A_{YM}} k^2} = \eta_{A_{C_{YM}}} \tag{4.80}$$

$$p_A \cdot \eta_{A_{YM}} = \eta_{A_{YM}} - \frac{\#f_{A_C} + \text{norm.}}{Z_{A_{YM}} k^2} = \eta_{A_{A_{YM}}}. \tag{4.81}$$

The normalisation is shown in Fig. 4.13, where the flow matches $\eta_{A_{YM}}$ in the IR and $\eta_{C_{YM}}$ in the UV.

Chapter 5

The phase diagram at imaginary chemical potential

The physical quark masses vary over a wide range, from a few MeV up to 10^2 GeV, see Tab. 5.1. Consequently the lighter quarks contribute more to the dynamics of QCD as the heavy quarks. The two lightest quarks are the u and the d and are compared to all other quarks nearly degenerate and massless. Moreover one could also argue that the s belongs to the light quarks, as the remaining c, b and t are much heavier in comparison. It is therefore a reasonable approximation to study QCD with $N_f = 2$ or $N_f = 2 + 1$ flavours. This also agrees with the intrinsic scale of QCD, Λ_{QCD}, which is around 200 MeV. The order of this scale is the important dynamical regime of QCD. It is also the regime, where the QCD phase transition takes place.

u	**c**	**t**
1-3 MeV	1 GeV	170 GeV
d	**s**	**b**
4-5 MeV	100 MeV	4 GeV

Table 5.1: The rounded quark masses from [181] . The u and the d quark are nearly degenerate and together with the s they are much lighter than the other three quarks.

At vanishing chemical potential but non-zero temperature one can depict the confinement–deconfinement and the chiral phase transitions as functions of the three light quark masses, see Fig. 5.1 and Ref. [182].

In the $N_f = 3$ chiral limit QCD exhibits at high temperatures exact chiral symmetry which is broken at low temperatures and the phase transition is a first order transition. As seen by lattice simulations, see e.g. [76] and references therein, the area of first order transition is extended from the chiral limit to an area for a number of quark masses. For infinitely heavy quarks and $N_f = 3$, QCD is a pure $SU(3)$ gauge theory. Here one finds a first order confinement–deconfinement transition [147, 183]. Inbetween, the transitions soften

to crossovers, and the first order regions end in second order lines. The point with physical quark masses seems to lie in the crossover area [80, 86, 87, 91, 183, 184].

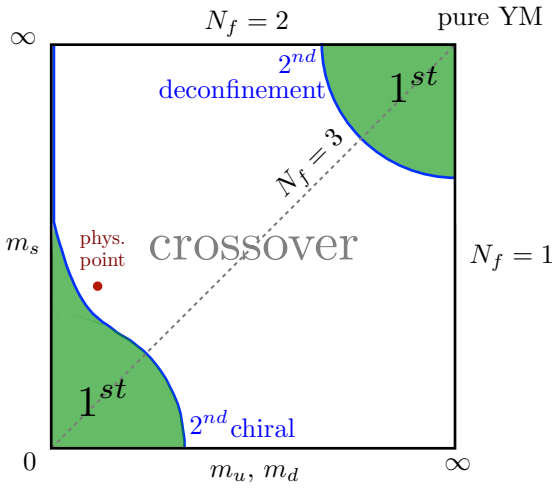

Figure 5.1: A sketch of the phase transitions for vanishing chemical potential in the quark mass plane, the so-called Columbia plot [182]. The first order regions are coloured in green, the second order transition lines are indicated with the blue lines and the white area stands for the crossover region. In the lower left corner all three quark masses are equal and vanish, so there we find the chiral limit with $N_f = 3$. The upper left corner has only two dynamical quarks with equal masses, so we find the $N_f = 2$ chiral limit. In the upper right corner all quark masses are equal but infinite, hence we are left with a pure $SU(3)$ gauge theory and no dynamical quarks. In the lower right corner we find only one dynamical massless quark flavour, so $N_f = 1$ in the chiral limit. On the diagonal all quarks have the same mass which is greater than zero and smaller than infinity appart from the corners and as we go away from the diagonal we have all possibilities for $N_f = 1 + 1 + 1$ or if we walk along a parallel to the m_u, m_d axis $N_f = 2 + 1$.

Extending this picture to non-zero chemical potential, one obtains a three dimensional plot. The second order transition lines now become critical surfaces and the physical point becomes a line. To determine the order of the phase transition in the QCD phase diagram spanned by temperature and chemical potential, it is crucial to know in which direction the critical surface bends.

If it bends away from the physical line, there will be no first order transition in the phase diagram with physical quark masses so one only observes a crossover when increasing the chemical potential. This is called the non-standard scenario and is depicted in Fig. 5.2.

On the other hand, if the critical surface bends towards the physical line, it pierces it and the line possibly stays in the first order area. This means that at low chemical potentials one observes a crossover, then a second order point followed by a first order transition line. This is called the standard scenario, see Fig. 5.3, as lattice calculations indicate a crossover

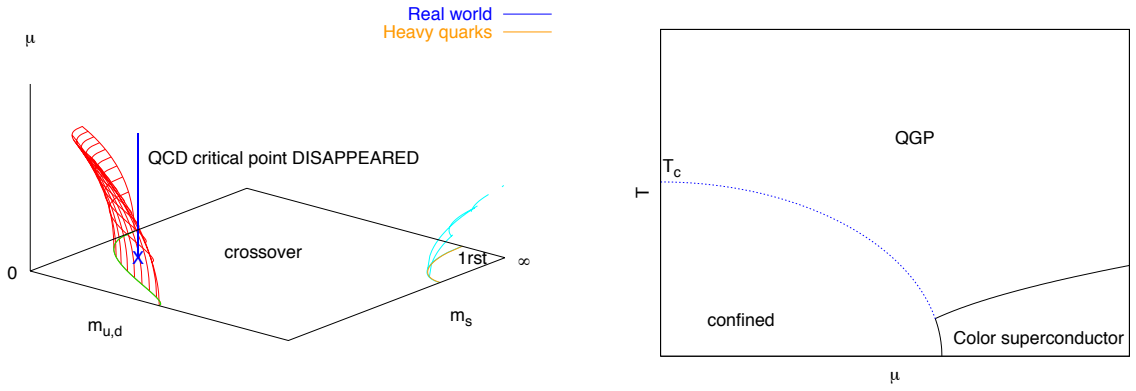

Figure 5.2: The non-standard scenario. The Columbia plot (left panel) for non-zero chemical potential and the corresponding phase diagram (right panel) both taken from Ref. [115]. The physical line does not pierce the critical surface as the first order regime shrinks with increasing chemical potential and as a result there is no critical endpoint and first order phase transition in the phase diagram.

at small chemical potentials and model studies which are valid at finite chemical potential and small temperatures indicate a first order transition, see e.g. [93] and [80] and references therein.

At the moment it is not clear which of these scenarios is realised in nature and whether the critical surface changes from bending outwards to inwards and vice versa, it could even change several times resulting in more than one second order point or simply shifting the location of the second order point to high values of the chemical potential.

One can now imagine extending the Columbia plot not only in the real chemical potential direction but also in the imaginary chemical potential direction, by using the square of chemical potential as a variable. The critical second order surface at $\mu^2 < 0$ stores information about the behaviour at $\mu^2 > 0$ as the two are smoothly connected, see Fig. 5.4. At least for small to moderate chemical potentials one should be able to deduce the bending of the phase boundary.

With the FRG approach, we can study the phase diagram at imaginary and vanishing chemical potential and compare to lattice studies. The comparison with lattice QCD calculations at imaginary and zero chemical potential gives an estimate of the quality of our approximation. In future analyses this can then be used to give constraints to lattice estimates and expansions for real chemical potential.

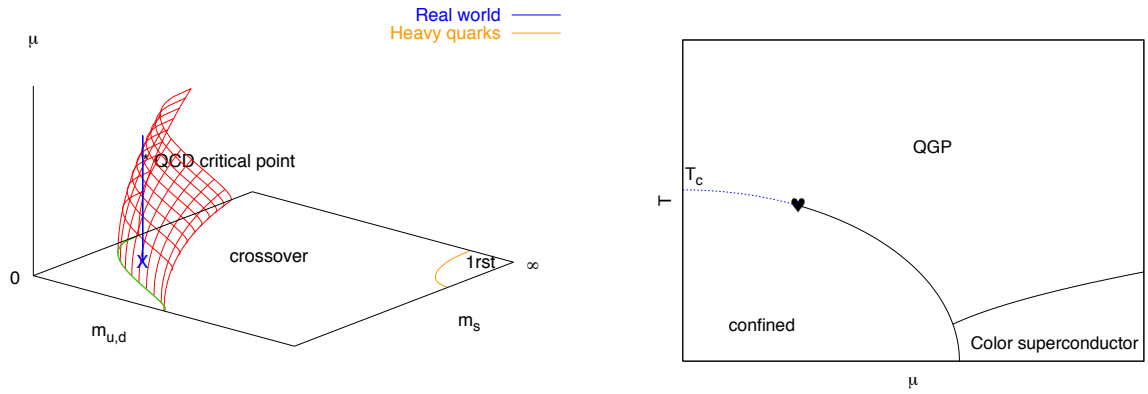

Figure 5.3: The standard scenario. The Columbia plot for non-zero chemical potential and the phase diagram taken from Ref. [115]. The second order point appears due to the intersection of the critical surface and the physical line. For larger chemical potential we stay in the first order regime.

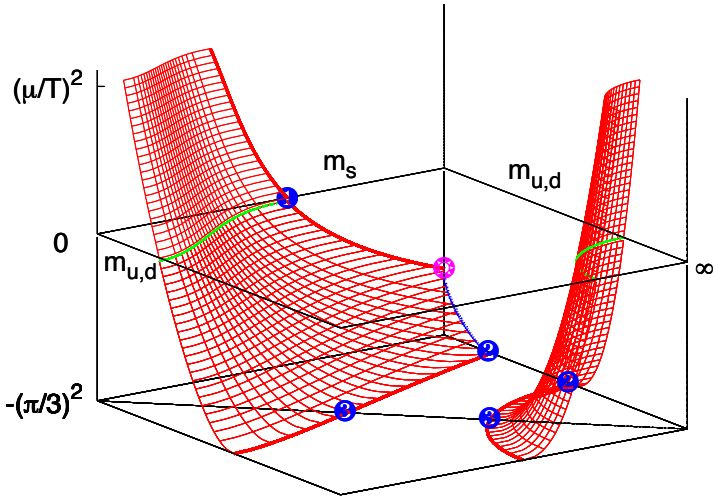

Figure 5.4: The Columbia plot including chemical potential squared. Imaginary chemical potential corresponds to $\mu^2 < 0$ and real chemical potential is plotted for $\mu^2 > 0$. The plot was taken from Ref. [185].

5.1 The Roberge–Weiss phase transition

At imaginary chemical potential θ, which is related to real chemical potential μ by $\theta = -i\mu\beta$ with $\beta = 1/T$, the QCD phase diagram looks qualitatively different than at real chemical potential. QCD shows a periodicity of $2\pi/N$ in θ [186]: Following the line of arguments of Ref. [186], the partition function of QCD with imaginary chemical potential is given by[1]

$$Z[\theta] = \int \mathcal{D}\psi\, \mathcal{D}\bar{\psi}\, \mathcal{D}A \exp\left\{ \int_x \bar{\psi}(i\not{D} + im - \gamma_0\theta/\beta)\psi + \frac{1}{4}F^a_{\mu\nu}F^a_{\mu\nu} \right\}. \tag{5.1}$$

It follows then with the gauge transformations that the fields ψ and A_μ transform as

$$\psi \to U\psi, \quad A_\mu \to UA_\mu U^{-1} - \frac{i}{g}(\partial_\mu U)U^{-1}, \tag{5.2}$$

where $U \in SU(N)$ and $U(\beta, x) = e^{2\pi ik/N}U(0, x)$ with $k \in \mathbb{N}$. This means that the transformations U are periodic up to the center elements $e^{2\pi ik/N}$. The action and the measure in eq. (5.1) are periodic under such a transformation, however the boundary conditions of the quarks are not

$$\psi(\beta, x) = e^{2\pi ik/N}e^{i\theta}\psi(0, x). \tag{5.3}$$

Inserting (5.3) into the partition function (5.1) one obtains the periodicity in θ

$$Z[\theta] = Z\left[\theta + \frac{2\pi k}{N}\right]. \tag{5.4}$$

This is called the Roberge–Weiss (RW) periodicity. Quantities that are related to the partition function such as the chiral condensate show this periodicity.

Furthermore at high temperatures the free energy shows discontinuities at $\theta = 2\pi(k + \frac{1}{2})/N$ and none at low temperatures, this is called the RW phase transition. The Polyakov loop, which is not invariant under the center transformation (5.2) with $\theta \to \theta + 2\pi k/N$, can be modified such that it respects this periodicity $\langle L\rangle(\theta) = \langle L\rangle e^{i\theta}$. Then one can study the these transitions by looking at $\langle L\rangle(\theta)$. The Polyakov loop shows discontinuities at $\theta \to \theta + 2\pi k/N$, signaling first order transitions, however they are transitions in the first order transitions, however they are transitions in the phase of the Polyakov loop and not the usual deconfinement transition [187]. Hence they are called Polyakov loop RW transitions.

One can now sketch a phase diagram for μ^2: for imaginary chemical potential it shows the periodically occurring Polyakov loop RW transitions which connects smoothly to real chemical potential, see Fig. 5.5. The RW endpoint is a first order point in the limit for small and large quark masses and weakens for intermediate. The second order transitions end in the first order transitions in the vicinity of the RW endpoint (Polyakov loop RW transitions) [188–193].

[1] Note that here in contradistinction to the following chapters the factor 2π does not appear in the partition function so that the periodicity we derive is given by Eqn. (5.4). In the rest of this thesis we use the definitions $2\pi\theta = -i\mu\beta$ such that the partition function is periodic under $\theta \to \theta + \frac{k}{N}$. We utilise this redefinition for an improved readability.

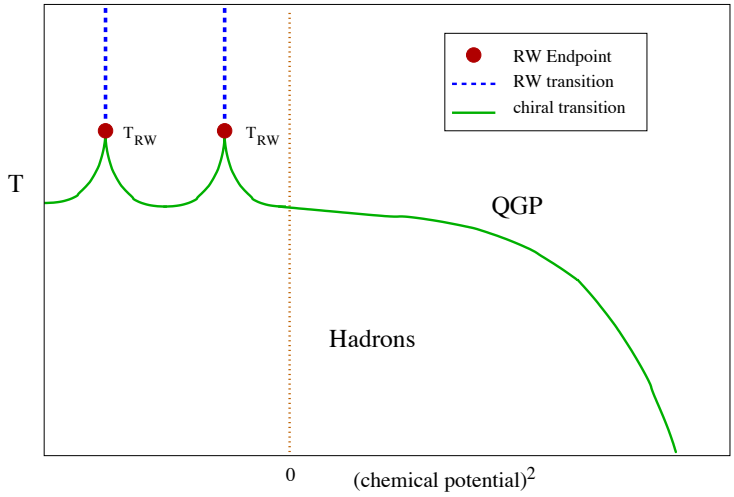

Figure 5.5: A sketch of the QCD phase diagram including chemical potential squared μ^2. For $\mu^2 > 0$, the picture is the same as in Fig. 1.1, for $\mu^2 < 0$, the phase transitions end in the RW endpoints and are followed by the RW phase transition for the Polyakov loop.

5.2 Dual order parameters

As introduced in Sec 2.5, the Polyakov loop serves as an order parameter for the confinement–deconfinement phase transition as it is sensitive to center transformations and it is connected to the free energy of a quark, where a non-vanishing value of $\langle L \rangle$ signals center symmetry breaking. This also means that any observable that transforms non-trivially under center transformations serves as an order parameter, as it vanishes in the symmetric phase and it is non-zero in the broken phase. This has been studied in [194–197], where the spectral properties of the Dirac operator have been related to the expectation value of the Polyakov loop. The relation stems from the observation that, in contradistinction to the gauge fields, the periodicity properties of the quark fields change under application of a gauge transformation U_z,

$$\psi^{U_z}(t+\beta,\vec{x}) = -z\psi^{U_z}(t,\vec{x})\,. \tag{5.5}$$

We can generalise the condition (5.5) such that it is enclosed in boundary conditions that depend on an angle θ

$$\psi_\theta(t+\beta,\vec{x}) = -e^{2\pi i\theta}\psi_\theta(t,\vec{x})\,. \tag{5.6}$$

Here all possible boundary conditions for the quark fields are included, especially the ones given by (5.5) with the center phases $z = \mathbb{1}\, e^{2\pi i\theta_z}$ and $\theta_z = 0, 1/3, 2/3$ for $SU(3)$. The quarks with the boundary conditions in (5.6) can be rewritten in terms of physical quarks with anti-periodic boundary conditions

$$\psi_\theta(x) = e^{2\pi\theta i\, t/\beta}\psi(x) \quad \text{with} \quad \psi(x) = \psi_{\theta=0}(x)\,. \tag{5.7}$$

This means that for vanishing angle θ we retrieve the physical quarks. Later, when we consider a phase diagram, where we vary θ, we actually look at different theories where the

difference stems from the different phases θ of the quarks. This means that only for vanishing θ we recover QCD, for all other values of θ we find a theory similar to QCD but with the quarks having boundary conditions that are not the physical ones. In the next steps we show that introducing this angle is formally the same thing as introducing an imaginary chemical potential [68], and see also [69].

Due to the periodicity in θ, see Eqn. (5.7), general observables that depend on the quark fields $\mathcal{O}_\theta = \langle O[\psi_\theta] \rangle$ can be represented in a Fourier decomposition,

$$\mathcal{O}_\theta = \sum_{l \in \mathbb{Z}} e^{2\pi i l \theta} O_l \,, \tag{5.8}$$

where we call the moments O_l dual observables. A center transformation (5.5) can be rewritten as a shift in $\theta \to \theta + \theta_z$, and implies that the moments O_l change under a center sensitive gauge transformation U_z into $z^l O_l$. Therefore every moment O_l with $l \in \mathbb{Z}$ and $l \bmod N_c \neq 0$ has to vanish in the center-symmetric phase as it is proportional to a sum over the center elements z

$$\sum_{z \in \mathcal{Z}} z^l = N_c \delta_{l \bmod N_c, 0}. \tag{5.9}$$

One example for a dual observable is $\mathcal{L}_\theta = e^{2\pi i \theta} \langle L \rangle$, which reflects the boundary conditions (5.6). The observables $\mathcal{O}_\theta$ can either be evaluated in QCD with anti-periodic quarks [194–197], or in QCD at imaginary chemical potential, QCD$_\theta$, with quarks having θ-dependent boundary conditions [68].

In summary, the moments $O_l \not\equiv 0$ with $l \mod N_c \neq 0$ are order parameters for the confinement–deconfinement phase transition for both, QCD and QCD$_\theta$. In particular the first moment O_1 is an order parameter for all N_c,

$$\tilde{\mathcal{O}} = \int_0^1 d\theta \, e^{-2\pi i \theta} \mathcal{O}_\theta \,, \tag{5.10}$$

so one example is the dual Polyakov loop which is in QCD $\langle L \rangle$.

Now we consider QCD$_\theta$. Its generating functional is given by

$$Z_\theta[J] = \int dA \, d\psi_\theta d\bar{\psi}_\theta \, \mathrm{e}^{-S[A,\psi_\theta,\bar{\psi}_\theta] + \int J \phi_\theta} \,, \tag{5.11}$$

with the θ-dependent fields $\phi_\theta = (A, \psi_\theta, \bar{\psi}_\theta, ...)$ and the source $J = (J_A, \bar{\eta}, \eta, ...)$. The dots stand for the ghost and composite hadronic fields, see e.g. [31, 60]. Here, S denotes the standard QCD action, see Eqn. (2.1), and includes a Dirac action with θ-dependent quark fields

$$\int \bar{\psi}_\theta \left(i \not{D} + im \right) \psi_\theta = \int \bar{\psi} \left(i \not{D} + im - 2\pi \frac{1}{\beta} \gamma_0 \theta \right) \psi \,. \tag{5.12}$$

The rhs of Eqn. (5.12) is simply the Dirac action with an imaginary chemical potential θ which is related to real chemical potential $\mu = 2\pi i \, \theta / \beta$, see Eqn. (5.1). If θ takes one of the

center values θ_z, we can define $\psi^{U_z} = \psi_{\theta_z}$ with the transformations U_z as in (5.5) and an anti-periodic quark field ψ. The center phases θ_z can now be absorbed in center transformations of the gauge field $A \to A^{U_z^\dagger}$. If we look at the generating functional Z_θ, we find that for vanishing current J it obeys the RW periodicity [186], see also [198–201],

$$Z_\theta[0] = Z_{\theta+1/N_c}[0]\,, \tag{5.13}$$

which on the other hand also means that the symmetry is broken if a source term proportional to J is present. Furthermore, any observable that depends on the quark fields, $\mathcal{O}_\theta$ in QCD_θ is RW-symmetric for vanishing current $J = 0$. Hence only the center-symmetric Fourier coefficients $O_{N_c l}$ are non-zero, whereas all other vanish identically: $O_l \equiv 0$ for $l \neq N_c l$ and we are not able to see a phase transition. This means that if RW periodicity is not somehow broken explicitly, all O_l vanish. And the introduction of a non-vanishing current J_A for the gauge field breaks the RW-symmetry, and leads to $O_l \neq 0$ for $l \mod N_c \neq 0$. This is implemented e.g. by a θ-independent gauge-field background φ.

So we find that the dual observables with $l \mod N_c \neq 0$ are order parameters for confinement. One simple and easily accessible confinement order parameter in QCD_θ is the dual density

$$\tilde{n}[\phi_J] \equiv \int_0^1 d\theta\, e^{-2\pi i\theta} n_\theta = \mathrm{i}\beta \int_0^1 d\theta\, e^{-2\pi i\theta} \ln Z_\theta[J]\,, \tag{5.14}$$

where $\phi_J = \langle\phi\rangle_J$. The density n_θ is the derivative of the partition function with respect to the chemical potential $2\pi\,\theta/\beta$,

$$n_\theta[\phi_J] = \int d^4x\, \langle\bar{\psi}\gamma_0\psi\rangle_\theta = \frac{\beta}{2\pi}\partial_\theta \ln Z_\theta[J]\,. \tag{5.15}$$

On the rhs of Eqn. (5.14) we have integrated by parts and used that $Z_0[J] = Z_1[J]$. Eqn. (5.14) tells us that the dual density $\tilde{n}[\phi]$ is proportional to the first moment of the grand canonical potential $Z_1(J)$ in the presence of a gauge field background φ so with explicitly broken RW symmetry. We now perform integration by parts and obtain the fermionic pressure difference $\Delta P(T,\theta) = P(T,\theta) - P(T,0)$, see Fig. 5.6. At $\theta = 1/2$ it shows a maximum in the direction of imaginary chemical potential for all temperatures, as θ differs here maximally from zero. Here it grows proportional to T^3 as it is proportional to the first moment of the grand canonical potential and the integrated θ-dependence is expected to be leading order. Fig. 5.6 shows also that the pressure difference at low temperatures no longer depends on imaginary chemical potential or the boundary conditions of the quark fields, as it is completely flat [202]. This means that at low temperatures the difference between the boundary conditions of the quarks does not play a role.

The above analysis for the dual density extends to general observables $\mathcal{O}_\theta[\phi_J]$. They give observables in different theories distinguished by the boundary condition. Hence the order parameters $\tilde{\mathcal{O}}$ in (5.10) in the presence of a fixed background $\phi_J = \langle\phi\rangle_J$ vanish only if QCD_θ is in the center symmetric phase for all boundary conditions. Therefore e.g. the pressure

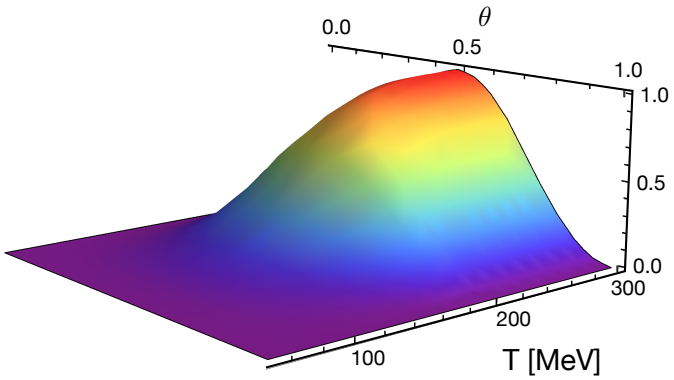

Figure 5.6: The pressure difference $\Delta P(T, \theta)$ as a function of temperature and imaginary chemical potential.

difference, see Fig. 5.6, does not vanish everywhere.

However, the transition temperature in QCD, $T_{\text{conf}} = T_{\text{conf}}(\theta = 0)$, is a lower bound for $T_{\text{conf}}(\theta)$, which can be seen in Fig. 5.11. Thus, the dual phase transition temperatures $\tilde{T}_{\text{conf}}$ are identical with the physical one, $\tilde{T}_{\text{conf}} = T_{\text{conf}}$.

Some interesting properties of dual order parameters can be accessed analytically. To that end it is convenient to study observables in terms of the quantum effective action 3.2. The current J is given by the derivative of the effective action with respect to ϕ, so $J = \delta\Gamma[\phi]/\delta\phi$, and vanishes on the equations of motion with the θ-dependent mean value $\bar{\phi}_\theta = \phi_{J=0}$. For example, the dual density (5.14) is then given by

$$\tilde{n}[\phi] = -i\beta \int_0^1 d\theta \, e^{-2\pi i\theta} \Gamma[\phi] \,. \tag{5.16}$$

As discussed above for $\phi = \bar{\phi}_\theta$, the dual observables vanish so that $\tilde{n}[\bar{\phi}_\theta] = 0$. This follows from the RW-symmetry of $\Gamma[\bar{\phi}_\theta]$ which is a consequence of that of Z_θ. For its direct proof it is sufficient to examine $\Gamma[\phi]$ for constant gauge field configurations A_0 in the Cartan subalgebra. The θ-dependence of the effective action $\Gamma[\phi]$ is found in the sums of terms with fermionic Matsubara frequencies, so in the zero component of the Dirac action,

$$iD_0 - 2\pi T\theta = 2\pi T \left(\left(n + \frac{1}{2} - \theta \right) \mathbb{1}_3 + \frac{\beta g A_0}{2\pi} \right) , \tag{5.17}$$

where here the background field A_0 is spanned by the three- and the eight-direction in the Cartan subalgebra for $N_c = 3$

$$\frac{\beta g A_0}{2\pi} = \frac{\varphi_3}{2\pi} \frac{\lambda^3}{2} + \frac{\varphi_8}{2\pi} \frac{\lambda^8}{2} . \tag{5.18}$$

The λ^3 and λ^8 are the Gell-Mann matrices in the fundamental representation, see App. A.3. Most of the θ-dependence can be reabsorbed in a θ-dependent gauge field $A_0(\theta)$. Where

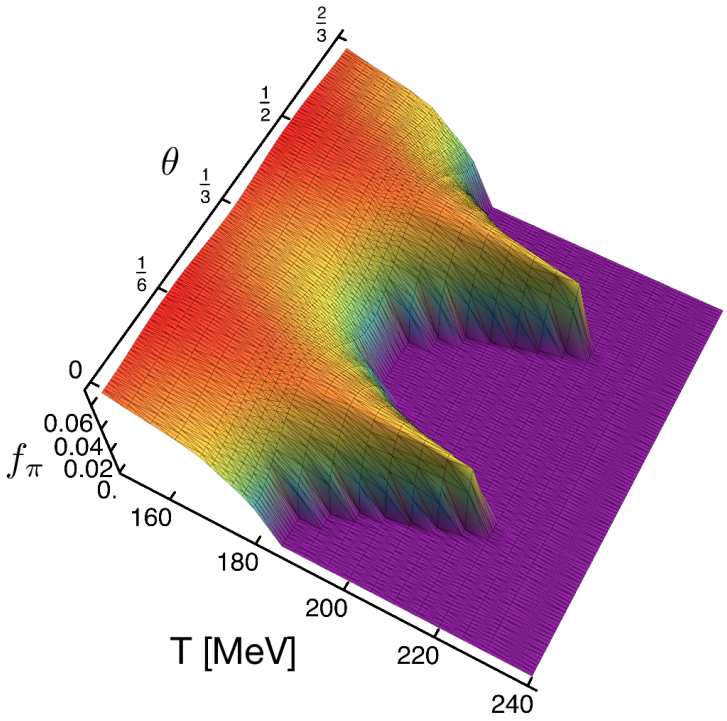

Figure 5.7: The pion decay constant as a function of imaginary chemical potential and temperature. The value $\theta = 0$ corresponds to QCD at vanishing chemical potential. The periodicity in θ is apparent. f_π vanishes above the transition and is finite below.

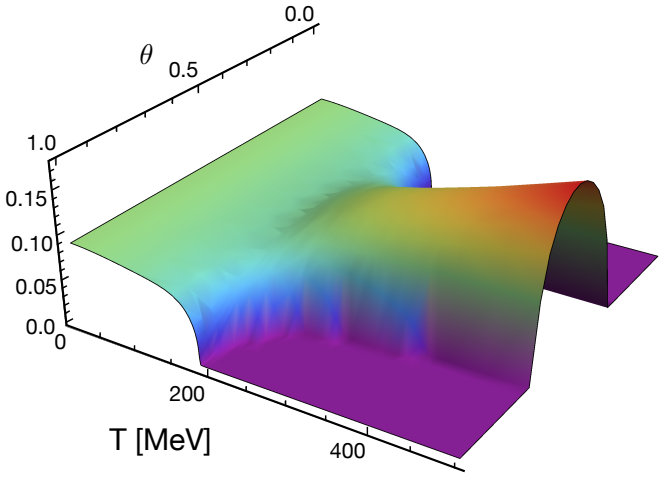

Figure 5.8: The dual quark mass parameter as a function of temperature and imaginary chemical potential. The RW symmetry is not broken, hence it does not vanish everywhere above the phase transition.

Eqn. (5.17) then reads

$$2\pi T \left(\left(n + \frac{1}{2} \right) \mathbb{1}_3 + \frac{1}{4\pi} \begin{pmatrix} \varphi_3 + \frac{\varphi_8}{\sqrt{3}} - 2(2\pi)\theta & 0 & 0 \\ 0 & -\varphi_3 + \frac{\varphi_8}{\sqrt{3}} - 2(2\pi)\theta & 0 \\ 0 & 0 & -\frac{2\varphi_8}{\sqrt{3}} - 2(2\pi)\theta \end{pmatrix} \right). \tag{5.19}$$

We then use the substitutions $\hat{\varphi}_3 = \varphi_3 + 3(2\pi)\theta$ and $\hat{\varphi}_8 = \varphi_8 + \sqrt{3}(2\pi)\theta$. Then we find the simple expression

$$2\pi T \left(\left(n + \frac{1}{2} \right) \mathbb{1}_3 + \frac{1}{4\pi} \begin{pmatrix} \hat{\varphi}_3 + \frac{\hat{\varphi}_8}{\sqrt{3}} - 6(2\pi)\theta & 0 & 0 \\ 0 & -\hat{\varphi}_3 + \frac{\hat{\varphi}_8}{\sqrt{3}} & 0 \\ 0 & 0 & -\frac{2\varphi_8}{\sqrt{3}} \end{pmatrix} \right). \tag{5.20}$$

We can extend this to general N_c and it is now clear that the RW-symmetry is explicit in the Matsubara frequencies

$$2\pi T \left(n + \frac{1}{2} + \frac{1}{4\pi}\Phi_i - N_c\, \delta_{i1}\, \theta \right), \quad i = 1, ..., N_c\,, \tag{5.21}$$

where the Φ_i's are the eigenvalues of the matrix $\hat{\varphi} = 2\beta g A_0(\theta)$: the shift $\theta \to \theta + \theta_z$ is absorbed in a center gauge transformation of the φ_i's as well as in a shift of the Matsubara sum

$$\theta \to \theta + \theta_z \tag{5.22}$$

$$\varphi_3 \to \varphi_3 + 3(2\pi)\theta_z \tag{5.23}$$

$$\varphi_8 \to \varphi_8 + 3(2\pi)\theta_z. \tag{5.24}$$

Under this combined transformation the $\hat{\varphi}_i$'s are invariant and so is the effective action. In particular we conclude from the above that any expansion scheme based on fixed field variables $\hat{\varphi}_i$ is form-invariant under the transformation $\theta \to \theta + \theta_z$. Moreover, the observables $\mathcal{O}_\theta[\bar{\phi}_\theta]$ are invariant, and therefore also $\tilde{\mathcal{O}}[\bar{\phi}_\theta] \equiv 0$. In turn, observables $\tilde{\mathcal{O}}[\phi]$ with θ-independent gauge field background φ are order parameters for confinement as such a background explicitly breaks the RW-symmetry. In particular this includes $\tilde{\mathcal{O}}[\phi]$ with $\varphi = \bar{\varphi} = \bar{\varphi}_{\theta=0}$ and $\varphi = 0$.

One can then find simple observables $\tilde{\mathcal{O}}[\phi]$ which follow directly from the vertices $\Gamma^{(n)}[\phi]$ in QCD$_\theta$. This includes the dual density (5.16) as well as the dual chiral condensate with $\mathcal{O}_\theta[\phi_J] = \int d^4x\, \langle \bar{\psi}_\theta \psi_\theta \rangle_J$ for either $\varphi_J = \bar{\varphi}_{\theta=0}$ and for $\varphi_J = 0$. The first case with $\bar{\varphi}$ relates to the lattice computations in QCD of dual order parameters [194–196]. The latter choice has been used implicitly in [197, 203].

An even simpler observable is the dual quark mass parameter $\tilde{\mathcal{M}}$ with

$$\mathcal{M}_\theta[\phi] \sim \operatorname{tr} \Gamma^{(2)}_{\bar{\psi}\psi}[\phi](p = 0). \tag{5.25}$$

The specific choice $\mathcal{M}_\theta[\bar{\phi}_\theta]$ is directly related to the pion decay constant f_π in QCD$_\theta$, see Fig 5.8. Due to the presence of a fixed background field it does not vanish in the broken and in the symmetric phase. At $\theta = 1/2$ closely above the phase transition it increases proportional to $\sqrt{T}$ and then linearly as the quarks effectively have bosonic Matsubara frequencies at $\theta = 1/2$. At $\theta = 0$ the dual quark mass is zero above the transition. For vanishing current it is related to the pion decay constant in QCD: the slice of the 3D plot at $\theta = 0$ is the (normalised) line shown in Fig. 5.9.

Another example is the modified Polyakov loop variable $L_\theta = e^{2\pi i\,\theta} L$ with $\mathcal{L}_\theta = \langle L_\theta \rangle$ and

$$L_{-\theta}[\varphi] = \frac{1}{N_c} \sum_{i=1}^{N_c} e^{2\pi i \left(\frac{1}{4\pi} \Phi_i[\hat{\varphi}] + N_c \delta_{i1} \theta \right)} . \tag{5.26}$$

$L_{-\theta}$ is invariant under $\theta \to \theta + \theta_z$ at fixed $\hat{\varphi}$. Hence, the Fourier coefficient O_{-1} vanishes, $\int_0^1 d\theta \langle L \rangle = 0$, which leads to $\tilde{\mathcal{L}}[\bar{\phi}_\theta] = 0$. In turn, $\tilde{L}[\bar{\phi}] = L[\bar{\varphi}]$ simply is the Polyakov loop variable introduced in [137, 146] as an order parameter for confinement.

The representation of the Polyakov loop in (5.26) leads to an interesting observation: in quenched QCD the $\mathcal{O}_\theta$ are given by sums from $i = 1$ to $i = N_c$ of terms which only depend on θ via the Matsubara frequencies (5.21). Thus, any observable $\tilde{\mathcal{O}}$ in (5.10) obeys

$$\tilde{\mathcal{O}}[\phi] = \int_0^1 d\theta\, e^{-2\pi i \theta} \mathcal{O}_\theta[0]\, L[\varphi] = \tilde{\mathcal{O}}[0]\, L[\varphi] , \tag{5.27}$$

for θ-independent gauge field background φ and vanishing quark and mesonic backgrounds. In (5.27) we have used that the $\Phi_i[\varphi]$-dependence of the Matsubara sums can be redistributed to the phase factor by shifting $\theta \to \theta + \Phi_i[\varphi]/(4\pi)$ in each term. In fully dynamical QCD$_\theta$ the factorisation (5.27) only holds approximately.

5.3 RW invariance of the Polyakov loop potential

Also the non-perturbative Polyakov loop potential shows the RW invariance under the shift $\theta \to \theta + \theta_z$. As before in the zero component of the Dirac term this shift can be absorbed in the gauge fields. The Polyakov loop potential is given by a component from the glue sector and one from the matter sector, see Eqn. (5.28). This means that in addition to the eigenvalues of the zero component of the Dirac operator in the fundamental representation we also need them in the adjoint representation. The Dirac operator there is given by a 8×8 matrix with bosonic Matsubara frequencies, see App. A.3.1. Then we can express the Polyakov loop potential

$$\begin{aligned} V_{\rm PL} \;=\; & V_{\rm glue} \left[\pm\hat{\varphi}_3 + 3(2\pi)\theta, \pm\frac{\hat{\varphi}_3 + \sqrt{3}\hat{\varphi}_8}{2} + 3(2\pi)\theta, \pm\frac{\hat{\varphi}_3 - \sqrt{3}\hat{\varphi}_8}{2} \right] \\ & + V_{\rm ferm} \left[\frac{\hat{\varphi}_3 + \frac{\hat{\varphi}_8}{\sqrt{3}}}{2} + 3(2\pi)\theta, \frac{-\hat{\varphi}_3 + \frac{\hat{\varphi}_8}{\sqrt{3}}}{2}, -\frac{\hat{\varphi}_8}{\sqrt{3}} \right] , \end{aligned} \tag{5.28}$$

with the RW transformation given in Eqn. (5.24) we find that the potential is invariant.

5.4 Results – The phase diagram

In our calculation of the phase diagram at imaginary chemical potential we use the truncation given in Sec. 4.1, where we include the back-reaction of the matter sector on the gauge sector through the vacuum polarisation from Refs. [89, 155]. The propagators for the pure Yang–Mills theory are the ones given in Subsec. 4.2.2, where temperature is explicitly included through the Matsubara sums. We also included a tiny explicit symmetry breaking term in the effective potential of the matter sector $U_{\text{break}} = -c\sigma$, simplifying our calculations significantly but without effecting the results. The initial conditions were chosen in the UV at the initial scale Λ_{UV}, see App. C.4. We implemented the threshold functions given in App. B.2. There, we assumed the Yukawa coupling to be non-zero but constant and the four-fermion coupling and its flow to vanish. The wave function renormalisation of the quark stays very close to 1 for all momenta, so we assume that $Z_\psi = 1$. We also set the anomalous dimension of the scalar fields to zero. The strong coupling α_s includes the full propagators from QCD within our approximation 4.1 and is given in Subsec. 4.2.3. The quarks are coupled to the gluon propagator (which also enters the running coupling α_s) via the anomalous dimension

$$\eta_A = \eta_{A_{YM}} + \Delta\eta_{A_q}. \tag{5.29}$$

At vanishing chemical potential we consider the order parameters of the chiral and the deconfinement phase transition, the Polyakov loop, the dual density and the pion decay constant, see Fig. 5.9. Above $T_c = 181$ MeV the pion decay constant vanishes and chiral

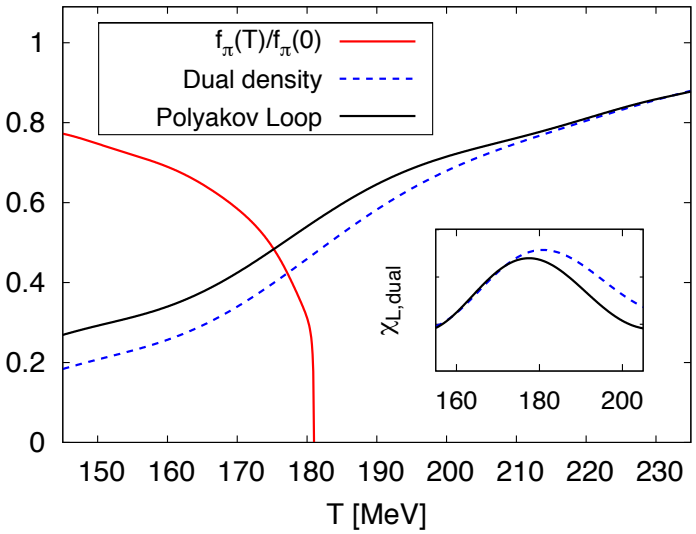

Figure 5.9: The pion decay constant, the dual density and the Polyakov loop as functions of temperature, $\chi_L = \partial_T L$, $\chi_{\text{dual}} = \partial_T \tilde{n}$.

symmetry is restored. The dual density $\tilde{n}[\bar{\phi}]$ and the Polyakov loop $L[\bar{\varphi}]$ both show a peak in their temperature derivative at $T_c \approx 178$ MeV. This provides a non-trivial consistency check

of our approximation as the Polyakov loop is computed from gluonic correlation functions, whereas the dual density is computed from matter correlation functions. We find that the chiral and the deconfinement transition agree within a few MeV. The comparison of the Polyakov loop $L[\bar{\varphi}]$ and the normalised dual density $\tilde{n}[\bar{\phi}]/\tilde{n}[0]$, see Fig. 5.10, shows that the factorisation (5.27) holds also in QCD approximately. Both, the dual density and the Polyakov loop differ only on the percent level, which is another consistency check for our approximation. The critical temperatures for the chiral and the confinement–deconfinement temperatures for $N_f = 2$ in Landau gauge in the chiral limit agree well within the widths of the crossover with lattice results, see e.g. [199, 204, 205].

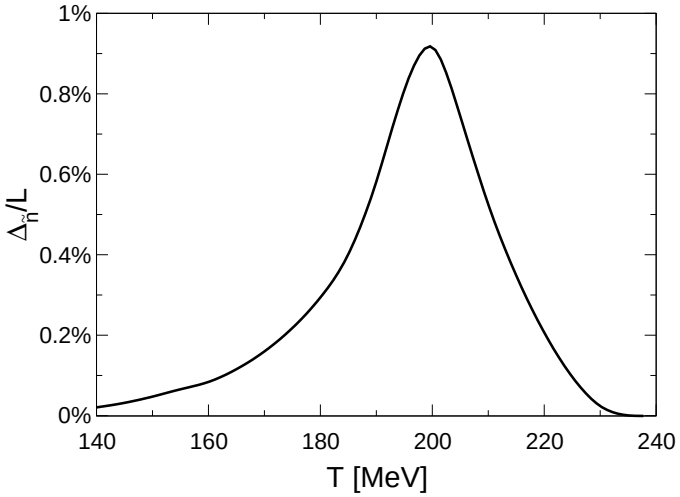

Figure 5.10: Comparison of the Polyakov loop and the dual density. Figure taken from [206].

Fig. 5.7 displays the pion decay constant as a function of imaginary chemical potential and temperature, which is proportional to the quark mass parameter $\mathcal{M}_\theta$ evaluated at $\bar{\phi}_\theta$, see Fig. 5.8. Here, in Fig. 5.7, the RW symmetry is not broken. For $T > T_{c,\chi}$ $f_\pi(\theta)$ vanishes and it is non-zero below $T_{c,\chi}$. Due to the chiral limit we find a second order transition. For vanishing temperature it approches 90 MeV. Fig. 5.11 is a plot of the QCD phase diagram at imaginary chemical potential. The chiral and the deconfinement transition agree within the width of the temperature derivative of the Polyakov loop throughout the phase diagram. The deconfinement transition occurs at lower critical temperatures than the chiral transition. This was also found by lattice computations [200, 207, 208]. In the PNJL, see e.g. [191], the lattice results have been reproduced by adjusting model parameters connected to an eight quark interaction. In our approach to QCD with imaginary chemical potential, the coinciding temperatures are a result solely due to the interplay of quantum interactions and have not been adjusted by hand. A first guess suggests that this is also the case at real chemical potential. An estimate of the corresponding quantum fluctuations within a PQM model also leads to coinciding critical temperatures at real chemical potential [90, 91, 100]. Also recent DSE results support this picture [84–86].

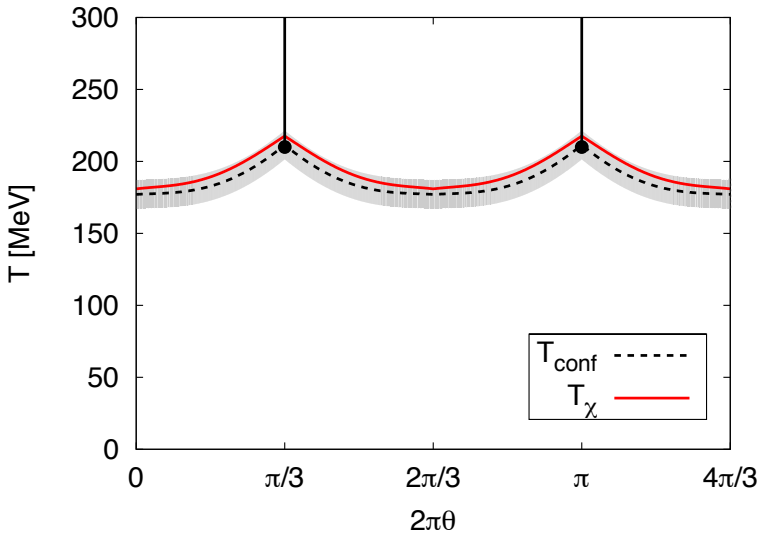

Figure 5.11: The QCD phase diagram at imaginary chemical potential. The grey band represents the width of the susceptibility of the Polyakov loop. The dashed line gives the crossover temperature, the solid line stands for the chiral phase transition. Black dots indicate the endpoints of the Polyakov loop RW transitions.

Chapter 6

The QCD phase diagram at real chemical potential

In the last chapter we presented the first results on $\mu = 0$ at non-zero temperature. In this chapter we apply the fully rebosonised flow equations and determine the masses of the matter sector at vanishing temperature and chemical potential. Next, we show preliminary results on the QCD phase diagram at real chemical potential. Then we compare the Yang–Mills and the glue Polyakov loop potential and explain how the matching of the YM and the glue temperature scales improve model studies, like the PQM model. Therefore we present results for the thermodynamic observables and compare them to lattice results.

6.1 Vanishing temperature and chemical potential

At vanishing temperature and vanishing chemical potential we study $N_f = 2$ QCD in the chiral limit given by the truncation in Eqn. (4.1). Here we make use of the fully rebosonised equations given in Sec. 4.3 and utilise the threshold functions given in App. B.1. Our initial conditions at vanishing chemical potential and temperature are given in App. C.3. Note that we do not fix the pion decay constant, but only match the coupling α_s to the 2-loop perturbative result in the UV. We apply the rebosonisation technique from Subsec. 3.4.2. Apart from the coupling in the UV, we do not fix any other values. Here, the gluon and ghost propagators are fully momentum dependent [152]. It is an upgrade of the setup we utilised at real chemical potential, see Sec. 6.2. Before incorporating non-vanishing temperature and quark chemical potential, we calculate the pion decay constant and the quark mass in the IR. The running of the coupling α_s is derived from the corresponding decoupling propagators [152], so that in the IR the coupling must vanish.

6.1.1 Results

At vanishing chemical potential and temperature we find the pion decay constant to be $f_\pi = 62.6$ MeV, the quark mass $M_\psi = 461.3$ MeV and the σ-mass $M_\sigma = 194$ MeV [70]. Although these values deviate from the physical ones we emphasise that this is work in

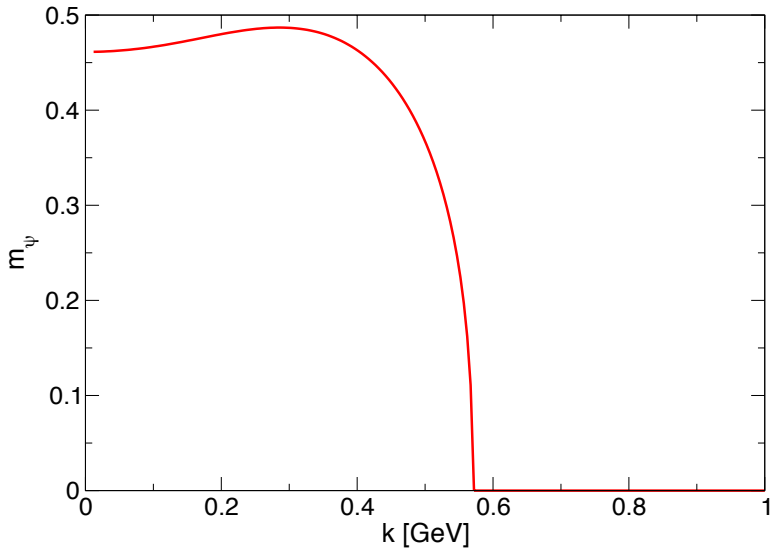

Figure 6.1: The quark mass as a function of momentum scale k at vanishing temperature and chemical potential. It is non-vanishing when chiral symmetry is broken.

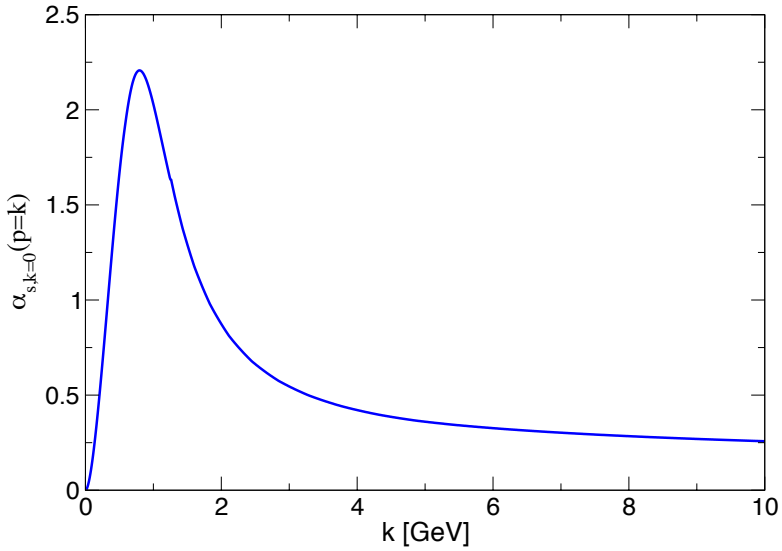

Figure 6.2: The running coupling $\alpha_{s,k=0}(p = k)$ at vanishing temperature and chemical potential for YM theory. Due to the decoupling behaviour of the propagators it vanishes in the IR. The data was obtained in [152].

progress. The definitions we used here are

$$f_\pi = \sigma_0, \quad M_\psi = h\,\sigma_0 \text{ and } M_\sigma = \sqrt{\lambda_\sigma}\sigma_0, \tag{6.1}$$

evaluated in the IR. All couplings and masses strongly depend on the strong coupling α_s, see the flow equations in Sec. 4.3, such that e.g. a small change in the normalisation leads to a large change in the results. For the values above we utilised the YM coupling from [152], see Fig. 6.2. For $k \to 0$, α_s also vanishes, as the ghost and gluon propagators exhibit a decoupling behaviour in the IR. Fig. 6.1 shows the scale dependent quark mass which is non-zero in the chiral symmetry broken phase and it vanishes the symmetric phase. We find stable flows for the couplings and anomalous dimensions where we show exemplarily the scale dependent Yukawa coupling in Fig. 4.11 and 4.12. The figures show that if we vary the initial conditions in the UV, the result in the IR does not change. Especially changing the initial UV scale, Λ_{UV}, yields interesting properties: the flow of the Yukawa coupling is driven to the solution when Λ_{UV} varies from $2 - 90$ GeV, however if Λ_{UV} is smaller, the flow cannot drive the system completely back to the correct solution as not enough momentum is left. This causes errors in the flow of the other couplings, as the mid-momentum regime is very important for the dynamics of the system. Therefore it is necessary to choose Λ_{UV} above 2 GeV, at least when keeping the initial conditions for the other couplings fixed. In Fig. 4.12 we keep Λ_{UV} fixed and change the other initial conditions and we also find very stable flows.

6.2 Finite μ and T

We study real chemical potential with two degenerate quark flavours in the chiral limit given by the truncation in Eqn. (4.1) and we include the momentum dependent wave function renormalisations [154] with the quark vacuum polarisation in the anomalous dimension of the gluon, see Sec. 4.7. We implement the same initial conditions as with imaginary chemical potential, see App. C.4. First we tried to include also a scale dependent gauge field background φ, however we find that the change to the results is minimal compared to the numerical effort, as the effective potential, the Polyakov loop potential, only builds up late in the flow, see Fig. 6.3. The small oscillations are due to the $3d$ regulator function but have little impact on the results. Therefore we drop the scale dependence of φ. Note that it still is temperature dependent. We fit the flow contribution of the ghost to the gluon propagator to the ones obtained earlier. We match them such that in the IR it coincides with the anomalous dimension for the gluon and in the UV with the anomalous dimension of the ghost, see Fig. 4.13. The flow includes the scale dependent scalar coupling λ_σ, the minimum of the effective potential κ and the trivial running of the symmetry breaking parameter c, the flow equations are given in Sec. 4.6. The Yukawa coupling has a non-vanishing value at Λ_{UV} but does not flow and is adjusted such that in the IR the pion decay constant is 90 MeV and the quark mass is 300 MeV. We match α_s at 10 GeV to the perturbative value. We do not match any other quantities, in particular we do not fit to thermodynamics from the lattice or else. The contraints on the Yukawa coupling amounts to bosonising the system in the UV.

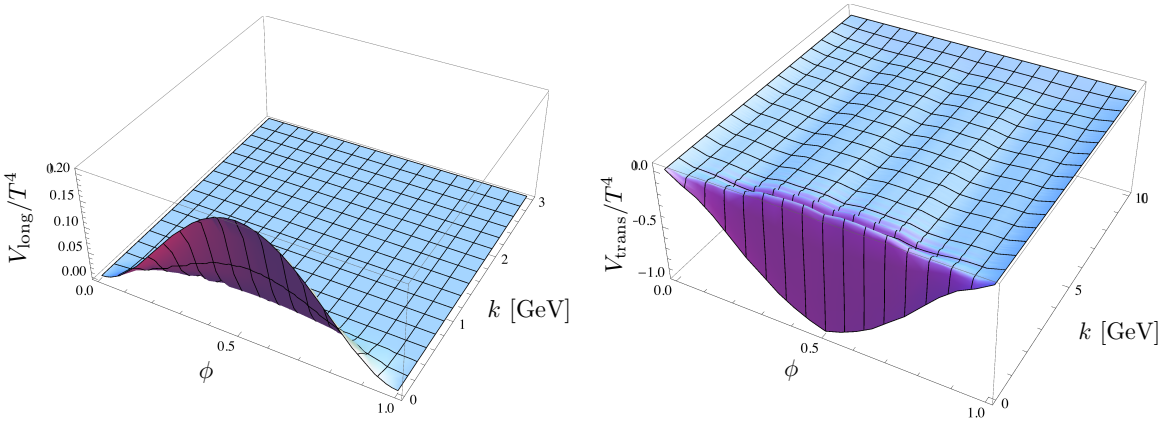

Figure 6.3: The longitudinal (left panel) and the transversal (right panel) component of the scale dependent effective potential for $SU(2)$. The final form of the potential builds up late in the flow.

6.2.1 Results

We show the $N_f = 2$ phase diagram in the chiral limit at real quark chemical potential, see Fig. 6.4. The chiral and the confinement–deconfinement transitions seem to agree within the width of the deconfinement crossover. Interestingly, the chiral transition seems to lie above the confinement–deconfinement transition, however this picture has not been clarified [71]. We find good agreement with DSE calculations [84–86] and FRG PQM model calculations [91, 100] for the critical temperatures of the transitions, see Fig. 6.5. From our preliminary results we estimate that if a critical endpoint exists, it seems to lie at larger chemical potential. Further analyses involving the full temperature (this includes the explicit and implicit temperature dependence) and momentum dependent propagators are necessary to support or disprove this guess [209]. Lattice calculations, see e.g. [210], DSE [84, 85] and PQM [91] results shown in Fig. 6.5 support this estimate.

Fig. 6.5 is an overlay of results for the QCD phase diagram from DSE [84], FRG model [91] and our FRG [71] calculations. All results display the chiral and the confinement–deconfinement transitions. The gray band stands for the width of the confinement–deconfinement crossover from Ref. [91] and within this width and also the width we find, see Fig. 6.4, the transitions agree. As mentioned before, all results estimate a critical endpoint at larger quark chemical potential.

6.3 Comparison of the glue and the Yang–Mills Polyakov loop potential

6.3.1 Matching the temperature scales

Models like the PQM or PNJL usually fit the dynamical glue sector at vanishing chemical potential and temperature to the Yang–Mills lattice thermodynamics and use the temperature

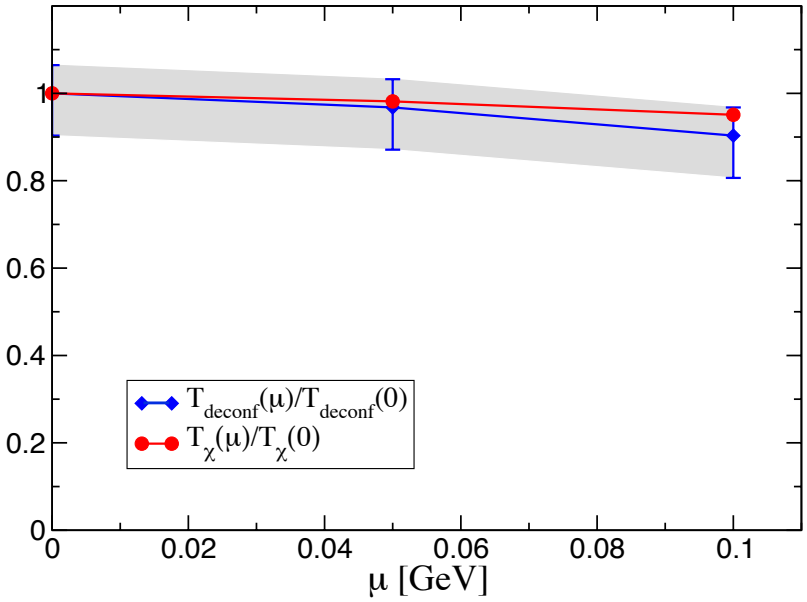

Figure 6.4: The phase diagram at real chemical potential [71]. The grey area corresponds to the width of the crossover associated with the width of the susceptibility of the Polyakov loop.

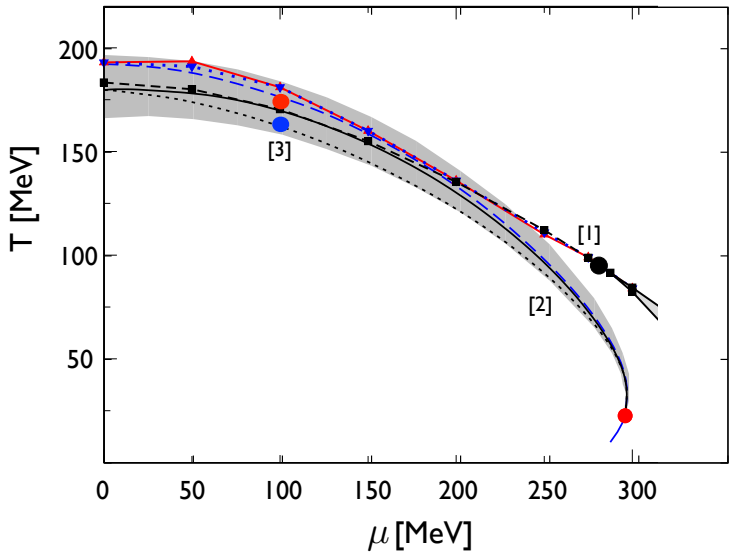

Figure 6.5: The QCD phase diagram from results obtained by DSE Ref. [84], given by data curves [1], FRG PQM model Ref. [91], see curves [2], and FRG Ref. [71], given by points [3]. This plot is an overlay of the results of the different groups. All results are in very good agreement. Here both the chiral and the confinement–deconfinement transitions are shown.

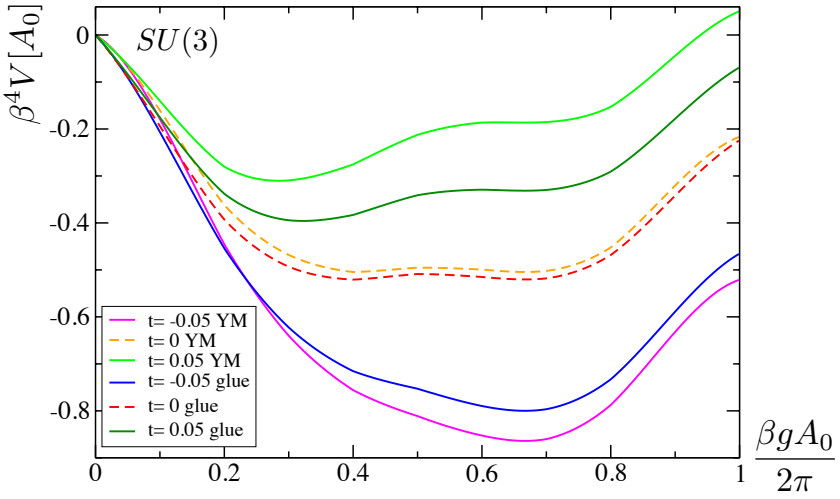

Figure 6.6: Comparison of the YM and the QCD glue potential for various reduced temperatures t. Note that here, only the glue potential of the full QCD Polyakov loop potential is plotted, the fermionic part differs in periodicity and has to be added to the glue part to obtain the full QCD potential. For the translation of the temperature scales only the glue potential is relevant.

dependency of the Polyakov loop for the Polyakov loop potential. The form of the Yang–Mills (only ghost and gluon contributions, so the pure gauge sector without any quark or matter contributions to the propagators) and the glue (contains also the vacuum polarisation of the gluon by the quarks and its feed-back to the ghosts) potential does not change, however the temperature scales do. The problem is that both scales, the Yang–Mills and the glue scale are very different. Parameters like the number of flavours and the chemical potential are one of two examples that change the pure gauge (Yang–Mills) scale. It is therefore beneficial for model studies to fit to the ansatz for the Polyakov loop potential to the glue scale. This was anticipated in [90] where the authors use a phenomenological HTL approximation to model the differences in the scales.

The Polyakov loop we implement depends on the expectation value of the zero component of the gauge field, $L[\langle A_0 \rangle]$, and is an upper limit via the Jensen inequality to the expectation value of the Polyakov loop variable which depends on the zero component of the gauge field, $\langle L[A_0] \rangle$, see Sec. 2.5. The Polyakov loop potential was derived in Sec. 2.7, where the pure Yang–Mills potential stems from [146] and the full glue potential was utilised in [68, 72]. In the current approximation the Yang–Mills Polyakov loop potential shows a phase transition at $T_c = 276$ MeV [146], whereas the glue potential shows a phase transition at $T_c = 203$ MeV [72]. To determine the scale factor translating the Yang-Mills temperature scale to the glue temperature scale, we can look at the form of the potentials, see Fig. 6.6.

Although the temperature scales differ, the form of the effective potential for the gauge

sector of QCD does not, see Fig. 6.6. We can use this property to fit the YM to the glue potential. Therefore we define the reduced temperatures

$$t_{\rm glue} = \frac{T - T_{\rm cr}^{\rm glue}}{T_{\rm cr}^{\rm glue}} \quad \text{and} \quad t_{\rm YM} = \frac{T - T_{\rm cr}^{\rm YM}}{T_{\rm cr}^{\rm YM}}, \tag{6.2}$$

where we find for the critical temperatures $T_{\rm cr}^{\rm glue} = 203$ MeV [72][1] and $T_{\rm cr}^{\rm YM} = 276$ MeV [146]. Then the comparison of the forms of the potential yields the translation of the two temperature scales

$$t_{\rm YM}(t_{\rm glue}) \approx 0.57\, t_{\rm glue}, \tag{6.3}$$

which can now serve as input for model studies. Note that this approximation holds only for small to moderate temperatures. At high temperatures the slope of Eqn. (6.3) saturates, where the potentials reach their asymptotic perturbative form, the Weiss potential, see Subsec. 2.7.1. Fig. 6.6 shows the comparison of the YM (light colours) and glue (dark colours) potential for various reduced temperatures t. The similarities of the form is apparent.

6.3.2 Results for the thermodynamics of a PQM model

We utilise the results for the change in the YM temperature scale in a PQM model with an logarithmic ansatz for the Polyakov loop potential [73]. Similar calculations have been performed in [211], where lattice propagators were utilised.

In the PQM model the Polyakov loop $\Phi(\vec{x})$ and its Hermitian conjugate $\bar{\Phi}(\vec{x})$ are given by

$$\Phi(\vec{x}) = \frac{1}{N_c}\langle \mathrm{Tr}\; L(\vec{x})\rangle, \quad \bar{\Phi}(\vec{x}) = \frac{1}{N_c}\langle \mathrm{Tr}\; L^\dagger(\vec{x})\rangle. \tag{6.4}$$

One can then construct an ansatz for the effective potential such that it captures confinement properties for pure $SU(3)$ YM theory. Usually the parameters of the model are fitted to the results of the Polyakov loop and the thermodynamic observables of lattice results in pure YM theory [126, 212, 213]. Here the effective potential is given by a logarithmic ansatz

$$\frac{U(\Phi,\bar{\Phi},T)}{T^4} = -\frac{1}{2}\, a(T)\, \Phi\bar{\Phi} + b(T)\, \log\left[1 - 6\,\Phi\bar{\Phi} + 4\,\left(\Phi^3 + \bar{\Phi}^3\right) - 3\,\left(\Phi\bar{\Phi}\right)^2\right] \tag{6.5}$$

where the explicit temperature dependency enters through the functions

$$a(T) = a_0 + a_1\left(\frac{T_0}{T}\right) + a_2\left(\frac{T_0}{T}\right)^2 \tag{6.6}$$

and

$$b(T) = b_3\left(\frac{T_0}{T}\right)^3. \tag{6.7}$$

The parameters have been adjusted to the lattice results [214, 215] of the Polyakov loop and the equation of state and are obtained from Ref. [213]. We then use the change in temperature

[1] Note that this is not the critical temperature obtained from the full QCD effective potential but only the contribution stemming from the glue part of the potential.

scale from YM to glue, see Eqn. (6.3) which also contains the back coupling of the matter sector to the pure YM sector, see e.g. Fig. 4.3,

$$\frac{U_{\rm YM}(\Phi,\bar{\Phi},T_{\rm YM})}{T_{\rm YM}^4} = \frac{U_{\rm glue}(\Phi,\bar{\Phi},T_{\rm glue})}{T_{\rm glue}^4}. \tag{6.8}$$

The grand canonical potential of the $N_f = 2+1$ PQM model further contains also a contribution from the quark-meson potential and the quarks. Where the mesonic potential is given by [99, 216]. The quark contribution contains a coupling to the mesons via terms proportional to the Yukawa coupling and a coupling to the glue sector through terms proportional to the Polyakov loop [99, 216].

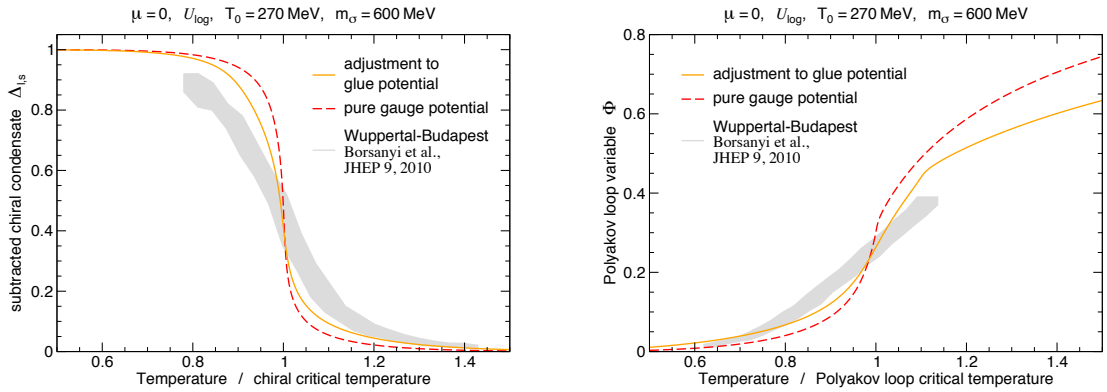

Figure 6.7: The order parameters from the PQM model with the glue temperature scale. The left panel shows the subtracted chiral condensate $\Delta_{l,s}$ and the right panel shows the Polyakov loop variable as functions of temperature normalised with the confinement–deconfinement or the chiral critical temperature. Both do not change drastically when one includes the glue temperature scale (orange solid lines), however they are smoother compared to the pure YM results (red dashed curves). The lattice data (grey) was taken from [217]. $\Delta_{l,s}$ is defined as the fraction of the difference of the non-strange and the strange chiral condensate at non-zero temperature divided by the same difference at zero temperature.

The thermodynamic observables we study in the following are pressure p, entropy density s and energy density ϵ and are derived from the grand canonical ensemble $\Omega = -T\ln Z/V$, where Z is the partition function and V is the volume and are given by

$$p = -\Omega \tag{6.9}$$
$$s = -\frac{\partial\Omega}{\partial T} \tag{6.10}$$
$$\epsilon = \Omega + Ts. \tag{6.11}$$

The results are shown in Figs 6.7, 6.8 and 6.9. The glue temperature scaling does not have a big effect on the order parameters of the chiral and the confinement–deconfinement transition,

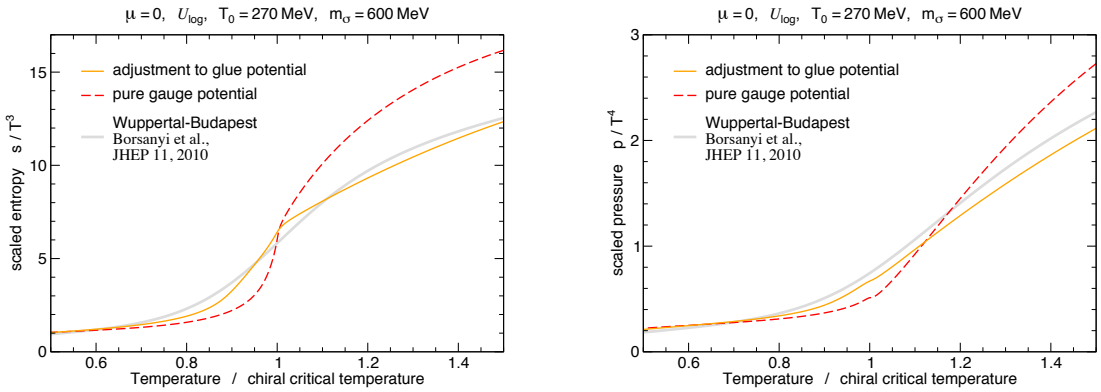

Figure 6.8: The left panel shows the entropy s/T^3 and the right panel shows the pressure p/T^4 as functions of temperature normalised with the chiral critical temperature. The lattice data stems from [217] and is given by the grey solid line. The red dashed curve utilises the pure YM temperatures in the Polyakov loop potential whereas the orange solid line includes the new improved glue temperature scaling. The new results agree very well with the lattice results.

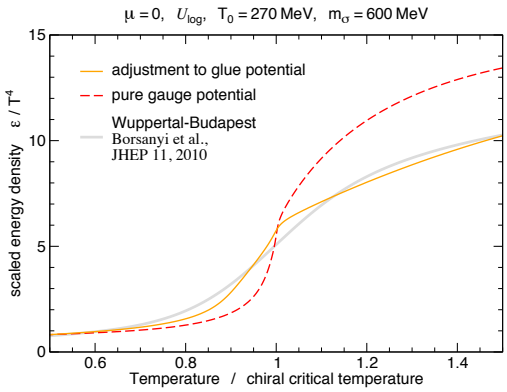

Figure 6.9: The energy density ϵ/T^4 as a function of temperature normalised to the chiral critical temperature. The energy density with the adjusted glue temperature (orange solid line) is in very good agreement with the lattice results (grey solid line).

however they are smoother than the pure YM results. The difference between the YM and the glue temperature scaling however does influence the thermodynamic observables. The entropy, the pressure and the energy density are in very good agreement with the lattice results. The results are improved significantly compared to the YM results.

Chapter 7

Conclusion

In this thesis we studied QCD with two degenerate massless quark flavours with the Functional Renormalisation Group at imaginary and real chemical potential. The aim was to investigate the chiral and the confinement–deconfinement transitions and their interplay in the QCD phase diagram.

To this end we derived the order parameters for both transitions, the chiral condensate for the matter sector of QCD and the Polyakov loop for the gauge sector. The information about the dynamics of the system is stored in the effective potentials from which the order parameters are derived, so the mesonic potential for the matter sector and the Polyakov loop potential for the gauge sector.

Due to the non-perturbative nature of QCD we applied the Functional Renormalisation Group. The flow of the effective average action is described by the Wetterich equation. Our ansatz included a vertex expansion up to third order in powers of the fields. The FRG is an ideal method to study the QCD phase diagram as it can in principle scan all temperatures and chemical potentials and has no difficulties at large coupling strengths or light quark masses. The rebosonisation technique enables the theory to form bound states naturally during the flow from the UV to the IR. We derived the general equations in Chap. 3.

In Chap. 4 we derived all technical details for our calculation. We specified the truncation which includes in the matter sector the sigma meson, the pions and the quarks, and the ghosts and gluons in the gauge sector. We coupled both through the full propagators containing the back-reaction of the others and solved the flow equations for the couplings and anomalous dimensions simultaneously. One key ingredient was the running of the strong coupling α_s which also captured the vacuum polarisation of the quark to the gluon propagator. In this chapter we also derived the flow equations and their rebosonised versions for all couplings within our truncation at zero and non-zero temperature and chemical potential.

In Chap. 5 we studied QCD at imaginary and vanishing chemical potential and non-zero temperature. To this end we derived the properties of the QCD phase diagram at imaginary chemical potential and suggested new order parameters, the dual order parameters, that actually stem from the matter sector of QCD but are sensitive to the confinement–deconfinement transition. We showed that imaginary chemical potential is formally the same as gener-

alised boundary conditions for the quark fields. Then we computed the order parameters, the Polyakov loop, the dual density and the pion decay constant at vanishing and imaginary chemical potential. At zero chemical potential we found a second order chiral transition and a critical temperature of $T_c = 181$ MeV. For the confinement–deconfinement crossover we computed the susceptibilities of the Polyakov loop and the dual density and found that both peak at about $T_c \approx 178$ MeV. Furthermore we calculated the deviation of the Polyakov loop and the dual density and found that they agree on the percent level. The critical temperatures also agreed within the width of the confinement–deconfinement crossover with lattice, DSE and FRG PQM model studies. Finally we computed the phase diagram at imaginary chemical potential and we found that for all values of the imaginary chemical potential the transitions agree. The phase diagram displays the Roberge–Weiss periodicity. The phase boundaries also agree with lattice studies.

In Chap. 6 we first used the rebosonised flow equations and included the anomalous dimensions for the scalar field and the quarks to determine the values of the masses of the matter sector in the IR, like the dynamical quark mass and the mass of the sigma-meson at vanishing temperature and chemical potential. We found very stable flows for the couplings, like the Yukawa and the scalar coupling, when we varied the initial conditions or the initial UV scale. We embeded the Yang–Mills coupling α_s obtained from a fully momentum dependent FRG YM study [152]. Unfortunately we also found that a small change in the normalisation changes the results as all flow equations for the couplings depend on it, especially the masses of the matter sector. Nevertheless the results are the first obtained with two degenerate massless flavours in QCD with the FRG in the chiral limit utilising the full rebosonised equations. Then we showed the phase diagram at real chemical potential for small to moderate values of the chemical potential where we combined the propagators obtained by [154] with the quark vacuum polarisation of the gluon. We also found that a scale dependence of the gauge field background does not affect the IR results of the effective potential, as it only builds up late in the flow. A comparison of our results for the chiral and the confinement–deconfinement transitions with DSE and FRG PQM model studies shows very good agreement. From these data a first estimate for the location of the critical endpoint in the QCD phase diagram suggested that it lies at larger chemical potential. Next we compared the Yang–Mills and the glue effective potentials of the gauge sector of QCD. We found that the form of the potentials hardly changes, however the temperature scales do. We matched the potentials and fit the reduced temperatures, such that we could translate the YM temperatures to the glue temperatures. Then we utilised this in a PQM model to improve the gauge dynamics. So instead of the YM scaling of the temperatures we used the glue scaling in an logarithmic ansatz for the effective potential for the Polyakov loop. We compared the results for the order parameters and the thermodynamic quantities such as the pressure, the entropy and the energy density and we found that the order parameters exhibit only small changes however the thermodynamic observables match the lattice results very well. This simple adaption of the glue temperature scale in the effective potential can thus improve model studies significantly.

The results we presented here are all in very good agreement with other non-perturbative methods. The next steps contain the fully momentum and temperature dependent propagators in the gauge sector and the corresponding strong running coupling α_s. Apart from a study of very light quarks, including the physical quark masses and going to $N_f = 2 + 1$ are very interesting thus leading to a map of the Columbia plot with FRG data. Another big step is including baryonic degrees of freedom, which are important at large chemical potential. This can be done in a similar fashion as it has already been done in Ultra Cold Atoms by the formation of trions. It seems that the combined effort will solve the mystery of the QCD phase diagram.

Appendix A

Notations and Conventions

A.1 Units

All units are natural units, where

$$\hbar = k_B = c = 1. \tag{A.1}$$

This implies that 1 meter and 1 Kelvin are

$$1\,\mathrm{m} \approx 5.1 \cdot 10^{12}\,\mathrm{MeV}^{-1} \tag{A.2}$$

and

$$1\,\mathrm{K} \approx 8.6 \cdot 10^{-11}\,\mathrm{MeV}. \tag{A.3}$$

This also means that a phase transition of about 200 MeV corresponds to a temperature of $2.3 \cdot 10^{12}$ K which easily exceeds the core temperature of the sun which is about 10^6 K. The proton has a size of about 1 fm= 10^{-15} m, the quarks and gluons are point-like in the standard model, so below 10^{-18} m. It is therefore necessary to go to extremely high energies in order to probe the phase transition of QCD in colliders or one can study it in the early universe (which is currently out of reach).

A.2 Dirac Algebra

We use the standard convention for the Hermitian γ-matrices. Due to a non-vanishing chemical potential or non-zero temperature, one has to pay attention to the Dirac traces, as some γ-matrices have dimension 4 and some have dimension 3. To do more elaborate calculations involving traces over more than six γ-matrices, it is advisable to utilise a CAS like Fleq [152], which can also take care of the different dimensions involved. So the anti-commutator for the $d = 4$ Hermitian γ-matrices in Euclidean space-time is given by

$$\{\gamma_\mu, \gamma_\nu\} = 2\delta_{\mu\nu}\mathbb{1}_4, \tag{A.4}$$

which are

$$\gamma^\mu = \begin{pmatrix} 0 & -i\tau^\mu \\ i\tau^\mu & 0 \end{pmatrix}, \gamma^5 = \begin{pmatrix} \mathbb{1}_2 & 0 \\ 0 & -\mathbb{1}_2 \end{pmatrix},$$

with $\gamma^5 = \gamma^1\gamma^2\gamma^3\gamma^0$, $\tau^\mu = (i\mathbb{1}_2, \tau^j)$ and the τ^j are the standard Pauli matrices, see App. A.3.

A.3 Generators and representations

The $SU(N)$ gauge group can be described in several irreducible representations. Two of them are the fundamental and the adjoint representation, both having different dimensions. The dimensions are related by the Casimir operators

$$d^{\text{fund}}\, C_2^{\text{fund}}(N) = d^{\text{adj}}\, C^{\text{fund}}(N). \tag{A.5}$$

For any matrices in the fundamental representation the trace of the generators of the $SU(N)$ is given by

$$\text{Tr}\; t^a t^b = C(N)\, \delta^{ab}. \tag{A.6}$$

And one finds in the *fundamental* representation for the Casimirs

$$\begin{aligned} C(N) &= \frac{1}{2} \\ C_2(N) &= \frac{N^2-1}{2N} \end{aligned} \tag{A.7}$$

and its dimension is $d^{\text{fund}} = N$. In the *adjoint* representation the Casimirs are given by

$$C(N) = N = C_2(N) \tag{A.8}$$

with the dimension $d^{\text{adj}} = N^2 - 1$. For the structure constants one obtains

$$f^{acd} f^{bcd} = C_2(N)\delta^{ab}. \tag{A.9}$$

The $SU(2)$ generators in the fundamental representation are given by the Pauli matrices

$$\tau^1 = \begin{pmatrix} 0 & 1 \\ 1 & 0 \end{pmatrix}, \tau^2 = \begin{pmatrix} 0 & -i \\ i & 0 \end{pmatrix}, \tau^3 = \begin{pmatrix} 1 & 0 \\ 0 & -1 \end{pmatrix},$$

and in $SU(3)$ they are given by the Gell–Mann matrices in the fundamental representation. Here we give the 3- and the 8-direction

$$\lambda^3 = \begin{pmatrix} 1 & 0 & 0 \\ 0 & -1 & 0 \\ 0 & 0 & 0 \end{pmatrix}, \qquad \lambda^8 = \frac{1}{\sqrt{3}} \begin{pmatrix} 1 & 0 & 0 \\ 0 & 1 & 0 \\ 0 & 0 & -2 \end{pmatrix}.$$

In the adjoint representation the two generators in $SU(3)$ are given by the 8×8 matrices

$$\begin{pmatrix} 0 & i & 0 & 0 & 0 & 0 & 0 & 0 \\ -i & 0 & 0 & 0 & 0 & 0 & 0 & 0 \\ 0 & 0 & 0 & 0 & 0 & 0 & 0 & 0 \\ 0 & 0 & 0 & 0 & \frac{i}{2} & 0 & 0 & 0 \\ 0 & 0 & 0 & -\frac{i}{2} & 0 & 0 & 0 & 0 \\ 0 & 0 & 0 & 0 & 0 & 0 & -\frac{i}{2} & 0 \\ 0 & 0 & 0 & 0 & 0 & \frac{i}{2} & 0 & 0 \\ 0 & 0 & 0 & 0 & 0 & 0 & 0 & 0 \end{pmatrix}, \quad \begin{pmatrix} 0 & 0 & 0 & 0 & 0 & 0 & 0 & 0 \\ 0 & 0 & 0 & 0 & 0 & 0 & 0 & 0 \\ 0 & 0 & 0 & 0 & 0 & 0 & 0 & 0 \\ 0 & 0 & 0 & 0 & \frac{i\sqrt{3}}{2} & 0 & 0 & 0 \\ 0 & 0 & 0 & -\frac{i\sqrt{3}}{2} & 0 & 0 & 0 & 0 \\ 0 & 0 & 0 & 0 & 0 & 0 & \frac{i\sqrt{3}}{2} & 0 \\ 0 & 0 & 0 & 0 & 0 & -\frac{i\sqrt{3}}{2} & 0 & 0 \\ 0 & 0 & 0 & 0 & 0 & 0 & 0 & 0 \end{pmatrix}.$$

A.3.1 Eigenvalues of the Dirac operator in the fundamental and adjoint representation

The eigenvalues of the zero component of the Dirac operator including imaginary chemical potential in the fundamental representation in the 3- and 8-direction are given by

$$\mathrm{EV}_i^{\mathrm{fund}} = \left\{ \frac{1}{2}\left(6(2\pi)\theta + \hat{\varphi}_3 + \frac{\hat{\varphi}_8}{\sqrt{3}}\right), \frac{1}{2}\left(-\hat{\varphi}_3 + \frac{\hat{\varphi}_8}{\sqrt{3}}\right), \frac{1}{2}\left(-\frac{2\hat{\varphi}_8}{\sqrt{3}}\right)\right\}. \tag{A.10}$$

In the adjoint representation we find for the zero component of the Dirac operator

$$iD_0 = 2\pi T \left(n\mathbb{1}_8 + \frac{1}{2\pi} \begin{pmatrix} 0 & -\varphi_3 & 0 & 0 & 0 & 0 & 0 & 0 \\ \varphi_3 & 0 & 0 & 0 & 0 & 0 & 0 & 0 \\ 0 & 0 & 0 & 0 & 0 & 0 & 0 & 0 \\ 0 & 0 & 0 & 0 & -\frac{\varphi_3}{2} - \frac{\sqrt{3}\varphi_8}{2} & 0 & 0 & 0 \\ 0 & 0 & 0 & \frac{\varphi_3}{2} + \frac{\sqrt{3}\varphi_8}{2} & 0 & 0 & 0 & 0 \\ 0 & 0 & 0 & 0 & 0 & 0 & \frac{\varphi_3}{2} - \frac{\sqrt{3}\varphi_8}{2} & 0 \\ 0 & 0 & 0 & 0 & 0 & \frac{\sqrt{3}\varphi_8}{2} - \frac{\varphi_3}{2} & 0 & 0 \\ 0 & 0 & 0 & 0 & 0 & 0 & 0 & 0 \end{pmatrix} \right).$$

Then we apply the same transformation as in the fundamental representation, see Eqn. (5.24) and we find for the eigenvalues of the glue part of the Polyakov loop potential

$$\mathrm{EV}_i^{\mathrm{adj}} = \left\{ \hat{\varphi}_3 + 3(2\pi)\theta, \frac{\hat{\varphi}_3 + \sqrt{3}\hat{\varphi}_8}{2} + 3(2\pi)\theta, \frac{\hat{\varphi}_3 - \sqrt{3}\hat{\varphi}_8}{2} \right\}. \tag{A.11}$$

Appendix B

Threshold functions

B.1 Threshold functions for $T = 0 = \mu$

These are the threshold functions for vanishing temperature and vanishing chemical potential. The letter B stands for boson and F for fermion, the number of space-time dimensions is $d = 4$.

The threshold functions for the anomalous dimensions are

$$\mathcal{M}_2(\bar{M}_F^2;\eta_F) = \left(1+\bar{M}_F^2\right)^{-4} \tag{B.1}$$

$$\mathcal{M}_4(\bar{M}_F^2;\eta_F) = \left(1+\bar{M}_F^2\right)^{-4} + \frac{1-\eta_F}{d-2}\left(1+\bar{M}_F^2\right)^{-3} - \left(\frac{1}{4}+\frac{1-\eta_F}{2d-4}\right)\left(1+\bar{M}_F^2\right)^{-2} \tag{B.2}$$

$$\mathcal{M}_{1,2}(\bar{M}_F^2,\bar{M}_B^2;\eta_F,\eta_B) = \left(1-\frac{\eta_B}{d+1}\right)(1+\bar{M}_F^2)^{-1}(1+\bar{M}_B^2)^{-2} \tag{B.3}$$

$$\mathcal{M}_{2,2}(\bar{M}_{B1}^2,\bar{M}_{B2}^2;\eta_B) = \left((1+\bar{M}_{B1}^2)^2(1+\bar{M}_{B2}^2)^2\right)^{-1}. \tag{B.4}$$

For the Yukawa coupling we find

$$L_{1,1}^{(FB)}(\bar{M}_F^2,\bar{M}_B^2;\eta_F,\eta_B) = \frac{2}{d}(1+\bar{M}_F^2)^{-1}(1+\bar{M}_B^2)^{-1}\Bigg\{\left(1-\frac{\eta_F}{d+1}\right)(1+\bar{M}_F^2)^{-1} + \left(1-\frac{\eta_B}{d+2}\right)(1+\bar{M}_B^2)^{-1}\Bigg\} \tag{B.5}$$

$$L_{1,2}^{(FB)}(\bar{M}_F^2;\eta_F,\eta_B) = \frac{2}{d}(1+\bar{M}_F^2)^{-2}\Bigg\{\left(1-\frac{2\eta_B}{d+2}+\frac{\eta_F}{d+1}\right) +2(1+\bar{M}_F^2)^{-1}\left(1-\frac{\eta_F}{d+1}\right)\Bigg\}, \tag{B.6}$$

and the flow of the four fermion coupling is proportional to

$$L_{1,1,1}^{(FB)}(\bar{M}_F^2,\bar{M}_{B1}^2,\bar{M}_{B2}^2;\eta_F,\eta_B) = \frac{2}{d}(1+\bar{M}_F^2)^{-2}(1+\bar{M}_{B1}^2)^{-1}(1+\bar{M}_{B2}^2)^{-1}\cdot \cdot\Bigg\{\left((1+\bar{M}_{B1}^2)^{-1}+(1+\bar{M}_{B2}^2)^{-1}\right)\left(1-\frac{\eta_B}{d+2}\right)+\left(2(1+\bar{M}_F^2)^{-1}-1\right)\left(1-\frac{\eta_F}{d+1}\right)\Bigg\}. \tag{B.7}$$

For the effective potential we have

$$l_n^B(\bar{M}_B^2;\eta_B) = \frac{2(\delta_{n,0}+n)}{d}\left(1-\frac{\eta_B}{d+2}\right)(1+\bar{M}_B^2)^{-n+1} \tag{B.8}$$

$$l_n^F(\bar{M}_F^2;\eta_F) = \frac{2(\delta_{n,0}+n)}{d}\left(1-\frac{\eta_F}{d+1}\right)(1+\bar{M}_F^2)^{-n+1}. \tag{B.9}$$

For the rebosonised equations, the substitution $\eta_\sigma \to \eta_\sigma - 2\dot{B}_1 p^2$ with $\dot{B}_1 = \frac{\partial_t \bar{\lambda}_\psi}{2\bar{h}^2}\frac{1}{k^2}$ has to be made in all of the above functions.

B.2 Threshold functions for finite T and μ

At finite temperature and chemical potential we use a $3d$ optimised regulator and we implement the threshold functions for the effective potential in the following way [89]

$$l_0^B(\bar{M}_B^2,\bar{T};\eta_B,Z_B) = \frac{2}{d-1}\frac{1}{\sqrt{1+\bar{M}_B^2}}\left(1-\frac{\eta_B}{d+1}\right)\frac{\frac{1}{2}+n_B(\bar{T},\bar{M}_B^2)}{\sqrt{Z_B}} \tag{B.10}$$

$$\begin{aligned} l_0^F(\bar{M}_F^2,\bar{T},\bar{\mu},\hat{\varphi};\eta_F,Z_F) &= \frac{1}{d-1}\frac{1}{\sqrt{1+\bar{M}_F^2}}\left(1-\frac{\eta_F}{d}\right)\cdot \\ &\quad \cdot\frac{1-n_F(\bar{T},\bar{M}_F^2,\bar{\mu},\hat{\varphi})-n_F(\bar{T},\bar{M}_F^2,-\bar{\mu},-\hat{\varphi})}{Z_F}, \end{aligned} \tag{B.11}$$

where the Bose–Einstein n_B and the Fermi–Dirac n_F distributions are given by

$$n_B(\bar{T},\bar{M}_B^2) = \frac{1}{e^{\frac{\sqrt{1+\bar{M}_B^2}}{\bar{T}}}-1} \tag{B.12}$$

$$n_F(\bar{T},\bar{M}_F^2,\bar{\mu},\hat{\varphi}) = \frac{1}{e^{\frac{\sqrt{1+\bar{M}_F^2}}{\bar{T}}-\frac{\bar{\mu}}{\bar{T}}-2\pi\, i\,\hat{\varphi}}+1} \tag{B.13}$$

The threshold functions for n larger than 0 are obtained by derivatives with respect to the masses

$$l_1^B = -\partial_{\bar{M}_B^2} l_0^B \tag{B.14}$$

$$l_1^F = -\partial_{\bar{M}_F^2} l_0^F \tag{B.15}$$

and so on for all higher n. For the pressure the threshold functions are

$$l_{\text{therm}}^B(\bar{M}_B^2,\bar{T};\eta_B,Z_B) = \frac{2}{d-1}\frac{1}{\sqrt{1+\bar{M}_B^2}}\left(1-\frac{\eta_B}{d+1}\right)\frac{n_B(\bar{T},\bar{M}_B^2)}{\sqrt{Z_B}} \tag{B.16}$$

(B.17)

$$\begin{aligned} l_{\text{therm}}^F(\bar{M}_F^2,\bar{T},\bar{\mu},\hat{\varphi};\eta_F,Z_F) &= \frac{1}{d-1}\frac{1}{\sqrt{1+\bar{M}_F^2}}\left(1-\frac{\eta_F}{d}\right)\cdot \\ &\quad \cdot\frac{n_F(\bar{T},\bar{M}_F^2,\bar{\mu},\hat{\varphi})-n_F(\bar{T},\bar{M}_F^2,-\bar{\mu},-\hat{\varphi})}{Z_F}. \end{aligned} \tag{B.18}$$

Appendix C

Details of the setup and initial conditions

C.1 $4d$ regulators at $T = 0$ and $\mu \neq 0$

For implementing a $4d$ regulator we basically have two choices, where the first does not depend on the chemical potential,

$$R_{\psi\bar{\psi}}^{4d,(\#1)}(q) = Z_{\psi}^{\perp} \not{q}\, r_{\psi}\left(\frac{q^2}{k^2}\right), \tag{C.1}$$

and the second one does

$$R_{\psi\bar{\psi}}^{4d,(\#2)}(q) = Z_{\psi}^{\perp} (\not{q} + i\gamma_0\mu)\, r_{\psi}\left(\frac{q^2}{k^2}\right). \tag{C.2}$$

Let's have a closer look at the regulators and see how their differences influence the resulting propagators. The zero component of the momentum of the second regulator is shifted by the chemical potential, which is not the case for the first one. Then the scale derivatives are

$$\partial_t R_{\psi\bar{\psi}}^{4d,(\#1)} = Z_{\psi}^{\perp} \not{q} \left(\partial_t r_{\psi} - \eta_{\psi}^{\perp} r_{\psi}\right) \tag{C.3}$$

$$\partial_t R_{\psi\bar{\psi}}^{4d,(\#2)} = Z_{\psi}^{\perp} (\not{q} + i\gamma_0\mu) \left(\partial_t r_{\psi} - \eta_{\psi}^{\perp} r_{\psi}\right), \tag{C.4}$$

with the final propagators

$$\begin{aligned} G_{\psi\bar{\psi}}^{4d,(\#1)} &= \left(Z_{\psi}^{\perp} \not{q}(1 + r_{\psi}) + Z_{\psi}^{\parallel} \gamma_0 i\mu - i M_{\psi,k}\right) \cdot \\ &\quad \left[(Z_{\psi}^{\parallel})^2 (q_0(1 + r_{\psi}) + i\mu)^2 + (Z_{\psi}^{\perp})^2 \vec{q}^2 (1 + r_{\psi})^2 + M_{\psi,k}^2\right]^{-1}, \end{aligned} \tag{C.5}$$

$$\begin{aligned} G_{\psi\bar{\psi}}^{4d,(\#2)} &= \left(Z_{\psi}^{\perp} (\not{q} + i\gamma_0\mu)(1 + r_{\psi}) - i M_{\psi,k}\right) \cdot \\ &\quad \left[(Z_{\psi}^{\perp})^2 (\not{q} + i\gamma_0\mu)^2 (1 + r_{\psi})^2 + M_{\psi,k}^2\right]^{-1}. \end{aligned} \tag{C.6}$$

This means that the second regulator shape function also cuts off chemical potential, whereas the first does not. The first one does not distinguish a chemical potential from the zero component of the momentum, which the second one does. This can be used to simplify the Dirac traces. Already the non-zero chemical potential breaks the $O(4)$ symmetry and this could in principle lead to an imaginary result of the Dirac traces.

C.2 Details on the quark vacuum polarisation of the gluon

Here we give some more details to the calculation of the vacuum polarisation of the gluon propagator by the quarks and the result for $Z_\psi^\parallel \neq Z_\psi^\perp$. Therefore we evaluate the digram given in Fig. 4.5. We obtain for the digram before evaluating the integrations and the Matsubara sum with the $3d$ regulator specified in (4.16) for non-zero temperature and chemical potential

$$\begin{aligned}
&-16\, g^2\, C_2(N_c)\, N_c\, N_f\, Z_{A_k}^\perp\, T \sum_n \int \frac{d^3q}{(2\pi)^3} \left(\tilde{G}_{\psi\bar{\psi}}(q_0,\vec{q})\right)^2 \tilde{G}_{\psi\bar{\psi}}(q_0+p_0,\vec{q}+\vec{p}) \cdot \\
&\quad \cdot \left(\partial_t r_\psi - \eta_{\psi,k}^\perp r_\psi\right) \cdot \\
&\quad \cdot \Big[\; (Z_\psi^\parallel)^2 (Z_\psi^\perp)^4\, q_0^2 \left(1 + r_\psi^{\vec{q}+\vec{p}}\right) \frac{1}{\vec{p}^2} (\vec{q}\cdot\vec{p})\, \vec{p}\cdot(\vec{q}+\vec{p}) \\
&\quad -2\, (Z_\psi^\parallel)^2 (Z_\psi^\perp)^4\, q_0(q_0+p_0) \left(1 + r_\psi^{\vec{q}}\right) \vec{q}^2 \\
&\quad -(Z_\psi^\perp)^6 \left(1 + r_\psi^{\vec{q}}\right)^2 \left(1 + r_\psi^{\vec{q}+\vec{p}}\right) \vec{q}^2\, \frac{1}{\vec{p}^2} (\vec{q}\cdot\vec{p})\, \vec{p}\cdot(\vec{q}+\vec{p}) \\
&\quad -2\, (Z_\psi^\perp)^4 \left(1 + r_\psi^{\vec{q}}\right) M_\psi^2\, \vec{q}^2 \\
&\quad -(Z_\psi^\perp)^4 \left(1 + r_\psi^{\vec{q}+\vec{p}}\right) M_\psi^2\, \frac{1}{\vec{p}^2} (\vec{q}\cdot\vec{p})\, \vec{p}\cdot(\vec{q}+\vec{p}) \Big]
\end{aligned} \tag{C.7}$$

where p is the loop momentum. Note that all couplings are dimensionful. And we defined

$$\tilde{G}_{\psi\bar{\psi}}(q_0,\vec{q}) = \left(\frac{\theta\left(k^2-\vec{q}^2\right)}{(Z_\psi^\parallel)^2 (q_0+i\mu)^2 + (Z_\psi^\perp)^2 k^2 + M_{\psi,k}^2} + \frac{\theta\left(\vec{q}^2-k^2\right)}{(Z_\psi^\parallel)^2 (q_0+i\mu)^2 + (Z_\psi^\perp)^2 \vec{q}^2 + M_{\psi,k}^2} \right). \tag{C.8}$$

Now we have to perform the derivatives ∂_p^2, integrate and set $p=0$. It is useful to utilise the integrations in Ref. [155] in App. C. Note that the functions $r_\psi^{\vec{q}+\vec{p}}$ and $\tilde{G}_{\psi\bar{\psi}}(q_0+p_0,\vec{q}+\vec{p})$ depend on p. Then we find for the result

$$\begin{aligned}
&-16\, g^2\, C_2(N_c)\, N_c\, N_f\, Z_{A_k}^\perp\, \frac{1}{(2\pi)^2}\, T \sum_n \\
&\qquad \Big[\frac{1}{5} (Z_\psi^\parallel)^2 (Z_\psi^\perp)^4\, q_0^2\, k^3\, (\hat{G}_{\psi\bar{\psi}})^3\, (-3+2\eta_\psi^\perp) \\
&\qquad + \frac{14}{15} (Z_\psi^\parallel)^2 (Z_\psi^\perp)^6\, q_0^2\, k^5\, (\hat{G}_{\psi\bar{\psi}})^4 \\
&\qquad + \frac{1}{5} (Z_\psi^\perp)^6\, k^5\, (\hat{G}_{\psi\bar{\psi}})^3\, (3-2\eta_\psi^\perp) \\
&\qquad + \frac{2}{5} (Z_\psi^\perp)^6\, k^7\, (\hat{G}_{\psi\bar{\psi}})^4 \\
&\qquad + \frac{14}{15} (Z_\psi^\perp)^4\, M_\psi^2\, k^5\, (\hat{G}_{\psi\bar{\psi}})^4 \\
&\qquad + \frac{1}{5} (Z_\psi^\perp)^4\, M_\psi^2\, k^3\, (\hat{G}_{\psi\bar{\psi}})^3 (-3+2\eta_\psi^\perp) \Big].
\end{aligned} \tag{C.9}$$

Here we used the shorthand

$$\hat{G}_{\psi\bar{\psi}} = \left[(Z_\psi^\parallel)^2 (q_0+i\mu)^2 + (Z_\psi^\perp)^2 k^2 + M_{\psi,k}^2 \right]^{-1}. \tag{C.10}$$

C.3 Initial conditions at $T = 0 = \mu$

For vanishing temperature and chemical potential we chose the following initial conditions for the couplings

$$\begin{aligned} \Lambda_{UV} &= 10\,\text{GeV} && \text{(C.11)} \\ \epsilon(\Lambda_{UV}) = \frac{m_\sigma^2}{k^2} &= 4.89 && \text{(C.12)} \\ h(\Lambda_{UV}) &= 0.001 && \text{(C.13)} \\ \lambda_\sigma(\Lambda_{UV}) &= 0.001, && \text{(C.14)} \end{aligned}$$

The scalar and the Yukawa coupling cannot be set to 0 exactly, as they would otherwise not start to flow but remain at 0. We have varied the initial conditions and the results are stable, see Fig. 4.12. We have also varied the initial momentum scale Λ_{UV}, the flow is fast driven to the stable solution, the results in the IR hardly change. However one has to be careful not start too far in the IR as the flow cannot relax fast enough below $k = 2\,\text{GeV}$, see Fig. 4.11.

C.4 Initial conditions at finite T and imaginary chemical potential

At finite temperature and imaginary chemical potential we use the following initial conditions

$$\begin{aligned} \Lambda_{UV} &= 10\,\text{GeV} && \text{(C.15)} \\ \alpha_s(M_{Z_0}) &= 0.1184 && \text{(C.16)} \\ \epsilon(\Lambda_{UV}) &= 0.37803 && \text{(C.17)} \\ h(\Lambda_{UV}) &= 10/3 && \text{(C.18)} \\ \lambda_\sigma(\Lambda_{UV}) &= 300, && \text{(C.19)} \end{aligned}$$

which have been chosen such that in the IR in the chiral limit we have

$$\begin{aligned} m_\psi &= 0.3\,\text{GeV} && \text{(C.20)} \\ f_\pi &= 0.09\,\text{GeV}. && \text{(C.21)} \end{aligned}$$

Note that in contradistinction to the initial conditions specified in C.3, we include a small symmetry breaking parameter c, which simplifies our numerical effort such that we bosonise at the initial scale $k = \Lambda_{UV}$ and then keep the flow of the Yukawa coupling and the four-fermion coupling at zero.

List of Figures

Permission for Figures

Figure 2.1 on page 13 was printed with kind permission from Springer Science and Business Media and appeared in [74].

Figure 4.4 on page 47 and Figure 4.7 on page 50 were printed with kind permission from Prof. Dr. Jan M. Pawlowski, Heidelberg University, the figures appeared in [146].

Figure 5.2 on page 63 and Figure 5.3 on page 64 were printed with kind permission from Prof. Dr. Owe Philipsen, University of Frankfurt and appeared in [115].

Figure 5.4 on page 64 was printed with kind permission from Prof. Dr. Owe Philipsen, University of Frankfurt and appeared in [76].

Bibliography

[1] H. D. Politzer. Reliable perturbative results for strong interactions? *Phys.Rev.Lett.*, 30:1346–1349, 1973.

[2] D. J. Gross and F. Wilczek. Ultraviolet behavior of non-abelian gauge theories. *Phys.Rev.Lett.*, 30:1343–1346, 1973.

[3] Peter Braun-Munzinger and Johanna Stachel. The quest for the quark-gluon plasma. *Nature*, 448:302–309, 2007.

[4] Hugo Pereira Da Costa. J/ψ production in pp and Pb-Pb with ALICE at the LHC. *AIP Conf.Proc.*, 1441:859–861, 2012.

[5] L. Massacrier. Vector meson production in the dimuon channel in the ALICE experiment at the LHC. *Acta Phys.Polon.Supp.*, 5:477–484, 2012.

[6] Eugenio Scapparone. Latest results from ALICE. 2011. arXiv:1111.2685.

[7] Edward V. Shuryak. What RHIC experiments and theory tell us about properties of quark-gluon plasma? *Nucl.Phys.*, A750:64–83, 2005.

[8] Andreas Schmitt. Dense matter in compact stars: A pedagogical introduction. *Lect.Notes Phys.*, 811:1–111, 2010.

[9] GSI. The QCD phase diagram. *copyright: GSI Helmholtzzentrum fuer Schwerionenforschung GmbH, taken from www.gsi.de.*

[10] S. Durr, Z. Fodor, J. Frison, C. Hoelbling, R. Hoffmann, et al. Ab-Initio Determination of Light Hadron Masses. *Science*, 322:1224–1227, 2008.

[11] Philippe de Forcrand, Seyong Kim, and Owe Philipsen. A QCD chiral critical point at small chemical potential: Is it there or not? *PoS*, LAT2007:178, 2007.

[12] G. Endrodi, Z. Fodor, S.D. Katz, and K.K. Szabo. The Nature of the finite temperature QCD transition as a function of the quark masses. *PoS*, LAT2007:182, 2007.

[13] J. Braun, B. Klein, H.-J. Pirner, and A.H. Rezaeian. Volume and quark mass dependence of the chiral phase transition. *Phys.Rev.*, D73:074010, 2006.

[14] Jens Braun and Bertram Klein. Scaling functions for the O(4)-model in d=3 dimensions. *Phys.Rev.*, D77:096008, 2008.

[15] Jens Braun, Bertram Klein, and Piotr Piasecki. On the scaling behavior of the chiral phase transition in QCD in finite and infinite volume. *Eur.Phys.J.*, C71:1576, 2011.

[16] Jens Braun, Bertram Klein, and Bernd-Jochen Schaefer. On the Phase Structure of QCD in a Finite Volume. *Phys.Lett.*, B713:216–223, 2012.

[17] Bertram Klein, Jens Braun, and Piotr Piasecki. Scaling behavior in two-flavor QCD, finite quark masses and finite volume effects. *PoS*, LATTICE2011:199, 2011.

[18] P. Hasenfratz and F. Karsch. Chemical Potential on the Lattice. *Phys.Lett.*, B125:308, 1983.

[19] John B. Kogut, H. Matsuoka, M. Stone, H.W. Wyld, Stephen H. Shenker, et al. Chiral Symmetry Restoration in Baryon Rich Environments. *Nucl.Phys.*, B225:93, 1983.

[20] Yoichiro Nambu and G. Jona-Lasinio. Dynamical Model of Elementary Particles Based on an Analogy with Superconductivity. 1. *Phys.Rev.*, 122:345–358, 1961.

[21] Yoichiro Nambu and G. Jona-Lasinio. Dynamical model of elementary particles based on an analogy with superconductivity. II. *Phys.Rev.*, 124:246–254, 1961.

[22] Peter N. Meisinger and Michael C. Ogilvie. Chiral symmetry restoration and Z(N) symmetry. *Phys.Lett.*, B379:163–168, 1996.

[23] Robert D. Pisarski. Quark gluon plasma as a condensate of SU(3) Wilson lines. *Phys.Rev.*, D62:111501, 2000.

[24] Kenji Fukushima. Chiral effective model with the Polyakov loop. *Phys.Lett.*, B591:277–284, 2004.

[25] E. Megias, E. Ruiz Arriola, and L.L. Salcedo. Polyakov loop in chiral quark models at finite temperature. *Phys.Rev.*, D74:065005, 2006.

[26] C. Sasaki, B. Friman, and K. Redlich. Susceptibilities and the Phase Structure of a Chiral Model with Polyakov Loops. *Phys.Rev.*, D75:074013, 2007.

[27] U. Ellwanger and C. Wetterich. Evolution equations for the quark - meson transition. *Nucl.Phys.*, B423:137–170, 1994.

[28] Holger Gies and Christof Wetterich. Renormalization flow of bound states. *Phys.Rev.*, D65:065001, 2002.

[29] Holger Gies and Christof Wetterich. Renormalization flow from UV to IR degrees of freedom. *Acta Phys.Slov.*, 52:215–220, 2002.

[30] Holger Gies and Christof Wetterich. Universality of spontaneous chiral symmetry breaking in gauge theories. *Phys. Rev.*, D69:025001, 2004.

[31] Jan M. Pawlowski. Aspects of the functional renormalisation group. *Annals Phys.*, 322:2831–2915, 2007.

[32] S. Floerchinger and C. Wetterich. Exact flow equation for composite operators. *Phys.Lett.*, B680:371–376, 2009.

[33] S. Floerchinger. Exact Flow Equation for Bound States. *Eur.Phys.J.*, C69:119–132, 2010.

[34] L.P. Kadanoff. Scaling laws for Ising models near T(c). *Physics*, 2:263–272, 1966.

[35] Franz J. Wegner and Anthony Houghton. Renormalization group equation for critical phenomena. *Phys.Rev.*, A8:401–412, 1973.

[36] Kenneth G. Wilson. Renormalization group and critical phenomena. 1. Renormalization group and the Kadanoff scaling picture. *Phys.Rev.*, B4:3174–3183, 1971.

[37] Kenneth G. Wilson. Renormalization group and critical phenomena. 2. Phase space cell analysis of critical behavior. *Phys.Rev.*, B4:3184–3205, 1971.

[38] Christof Wetterich. Exact evolution equation for the effective potential. *Phys.Lett.*, B301:90–94, 1993.

[39] Holger Gies. Introduction to the functional RG and applications to gauge theories. 2006. hep-ph/0611146.

[40] Juergen Berges, Nikolaos Tetradis, and Christof Wetterich. Nonperturbative renormalization flow in quantum field theory and statistical physics. *Phys.Rept.*, 363:223–386, 2002.

[41] K. Aoki. Introduction to the nonperturbative renormalization group and its recent applications. *Int. J. Mod. Phys.*, B14:1249–1326, 2000.

[42] M. Reuter. Effective Average Actions and Nonperturbative Evolution Equations. 1996. hep-th/9602012.

[43] M. Salmhofer and C. Honerkamp. Fermionic renormalization group flows: Technique and theory. *Prog. Theor. Phys.*, 105:1–35, 2001.

[44] B. Delamotte, D. Mouhanna, and M. Tissier. Nonperturbative renormalization group approach to frustrated magnets. *Phys. Rev.*, B69:134413, 2004.

[45] C. Bagnuls and C. Bervillier. Exact renormalization group equations. An Introductory review. *Phys.Rept.*, 348:91, 2001.

[46] Igor Boettcher, Jan M. Pawlowski, and Sebastian Diehl. Ultracold atoms and the Functional Renormalization Group. 2012. arXiv:1204.4394.

[47] Janos Polonyi. Lectures on the functional renormalization group method. *Central Eur.J.Phys.*, 1:1–71, 2003.

[48] Bertrand Delamotte. An Introduction to the nonperturbative renormalization group. 2007. cond-mat/0702365.

[49] Oliver J. Rosten. Fundamentals of the Exact Renormalization Group. *Phys.Rept.*, 511:177–272, 2012.

[50] Jens Braun. Fermion Interactions and Universal Behavior in Strongly Interacting Theories. *J.Phys.G*, G39:033001, 2012.

[51] Jean-Paul Blaizot. Non Perturbative Renormalization Group and Bose-Einstein Condensation. 2008. arXiv:0801.0009.

[52] S. Diehl, S. Floerchinger, H. Gies, J.M. Pawlowski, and C. Wetterich. Functional renormalization group approach to the BCS-BEC crossover. *Annalen Phys.*, 522:615–656, 2010.

[53] Michael M. Scherer, Stefan Floerchinger, and Holger Gies. Functional renormalization for the BCS-BEC crossover. 2010. arXiv:1010.2890.

[54] Michael C. Birse. The Renormalisation group and nuclear forces. *Phil.Trans.Roy.Soc.Lond.*, A369:2662–2678, 2011.

[55] Stefan Floerchinger, Sergej Moroz, and Richard Schmidt. Efimov physics from the functional renormalization group. *Few Body Syst.*, 51:153–180, 2011.

[56] B. Friman, K. Hebeler, and A. Schwenk. Renormalization group and Fermi liquid theory for many-nucleon systems. 2012. arXiv:1201.2510.

[57] R.J. Furnstahl. The Renormalization Group in Nuclear Physics. 2012. arXiv:1203.1779.

[58] Uwe C. Tauber. Renormalization Group: Applications in Statistical Physics. *Nucl.Phys.Proc.Suppl.*, 228C:3, 2012.

[59] Jurgen Berges and David Mesterhazy. Introduction to the nonequilibrium functional renormalization group. 2012. arXiv:1204.1489.

[60] Daniel F. Litim and Jan M. Pawlowski. On gauge invariant Wilsonian flows. pages 168–185, 1998. hep-th/9901063.

[61] Bernd-Jochen Schaefer and Jochen Wambach. Renormalization group approach towards the QCD phase diagram. *Phys.Part.Nucl.*, 39:1025–1032, 2008.

[62] Daniel F. Litim. Fixed Points of Quantum Gravity and the Renormalisation Group. 2008. arXiv:0810.3675.

[63] Roberto Percacci. Asymptotic Safety. 2007. arXiv:0709.3851.

[64] Martin Reuter and Frank Saueressig. Quantum Einstein Gravity. *New J.Phys.*, 14:055022, 2012.

[65] H. Schoeller. A perturbative nonequilibrium renormalization group method for dissipative quantum mechanics. Real-time RG in frequency space (RTRG-FS). *European Physical Journal Special Topics*, 168:179–266, February 2009.

[66] Walter Metzner, Manfred Salmhofer, Carsten Honerkamp, Volker Meden, and Kurt Schonhammer. Functional renormalization group approach to correlated fermion systems. *Rev.Mod.Phys.*, 84:299, 2012.

[67] Babette Dobrich and Astrid Eichhorn. Can we see quantum gravity? Photons in the asymptotic-safety scenario. *JHEP*, 1206:156, 2012.

[68] Jens Braun, Lisa M. Haas, Florian Marhauser, and Jan M. Pawlowski. Phase Structure of Two-Flavor QCD at Finite Chemical Potential. *Phys.Rev.Lett.*, 106:022002, 2011.

[69] Lisa M. Haas, Jens Braun, and Jan M. Pawlowski. On the QCD phase diagram at finite chemical potential. *AIP Conf.Proc.*, 1343:459–461, 2011.

[70] Jens Braun, Leonard Fister, Lisa M. Haas, and Jan M. Pawlowski. in preparation.

[71] Jens Braun, Lisa M. Haas, and Jan M. Pawlowski. unpublished results.

[72] Jens Braun, Lisa M. Haas, and Jan M. Pawlowski. in preparation.

[73] Lisa M. Haas, Jan M. Pawlowski, Juergen Schaffner-Bielich, and Rainer Stiele. in preparation.

[74] Siegfried Bethke. The 2009 World Average of alpha(s). *Eur.Phys.J.*, C64:689–703, 2009.

[75] Kenji Fukushima and Tetsuo Hatsuda. The phase diagram of dense QCD. *Rept.Prog.Phys.*, 74:014001, 2011.

[76] Owe Philipsen. Status of the QCD phase diagram from lattice calculations. 2011. arXiv:1111.5370.

[77] Mei Huang. QCD Phase Diagram at High Temperature and Density. 2010. arXiv:1001.3216.

[78] M.A. Stephanov. QCD phase diagram: An Overview. *PoS*, LAT2006:024, 2006.

[79] Bernd-Jochen Schaefer and Mathias Wagner. On the QCD phase structure from effective models. 2008. arXiv:0812.2855.

[80] Wolfram Weise. Nuclear chiral dynamics and phases of QCD. *Prog.Part.Nucl.Phys.*, 67:299–311, 2012.

[81] Masataka Fukugita, Masanori Okawa, and Akira Ukawa. Finite size scaling study of the deconfining phase transition in pure SU(3) lattice gauge theory. *Nucl.Phys.*, B337:181, 1990.

[82] Szabolcs Borsanyi et al. Transition temperature and the equation of state from lattice QCD, Wuppertal-Budapest results. *Acta Phys.Polon.Supp.*, 4:593–602, 2011.

[83] A. Bazavov, T. Bhattacharya, M. Cheng, C. DeTar, H.T. Ding, et al. The chiral and deconfinement aspects of the QCD transition. *Phys.Rev.*, D85:054503, 2012.

[84] Christian S. Fischer, Jan Luecker, and Jens A. Mueller. Chiral and deconfinement phase transitions of two-flavour QCD at finite temperature and chemical potential. *Phys.Lett.*, B702:438–441, 2011.

[85] Jan Luecker and Christian S. Fischer. Two-flavor QCD at finite temperature and chemical potential in a functional approach. *Prog.Part.Nucl.Phys.*, 67:200–205, 2012.

[86] Christian S. Fischer and Jan Luecker. Propagators and phase structure of Nf=2 and Nf=2+1 QCD. 2012. arXiv:1206.5191.

[87] Y. Aoki, G. Endrodi, Z. Fodor, S.D. Katz, and K.K. Szabo. The Order of the quantum chromodynamics transition predicted by the standard model of particle physics. *Nature*, 443:675–678, 2006.

[88] C. DeTar and U.M. Heller. QCD Thermodynamics from the Lattice. *Eur.Phys.J.*, A41:405–437, 2009.

[89] Jens Braun. The QCD Phase Boundary from Quark-Gluon Dynamics. *Eur. Phys. J.*, C64:459–482, 2009.

[90] Bernd-Jochen Schaefer, Jan M. Pawlowski, and Jochen Wambach. The Phase Structure of the Polyakov–Quark-Meson Model. *Phys.Rev.*, D76:074023, 2007.

[91] Tina Katharina Herbst, Jan M. Pawlowski, and Bernd-Jochen Schaefer. The phase structure of the Polyakov–quark-meson model beyond mean field. *Phys.Lett.*, B696:58–67, 2011.

[92] Kenji Fukushima. Phase diagrams in the three-flavor Nambu-Jona-Lasinio model with the Polyakov loop. *Phys.Rev.*, D77:114028, 2008.

[93] M. Asakawa and K. Yazaki. Chiral restoration at finite density and temperature. *Nucl.Phys.*, A504:668–684, 1989.

[94] A. Barducci, R. Casalbuoni, S. De Curtis, Raoul Gatto, and Giulio Pettini. Chiral symmetry breaking in QCD at finite temperature and density. *Phys.Lett.*, B231:463, 1989.

[95] Frank Wilczek. Application of the renormalization group to a second order QCD phase transition. *Int.J.Mod.Phys.*, A7:3911–3925, 1992.

[96] Juergen Berges and Krishna Rajagopal. Color superconductivity and chiral symmetry restoration at nonzero baryon density and temperature. *Nucl.Phys.*, B538:215–232, 1999.

[97] Larry McLerran and Robert D. Pisarski. Phases of cold, dense quarks at large N(c). *Nucl.Phys.*, A796:83–100, 2007. 20 pages, 2 figures.

[98] Bernd-Jochen Schaefer. Critical structure of the QCD medium. *PoS*, CPOD07:032, 2007.

[99] Bernd-Jochen Schaefer and Mathias Wagner. The Three-flavor chiral phase structure in hot and dense QCD matter. *Phys.Rev.*, D79:014018, 2009.

[100] Tina Katharina Herbst, Jan M. Pawlowski, and Bernd-Jochen Schaefer. The Impact of Fluctuations on QCD Matter. 2012. arXiv:1202.0758.

[101] P. Braun-Munzinger, J. Stachel, and Christof Wetterich. Chemical freezeout and the QCD phase transition temperature. *Phys.Lett.*, B596:61–69, 2004.

[102] F. Karsch, E. Laermann, and A. Peikert. Quark mass and flavor dependence of the QCD phase transition. *Nucl.Phys.*, B605:579–599, 2001.

[103] Nils Strodthoff, Bernd-Jochen Schaefer, and Lorenz von Smekal. Quark-meson-diquark model for two-color QCD. *Phys.Rev.*, D85:074007, 2012.

[104] Naseemuddin Khan, Jan M. Pawlowski, and Michael M. Scherer. to be published.

[105] Tomas Brauner, Kenji Fukushima, and Yoshimasa Hidaka. Two-color quark matter: U(1)(A) restoration, superfluidity, and quarkyonic phase. *Phys.Rev.*, D80:074035, 2009.

[106] Jens O. Andersen and Tomas Brauner. Phase diagram of two-color quark matter at nonzero baryon and isospin density. *Phys.Rev.*, D81:096004, 2010.

[107] J.B. Kogut, D.K. Sinclair, S.J. Hands, and S.E. Morrison. Two color QCD at nonzero quark number density. *Phys.Rev.*, D64:094505, 2001.

[108] Simon Hands, Seyong Kim, and Jon-Ivar Skullerud. Deconfinement in dense 2-color QCD. *Eur.Phys.J.*, C48:193, 2006.

[109] Simon Hands, Philip Kenny, Seyong Kim, and Jon-Ivar Skullerud. Lattice Study of Dense Matter with Two Colors and Four Flavors. *Eur.Phys.J.*, A47:60, 2011.

[110] Krishna Rajagopal and Frank Wilczek. The Condensed matter physics of QCD. 2000. hep-ph/0011333.

[111] Mark G. Alford, Andreas Schmitt, Krishna Rajagopal, and Thomas Schafer. Color superconductivity in dense quark matter. *Rev.Mod.Phys.*, 80:1455–1515, 2008.

[112] Bertrand C. Barrois. Superconducting Quark Matter. *Nucl.Phys.*, B129:390, 1977.

[113] D. Bailin and A. Love. Superfluidity and Superconductivity in Relativistic Fermion Systems. *Phys.Rept.*, 107:325, 1984.

[114] Mark G. Alford, Jeffrey A. Bowers, and Krishna Rajagopal. Crystalline color superconductivity. *Phys.Rev.*, D63:074016, 2001.

[115] Owe Philipsen. Lattice QCD at non-zero temperature and baryon density. pages 273–330, 2010. Lectures given at the Summer School on 'Modern perspectives in lattice QCD', Les Houches, August 3-28, 2009, arXiv:1009.4089.

[116] Y. Aoki, Z. Fodor, S.D. Katz, and K.K. Szabo. The QCD transition temperature: Results with physical masses in the continuum limit. *Phys.Lett.*, B643:46–54, 2006.

[117] Y. Aoki et al. The QCD transition temperature: results with physical masses in the continuum limit II. *JHEP*, 06:088, 2009.

[118] Z. Fodor. QCD thermodynamics on the lattice: Approaching the continuum limit with physical quark masses. *J.Phys.Conf.Ser.*, 230:012013, 2010.

[119] M. Cheng, N.H. Christ, S. Datta, J. van der Heide, C. Jung, et al. The Transition temperature in QCD. *Phys.Rev.*, D74:054507, 2006.

[120] Frithjof Karsch. Equation of state and more from lattice regularized QCD. *J.Phys.G*, G35:104096, 2008.

[121] S.P. Klevansky. The Nambu-Jona-Lasinio model of quantum chromodynamics. *Rev.Mod.Phys.*, 64:649–708, 1992.

[122] J. Berges, D.U. Jungnickel, and C. Wetterich. Two flavor chiral phase transition from nonperturbative flow equations. *Phys.Rev.*, D59:034010, 1999.

[123] Jens Braun and Holger Gies. Chiral phase boundary of QCD at finite temperature. *JHEP*, 06:024, 2006.

[124] Bernd-Jochen Schaefer and Jochen Wambach. The phase diagram of the quark meson model. *Nucl. Phys.*, A757:479–492, 2005.

[125] Jens Braun, Kai Schwenzer, and Hans-Jurgen Pirner. Linking the quark meson model with QCD at high temperature. *Phys.Rev.*, D70:085016, 2004.

[126] Claudia Ratti, Michael A. Thaler, and Wolfram Weise. Phases of QCD: Lattice thermodynamics and a field theoretical model. *Phys.Rev.*, D73:014019, 2006.

[127] V. Skokov et al. Meson fluctuations and thermodynamics of the Polyakov loop extended quark-meson model. *Phys.Rev.*, C82:015206, 2010.

[128] J. Hubbard. Calculation of partition functions. *Phys. Rev. Lett.*, 3:77–80, 1959.

[129] R. L. Stratonovich. On a method of calculating quantum distribution functions. *Soviet. Phys. Doklady.*, 2:416, 1958.

[130] Robert D. Pisarski and Frank Wilczek. Remarks on the Chiral Phase Transition in Chromodynamics. *Phys.Rev.*, D29:338–341, 1984.

[131] Krishna Rajagopal and Frank Wilczek. Static and dynamic critical phenomena at a second order QCD phase transition. *Nucl.Phys.*, B399:395–425, 1993.

[132] Alexander M. Polyakov. Thermal Properties of Gauge Fields and Quark Liberation. *Phys.Lett.*, B72:477–480, 1978.

[133] J. Greensite. The Confinement problem in lattice gauge theory. *Prog.Part.Nucl.Phys.*, 51:1, 2003.

[134] H. Reinhardt. Resolution of Gauss' law in Yang-Mills theory by gauge invariant projection: Topology and magnetic monopoles. *Nucl.Phys.*, B503:505–529, 1997.

[135] C. Ford, U.G. Mitreuter, T. Tok, A. Wipf, and J.M. Pawlowski. Monopoles, Polyakov loops and gauge fixing on the torus. *Annals Phys.*, 269:26–50, 1998.

[136] Oliver Jahn and F. Lenz. Structure and dynamics of monopoles in axial gauge QCD. *Phys.Rev.*, D58:085006, 1998.

[137] Florian Marhauser and Jan M. Pawlowski. Confinement in Polyakov Gauge. 2008. arXiv:0812.1144.

[138] Michael Strickland, Jens O. Andersen, Lars E. Leganger, and Nan Su. Hard-thermal-loop QCD Thermodynamics. *Prog.Theor.Phys.Suppl.*, 187:106–114, 2011.

[139] Jens O. Andersen, Lars E. Leganger, Michael Strickland, and Nan Su. Three-loop HTL QCD thermodynamics. *JHEP*, 1108:053, 2011.

[140] Jean-Paul Blaizot and Edmond Iancu. The Quark gluon plasma: Collective dynamics and hard thermal loops. *Phys.Rept.*, 359:355–528, 2002.

[141] Jean-Paul Blaizot, Edmond Iancu, and Anton Rebhan. Thermodynamics of the high temperature quark gluon plasma. 2003.

[142] Thomas Schafer and Derek Teaney. Nearly Perfect Fluidity: From Cold Atomic Gases to Hot Quark Gluon Plasmas. *Rept.Prog.Phys.*, 72:126001, 2009.

[143] Nathan Weiss. The Effective Potential for the Order Parameter of Gauge Theories at Finite Temperature. *Phys.Rev.*, D24:475, 1981.

[144] David J. Gross, Robert D. Pisarski, and Laurence G. Yaffe. QCD and Instantons at Finite Temperature. *Rev.Mod.Phys.*, 53:43, 1981.

[145] J. Braun, H. Gies, and H.-J. Pirner. RG flow of the Polyakov-loop potential: First status report. *AIP Conf.Proc.*, 775:162–172, 2005.

[146] Jens Braun, Holger Gies, and Jan M. Pawlowski. Quark Confinement from Color Confinement. *Phys. Lett.*, B684:262–267, 2010.

[147] Jens Braun, Astrid Eichhorn, Holger Gies, and Jan M. Pawlowski. On the Nature of the Phase Transition in SU(N), Sp(2) and E(7) Yang-Mills theory. *Eur.Phys.J.*, C70:689–702, 2010.

[148] Eric S. Swanson. A Primer on Functional Methods and the Schwinger-Dyson Equations. *AIP Conf.Proc.*, 1296:75–121, 2010.

[149] Daniel F. Litim. Optimization of the exact renormalization group. *Phys.Lett.*, B486:92–99, 2000.

[150] Leonard Fister and Jan Martin Pawlowski. Yang-Mills theory at non-vanishing temperature. 2011. arXiv:1112.5429.

[151] Leonard Fister and Jan M. Pawlowski. Yang-Mills correlation functions at finite temperature. 2011. arXiv:1112.5440.

[152] Leonard Fister. Dissertation, University of Heidelberg. 2012.

[153] Reinhard Alkofer and Lorenz von Smekal. The Infrared behavior of QCD Green's functions: Confinement dynamical symmetry breaking, and hadrons as relativistic bound states. *Phys.Rept.*, 353:281, 2001.

[154] Christian S. Fischer, Axel Maas, and Jan M. Pawlowski. On the infrared behavior of Landau gauge Yang-Mills theory. *Annals Phys.*, 324:2408–2437, 2009.

[155] Lisa M. Haas. Diploma thesis, University of Heidelberg. 2009.

[156] Michael E. Peskin and Daniel V. Schroeder. An Introduction to quantum field theory. 1995.

[157] S. Pokorski. Gauge field theories. 1987.

[158] L.D. Faddeev and V.N. Popov. Feynman Diagrams for the Yang-Mills Field. *Phys.Lett.*, B25:29–30, 1967.

[159] A. Sternbeck, E.-M. Ilgenfritz, M. Muller-Preussker, A. Schiller, and I.L. Bogolubsky. Lattice study of the infrared behavior of QCD Green's functions in Landau gauge. *PoS*, LAT2006:076, 2006.

[160] Fabian Rennecke. Work in progress.

[161] Attilio Cucchieri and Tereza Mendes. The Saga of Landau-Gauge Propagators: Gathering New Ammo. *AIP Conf.Proc.*, 1343:185–187, 2011.

[162] Lorenz von Smekal, Andreas Hauck, and Reinhard Alkofer. A solution to coupled Dyson-Schwinger equations for gluons and ghosts in Landau gauge. *Annals Phys.*, 267:1, 1998.

[163] Lorenz von Smekal, Reinhard Alkofer, and Andreas Hauck. The Infrared behavior of gluon and ghost propagators in Landau gauge QCD. *Phys.Rev.Lett.*, 79:3591–3594, 1997.

[164] Daniel Zwanziger. Nonperturbative Landau gauge and infrared critical exponents in QCD. *Phys.Rev.*, D65:094039, 2002.

[165] Christoph Lerche and Lorenz von Smekal. On the infrared exponent for gluon and ghost propagation in Landau gauge QCD. *Phys.Rev.*, D65:125006, 2002.

[166] Reinhard Alkofer, Markus Q. Huber, and Kai Schwenzer. Infrared singularities in Landau gauge Yang-Mills theory. *Phys.Rev.*, D81:105010, 2010.

[167] Markus Q. Huber, Axel Maas, and Lorenz von Smekal. Two- and three-point functions in two-dimensional Landau-gauge Yang-Mills theory: Continuum results. 2012. arXiv:1207.0222.

[168] I.L. Bogolubsky, E.M. Ilgenfritz, M. Muller-Preussker, and A. Sternbeck. The Landau gauge gluon and ghost propagators in 4D SU(3) gluodynamics in large lattice volumes. *PoS*, LAT2007:290, 2007.

[169] Attilio Cucchieri and Tereza Mendes. What's up with IR gluon and ghost propagators in Landau gauge? A puzzling answer from huge lattices. *PoS*, LAT2007:297, 2007.

[170] Philippe Boucaud, J-P. Leroy, A. Le Yaouanc, J. Micheli, O. Pene, et al. IR finiteness of the ghost dressing function from numerical resolution of the ghost SD equation. *JHEP*, 0806:012, 2008.

[171] A.C. Aguilar, D. Binosi, and J. Papavassiliou. Gluon and ghost propagators in the Landau gauge: Deriving lattice results from Schwinger-Dyson equations. *Phys.Rev.*, D78:025010, 2008.

[172] Axel Maas. Describing gauge bosons at zero and finite temperature. 2011. arXiv:1106.3942.

[173] Christian S. Fischer, Axel Maas, and Jan M. Pawlowski. Aspects of confinement from QCD correlation functions. *PoS*, CONFINEMENT8:043, 2008.

[174] Daniel Spielmann. Aspects of confinement in QCD from lattice simulations. Dissertation. Heidelberg University. 2011.

[175] Markus Q. Huber. On gauge fixing aspects of the infrared behavior of Yang-Mills Green functions. 2010. arXiv:1005.1775.

[176] Holger Gies. Running coupling in Yang-Mills theory: A flow equation study. *Phys. Rev.*, D66:025006, 2002.

[177] Jan M. Pawlowski, Daniel F. Litim, Sergei Nedelko, and Lorenz von Smekal. Infrared behaviour and fixed points in Landau gauge QCD. *Phys. Rev. Lett.*, 93:152002, 2004.

[178] Daniel F. Litim, Jan M. Pawlowski, Sergei Nedelko, and Lorenz von Smekal. Infrared QCD and the renormalisation group. 2004. hep-th/0410241.

[179] N. Tetradis and C. Wetterich. Critical exponents from effective average action. *Nucl.Phys.*, B422:541–592, 1994.

[180] D.U. Jungnickel and C. Wetterich. Effective action for the chiral quark-meson model. *Phys.Rev.*, D53:5142–5175, 1996.

[181] K. Nakamura et al. Review of particle physics. *J.Phys.G*, G37:075021, 2010.

[182] Frank R. Brown, Frank P. Butler, Hong Chen, Norman H. Christ, Zhi-hua Dong, et al. On the existence of a phase transition for QCD with three light quarks. *Phys.Rev.Lett.*, 65:2491–2494, 1990.

[183] H. Saito et al. Phase structure of finite temperature QCD in the heavy quark region. *Phys.Rev.*, D84:054502, 2011.

[184] T. Umeda et al. Equation of state in 2+1 flavor QCD with improved Wilson quarks by the fixed scale approach. *Phys.Rev.*, D85:094508, 2012.

[185] Claudio Bonati, Philippe de Forcrand, Massimo D'Elia, Owe Philipsen, and Francesco Sanfilippo. Constraints on the two-flavor QCD phase diagram from imaginary chemical potential. *PoS*, LATTICE2011:189, 2011.

[186] Andre Roberge and Nathan Weiss. Gauge theories with imaginary chemical potential and the phases of QCD. *Nucl. Phys.*, B275:734, 1986.

[187] Yuji Sakai, Kouji Kashiwa, Hiroaki Kouno, and Masanobu Yahiro. Phase diagram in the imaginary chemical potential region and extended Z(3) symmetry. *Phys.Rev.*, D78:036001, 2008.

[188] Massimo D'Elia and Francesco Sanfilippo. The Order of the Roberge-Weiss endpoint (finite size transition) in QCD. *Phys.Rev.*, D80:111501, 2009.

[189] Claudio Bonati, Guido Cossu, Massimo D'Elia, and Francesco Sanfilippo. The Roberge-Weiss endpoint in $N_f = 2$ QCD. *Phys.Rev.*, D83:054505, 2011.

[190] Philippe de Forcrand and Owe Philipsen. Constraining the QCD phase diagram by tricritical lines at imaginary chemical potential. *Phys.Rev.Lett.*, 105:152001, 2010.

[191] Yuji Sakai et al. Determination of QCD phase diagram from the imaginary chemical potential region. *Phys.Rev.*, D79:096001, 2009.

[192] David Scheffler, Michael Buballa, and Jochen Wambach. PNJL model analysis of the Roberge-Weiss transition endpoint at imaginary chemical potential. 2011.

[193] Kouji Kashiwa, Thomas Hell, and Wolfram Weise. Nonlocal Polyakov-Nambu-Jona-Lasinio model and imaginary chemical potential. *Phys.Rev.*, D84:056010, 2011.

[194] Christof Gattringer. Linking confinement to spectral properties of the Dirac operator. *Phys. Rev. Lett.*, 97:032003, 2006.

[195] Franziska Synatschke, Andreas Wipf, and Christian Wozar. Spectral sums of the Dirac-Wilson operator and their relation to the Polyakov loop. *Phys. Rev.*, D75:114003, 2007.

[196] Erek Bilgici et al. Dual quark condensate and dressed Polyakov loops. *Phys. Rev.*, D77:094007, 2008.

[197] Christian S. Fischer. Deconfinement phase transition and the quark condensate. *Phys. Rev. Lett.*, 103:052003, 2009.

[198] Jeroen C. Vink. On the spectrum of the staggered Dirac operator at finite chemical potential. *Nucl.Phys.*, B323:399, 1989.

[199] Slavo Kratochvila and Philippe de Forcrand. QCD at zero baryon density and the Polyakov loop paradox. *Phys.Rev.*, D73:114512, 2006. 21 pages, 7 figures Report-no: CERN-PH-TH-2006-007.

[200] Philippe de Forcrand and Owe Philipsen. The QCD phase diagram for small densities from imaginary chemical potential. *Nucl. Phys.*, B642:290–306, 2002.

[201] Yuji Sakai, Kouji Kashiwa, Hiroaki Kouno, and Masanobu Yahiro. Polyakov loop extended NJL model with imaginary chemical potential. *Phys.Rev.*, D77:051901, 2008.

[202] Lisa M. Haas, Jan M. Pawlowski, and Lorenz von Smekal. work in progress.

[203] Christian S. Fischer and Jens A. Mueller. Chiral and deconfinement transition from Dyson-Schwinger equations. *Phys.Rev.*, D80:074029, 2009.

[204] Liang-Kai Wu, Xiang-Qian Luo, and He-Sheng Chen. Phase structure of lattice QCD with two flavors of Wilson quarks at finite temperature and chemical potential. *Phys.Rev.*, D76:034505, 2007.

[205] V.G. Bornyakov, R. Horsley, S.M. Morozov, Y. Nakamura, M.I. Polikarpov, et al. Probing the finite temperature phase transition with N(f) = 2 nonperturbatively improved Wilson fermions. *Phys.Rev.*, D82:014504, 2010.

[206] Florian Marhauser. Confinement in Polyakov Gauge and the QCD phase diagram. 2009. Dissertation. Heidelberg University.

[207] Massimo D'Elia and Maria-Paola Lombardo. Finite density QCD via imaginary chemical potential. *Phys. Rev.*, D67:014505, 2003.

[208] Massimo D'Elia and Maria Paola Lombardo. QCD thermodynamics from an imaginary mu(B): Results on the four flavor lattice model. *Phys.Rev.*, D70:074509, 2004.

[209] Jens Braun, Leonard Fister, Lisa M. Haas, Jan M. Pawlowski, and Fabian Rennecke. work in progress.

[210] Owe Philipsen. What the lattice tells us about the existence of a critical point. *AIP Conf.Proc.*, 1343:462–464, 2011.

[211] Kenji Fukushima and Kouji Kashiwa. Polyakov loop and QCD thermodynamics from the gluon and ghost propagators. 2012. arXiv:1206.0685.

[212] O. Scavenius, A. Dumitru, and J.T. Lenaghan. The K / pi ratio from condensed Polyakov loops. *Phys.Rev.*, C66:034903, 2002.

[213] Simon Roessner, Claudia Ratti, and W. Weise. Polyakov loop, diquarks and the two-flavour phase diagram. *Phys.Rev.*, D75:034007, 2007.

[214] G. Boyd, J. Engels, F. Karsch, E. Laermann, C. Legeland, et al. Thermodynamics of SU(3) lattice gauge theory. *Nucl.Phys.*, B469:419–444, 1996.

[215] O. Kaczmarek, F. Karsch, P. Petreczky, and F. Zantow. Heavy quark anti-quark free energy and the renormalized Polyakov loop. *Phys.Lett.*, B543:41–47, 2002.

[216] Jonathan T. Lenaghan, Dirk H. Rischke, and Jurgen Schaffner-Bielich. Chiral symmetry restoration at nonzero temperature in the SU(3)(r) x SU(3)(l) linear sigma model. *Phys.Rev.*, D62:085008, 2000.

[217] Szabolcs Borsanyi et al. Is there still any T_c mystery in lattice QCD? Results with physical masses in the continuum limit III. *JHEP*, 1009:073, 2010.

[218] Douglas Adams. *So long and thanks for all the fish.* Pan Books, UK, 1984.

Acknowledgments

Special thanks go to Prof. Dr. Jan M. Pawlowski who gave me the opportunity to work on the topic of this thesis. I especially thank him for his outstanding patience, encouragement and his support throughout this thesis. I would like to thank him for the countless extremely helpful and enlightening discussions and explanations. I am very grateful that he made it possible for me to visit many workshops and schools and to always have an open ear and door. Thank you!

I would also like to thank Prof. Dr. Michael G. Schmidt for agreeing to be the second examiner of this thesis.

For an excellent scientific collaboration and endless very helpful and very enlightening discussions and explanations I am indebted to Prof. Dr. Jens Braun.

I would also like to thank my collaborators Mag. Leonard Fister, Dr. Florian Marhauser, Dipl.-Phys. Fabian Rennecke, Prof. Dr. Jürgen Schaffner–Bielich and Dipl.-Phys. Rainer Stiele for very enriching and productive collaborations.

Also, I want to thank Dipl.-Phys. Igor Boettcher, Dipl.-Phys. Nicolai Christiansen, Dr. Astrid Eichhorn, Prof. Dr. Christian S. Fischer, Dr. Stefan Floerchinger, Dr. Simon Friederich, MSc Naseemuddin Khan, Dr. Sergej Moroz, Dr. Michael M. Scherer, Dipl.-Phys. Fabian Spallek, Dr. Daniel Spielmann and Dr. habil. Lorenz von Smekal for many useful discussions.

I thank the HGSFP and especially Prof. Dr. Sandra Klevansky for their (financial) support during the last year.

For proof-reading I am very grateful to Prof. Dr. Jens Braun, Dipl.-Phys. Nicolai Christiansen, Dipl.-Biol. Helen Haas, Dipl.-Phys. Boris Nowak and Dipl.-Phys. Fabian Rennecke.

My thanks to all the people from the "Dachzimmer" for a friendly and joyful atmosphere!

I thank Hannes Haas for his love, support and Elternzeit and my son Finn for lighting up my day.

So long, and thanks for all the fish [218][1]

[1]Excerpt from Wikipedia: "So Long, and Thanks for All the Fish is the fourth book of the Hitchhiker's Guide to the Galaxy "trilogy" written by Douglas Adams. Its title is the message left by the dolphins when they departed Planet Earth just before it was demolished to make way for a hyperspace bypass, as described in The Hitchhiker's Guide to the Galaxy."